

UNIVERSITY OF APPLIED SCIENCES ASCHAFFENBURG

MASTER'S THESIS

CONNECTIVITY ESTIMATION OF HIGH DIMENSIONAL DATA RECORDED FROM NEURONAL CELLS

*A thesis submitted in fulfillment of the requirements
for the degree of Master of Engineering*

in the

Biomems lab
University of Applied Sciences Aschaffenburg

Author:
Stefano DE BLASI

Supervisors:
Christiane THIELEMANN
Manuel CIBA

28th September, 2018

Declaration of Authorship

I, Stefano De Blasi, declare that this thesis titled, *Connectivity estimation of high dimensional data recorded from neuronal cells* and the work presented in it are my own. I confirm that:

- This work was done wholly or mainly while in candidature for a research degree at the University of Applied Sciences (UAS) Aschaffenburg.
- Where any part of this report has previously been submitted for a degree at the UAS Aschaffenburg, this has been clearly stated.
- Where I have consulted the published work of others, this is always clearly attributed.
- Where I have quoted from the work of others, the source is always given. With the exception of such quotations, this thesis is entirely my own work.
- Some parts of this work are the pre-print versions of the publications I submitted during my candidature for a research degree at the UAS Aschaffenburg. These publications have not been submitted for a degree.
- I have acknowledged all main sources of help.
- Where the report is based on work done by myself jointly with others, I have made clear exactly what was done by others and what I have contributed myself.

Signed:

Date: 28th September, 2018

Author:
Stefano De Blasi
Prozelterner Weg 6
63933 Mönchberg

First examiner and supervisor:
Prof. Dr.-Ing. Christiane Thielemann

Second examiner:
Prof. Dr. Hans-Georg Stark

Supervisor:
M.Eng. Manuel Ciba

UAS Aschaffenburg
Faculty Engineering Sciences
Würzburger Straße 45
63743 Aschaffenburg



Contents

List of Figures	VI
Acronyms	VII
1. Motivation	1
2. Fundamentals	3
2.1. Elements of neuronal systems	3
2.2. Types of connectivity	5
2.2.1. Structural connectivity	5
2.2.2. Functional connectivity	6
2.2.3. Effective connectivity	6
2.3. Spike train data <i>in vitro</i>	6
2.3.1. Measurement of neuronal raw data in vitro	6
2.3.2. Signal preprocessing	8
3. Simulation framework for evaluation applications	10
3.1. Selection of a neuron model	10
3.2. Modeling of networks	11
3.2.1. Synaptic Weight Matrix	11
3.2.2. Delay Matrix	12
3.3. Network types	12
3.3.1. Regular networks	12
3.3.2. Random networks	12
3.3.3. Small-world networks	13
3.3.4. Scale-free networks	13
3.4. Neuronal network simulations	14
3.5. Results and discussion of simulation	16
3.6. Conclusion of simulation	19
4. Methods of connectivity estimation	20
4.1. Cross Correlation	21
4.1.1. Normalized Cross Correlation Histogram	21
4.1.2. Normalized Cross Correlation	21
4.2. Transfer Entropy	23
4.2.1. Delay One Transfer Entropy	23
4.2.2. Higher Order Transfer Entropy	24
4.2.3. Delayed Higher Order Transfer Entropy	24
4.2.4. Combined Higher Order Transfer Entropy	26
4.3. Total Spiking Probability Edges	27
4.4. Threshold calculation methods	30
4.4.1. Easy threshold calculation	30
4.4.2. Threshold calculation with surrogate data	30
4.5. Implementations	30

5. Evaluation of connectivity estimation	31
5.1. Evaluation tools	31
5.1.1. Simulation	31
5.1.2. ROC Curve	31
5.1.3. Confusion matrix	32
5.2. Accuracy of functional connectivity estimation	32
5.3. Accuracy of effective connectivity estimation by TSPE	35
5.4. Calculation time	36
5.5. Evaluation of threshold calculation	37
5.5.1. Easy threshold calculation	37
5.5.2. Threshold calculation with surrogate data	38
5.6. Conclusion of evaluation	39
6. Graph theory	41
7. Application of connectivity estimation	42
7.1. Setup of the experiment	42
7.2. Spike detection and sorting	44
7.3. Connectivity estimation with TSPE	45
7.4. Graph theory analysis	47
7.5. Network dynamics	48
7.5.1. Comparison of different stimuli	48
7.5.2. Long recording based analysis	48
7.5.3. Interchamber comparison	54
7.6. Discussion	55
8. Conclusion and outlook	56
Appendices	58

List of Figures

2.1. Structure of a typical neuron	4
2.2. Biological neural network <i>in vitro</i>	4
2.3. Types of connectivity	5
2.4. MEA and HDMEA chip	7
2.5. Layout of MEA and HDMEA	7
2.6. Spike detection	8
2.7. Binning types	9
3.1. Difference between random and scale-free neuronal networks	13
3.2. Neuronal network <i>in silico</i>	14
3.3. Effects of STDP	15
3.4. Samples of simulated spike trains	16
3.5. Analysis of SII and ER random network	17
3.6. Analysis of generated IC and BA scale-free network	18
4.1. Workflow of connectivity estimation	20
4.2. Cross Correlation	22
4.3. Principle of Coincidence Index	23
4.4. Principle of Delayed Transfer Entropy	25
4.5. Principle of CDHOTE	26
4.6. Principle of SPE	27
4.7. Design of edge and running total filters	28
4.8. Principle of TSPE	29
4.9. Spike dithering for generate surrogate data	30
5.1. Evaluation of connectivity estimation algorithms for different network topologies	33
5.2. Effects of the recording time on the accuracy of the connectivity estimation	34
5.3. Confusion matrices for connection types classified by TSPE	35
5.4. Comparison of calculation times of tested algorithms	36
7.1. Neurites in a micro-tunnel device	42
7.2. Experiment with four cultures	43
7.3. Example of spike sorting	44
7.4. Example of measured spike trains (1 min)	45
7.5. Example of an estimated connection	46
7.6. Results of estimated graphs	47
7.7. Network dynamics for different stimuli at DG	49
7.8. Network dynamics for HF stimulation at DG with long recordings	50
7.9. Network dynamics for HF stimulation at CA1 with long recordings	51
7.10. Network dynamics for HF stimulation at CA3 with long recordings	52
7.11. Network dynamics for HF stimulation at EC with long recordings	53
C.1. Comparison of neuronal models	61
D.1. Comparison of simulation software	62

Acronyms

APS	Active Pixel Sensor
BA	Barabasi–Albert
BaCaTeC	Bavaria California Technology Center
CA1	Cornu Ammonis 1
CA3	Cornu Ammonis 3
CC	Cross Correlation
CCW	Counter Clockwise
CDHOTE	Combined Delayed Higher Order Transfer Entropy
CH	Chattering
CI	Coincidence Index
CM	Connectivity Matrix
CMOS	Complementary Metal-Oxide Semiconductor
COBA	Conductance-Based
CTU	Czech Technical University
CUBA	Current-Based
CW	Clockwise
D1TE	Delay One Transfer Entropy
DG	Dentate Gyrus
DHOTE	Delayed Higher Order Transfer Entropy
DHOTE CI	Delayed Higher Order Transfer Entropy Coincidence Index
DIV	Days <i>in vitro</i>
DM	Delay Matrix
DTE	Delayed Transfer Entropy
DTE CI	Delayed Transfer Entropy Coincidence Index
EC	Entorhinal Cortex
ER	Erdos–Renyi
FIR	Finite Impulse Response

FLOP	Float Operation
FN	False Negative
FP	False Positive
FPR	False Positive Rate
FS	Fast Spiking
HDMEA	High Density Microelectrode Array
HF	High Frequency
HH	Hodgkin–Huxley
HOTE	Higher Order Transfer Entropy
HT	Hard Threshold
IB	Intrinsically Bursting
IC	Implementation of Catanzaro
IF	Integrate-and-Fire
K-S test	Kolmogorov-Smirnov test
LR	Long Recording
LTS	Low-Threshold Spiking
MCS	Multi Channel Systems
MEA	Microelectrode Array
MEX	MATLAB executable
MFR	Mean Firing Rate
MI	Mutual Information
MIND	Institute for Memory Impairments and Neurological Disorders
MPL	Mean Path Length
NCC	Normalized Cross Correlation
NCCCI	Normalized Cross Correlation Coincidence Index
NCCH	Normalized Cross Correlation Histogram
PDMS	Polydimethylsiloxane
PP	Paired Pulse
PTSD	Precise Timing Spike Detection
QBD	Quantile Based Detection
ROC	Receiver Operating Characteristic
RS	Regular Spiking
SD	Standard Deviation

SII	Standard Implementation of Izhikevich
SNR	Signal-to-Noise Ratio
SPE	Spiking Probability Edges
SS	Summer Semester
STDP	Spike-Timing Dependent Plasticity
SWDT	Sliding Window Differential Threshold
SWM	Synaptic Weight Matrix
TC	Thalamo-Cortical
TCM	Thresholded Connectivity Matrix
TE	Transfer Entropy
TETRA	Terrestrial Trunked Radio
TN	True Negative
TP	True Positive
TPR	True Positive Rate
TSPE	Total Spiking Probability Edges
UAS	University of Applied Sciences
UCI	University of California Irvine

1.

Motivation

The human brain consists of billions of nerve cells, so-called neurons, and is one of the most exciting mysteries of our time. Many neuroscientists study nervous systems in order to understand the brain, which is essential for human consciousness, motor control or memory and learning. Since brain diseases have devastating effects on our lives [1], the need for an improvement of our knowledge about these diseases and their causes is critical in order to develop more effective treatment. Fundamental understanding of the brain could even help to cure neural diseases like epilepsy, Parkinson's disease or Alzheimer's disease [2]. Moreover, developments such as bionic prostheses can restore the patient's lost senses. These developments are highly desirable and possible with acquired knowledge about our brain. For example, cochlear implants can be used to make a deaf person hear [3]. In addition, retinal prostheses, so-called bionic eyes, are currently attracting a lot of attention and are able to grant blind people visual perception [4].

To understand neural networks like the brain it is fundamentally necessary to know the topology of them first. How are single neurons connected with each other? Is there some kind of a connection map similar to power grids or motorways? Next, the information flow has to be analysed. How is an information designed and how is it processed by the brain? Are there similarities with already known information networks such as the Internet? Finally, by observing the information flow, we would be able to detect functions of certain neurons, what provides the basis for precise treatments or bionic interfaces.

Many issues are directly or indirectly connected to the international task understanding the human brain. There are many different approaches to solving these problems. For example, the biological technology of optogenetics has recently attracted international attention. It allows to use genetically modified cells in order to understand functions of rat brains by literally switching parts of a living rat brain on or off to observe effects on the behaviour of the subject [5]. An optical fiber goes directly through skin into the brain of living animals to stimulate certain areas or functions. This kind of experiments is called *in vivo* and is ethically questionable not only from the point of view of animal welfare organizations [6]. While countless researchers already work on mapping brains of humans or animals by using methods like optogenetics or reconstructions of dead rat brain slices [7] there are still many unsolved questions even at small networks with only thousands of neurons. Wouldn't it be more effective to understand small neural networks complexity first?

Microelectrode Arrays (MEAs) can be used to measure electrical signals of *in vitro* cultures, which means these experiments do not involve living animals. By detecting action potentials of a neuronal network there exist methods to make statements about connections between neurons. This task is called estimation of neuronal connectivity and it is part of cutting-edge fundamental research.

At the biomems lab of UAS Aschaffenburg, such *in vitro* experiments are carried out in order to learn more about external influences on neural systems by using cell-based biosensors in form of cultures on MEAs. The portfolio of the biomems labs is represented by three projects which could gain in significance in the future through connectivity estimation. Electrophysiological effects on neural network communication of human embryonic stem cell derived neurospheres are investigated [8]. In Aschaffenburg cell-based sensor chips are also used for neurotoxicity measurements in drinking water [9]. In addition, impacts of irradiation like Terrestrial Trunked Radio (TETRA) on neural *in vitro* networks cells are explored also in long-terms [10]. Observing a significant change in connectivity during these experiments would lead to important biological statements. Furthermore, with an ability to estimate connectivity there are several methods of graph theory to get even more knowledge

about the neural network like node degree, path length or efficiency, connection density or cost, hubs, centrality or robustness [11]. These parameters would improve the meaningfulness of future experiments. Moreover, network dynamics could be observed in experimental environment.

The main result of this thesis is the development of a novel connectivity estimation method, called *Total Spiking Probability Edges* (TSPE). Based on cross-correlation and edge filtering at different time scales this method is proposed and the theoretical framework is outlined in this work. TSPE enables the classification between inhibitory and excitatory connections by using recorded action potentials.

To compare this method learning about state of the art algorithms to estimate connectivity is necessary. After a research, promising algorithms are implemented and evaluated for further research topics, among others in the biomems lab of UAS Aschaffenburg. To evaluate these algorithms *in silico* networks are used, because of their known connectivity. This makes it possible to validate the correctness of our algorithm results. Therefore, a biophysically representative neuronal network simulation is needed first. Datasets were simulated in different ways and analysed in order to develop an evaluation framework. After a successful evaluation with *in silico* networks, *in vitro* experiments and their analyses complete this project.

2.

Fundamentals

This chapter covers relevant fundamentals which are necessary to understand the project beginning with some basics of neuronal systems. Section 2.2 provides knowledge about connectivity in neuronal networks. In Section 2.3, the extraction and preprocessing of neuronal data from real cultures *in vitro* is explained.

2.1. Elements of neuronal systems

A neuronal network consists of many neurons connected with each other. Each neuron has the ability to change its membrane potential, that is given by different ion concentrations within (intracellular) and outside (extracellular) the nerve cell. Changes are enabled by ion channels and pumps transferring mainly sodium ions Na^+ and potassium ions K^+ across the cell membrane. The flow of sodium ions produces an increase in membrane potential, leading to the rapid opening of even more channels (reaction series). This immense influx inactivates the sodium ion channels by polarization and activates the potassium ion channels (membrane potential decreases again). Between two neurons, information is transmitted using these described electrical pulses, so-called action potentials [12]. These pulses are generated by each individual neuron and sent to adjacent nerve cells along the connections of a network. In Figure 2.1, the structure of a typical neuron is illustrated. These neurons are connected to each other in a neuronal network (see Figure 2.2). The axon can be seen as the output of a neuron while dendrites are the inputs received from other neurons. Therefore, the way of an action potential consists basically of three parts:

- Axon of the emitting, also presynaptic, neuron
- Synapse connecting an axon and a dendrite
- Dendrite ending at the soma of a receiving, also postsynaptic, neuron

While the soma can be seen as a processing unit, it emits new action potentials depending on its input. Basically there are two types of neurons: Excitatory and inhibitory. Very simplified you may imagine a threshold for each soma, excitatory inputs add a value while inhibitory subtract another value. If the sum of these inputs is big enough to pass the postsynaptic threshold its neuron will emit an action potential, this process is also known as firing [14].

Neural networks are able to strengthen a synapse by using it, which is basically the ability to learn something. This hypothesis for learning processes in the brain is called Hebbian theory [15]. Since neuronal coding theories take only action potentials into account, the amplitude is not of interest. Thus, the important information of recorded neuronal data is the history of detected peaks, which are then called spikes. Temporal sequences of all spikes are referred to spike trains. In this work discussed connectivity estimation algorithms use such spike trains. Multiple spikes of a same emitting neuron in a short time are called bursts. Furthermore, in neuronal networks neurons may fire almost synchronously in short time intervals, which is known as network bursts.

Further information of neuronal systems can be found in literature like the books *Theoretical Neuroscience* by Dayan or *Neuronal Dynamics: From Single Neurons to Networks and Models of Cognition* by Gerstner [12, 14].

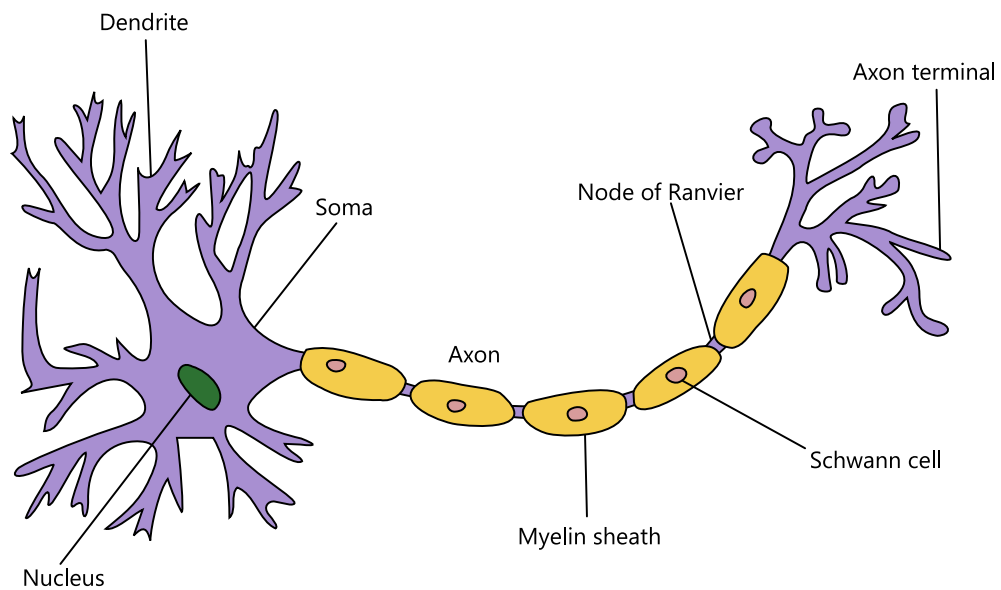


Figure 2.1. – Structure of a typical neuron: On the left-hand side dendrites are the input side of a neuron. The body of a neuron is called soma. Through an axon an action potential will be emitted to the axon terminals, which are the output side. The connection between a dendrite and terminal is a so-called synapse. Figure by [13].

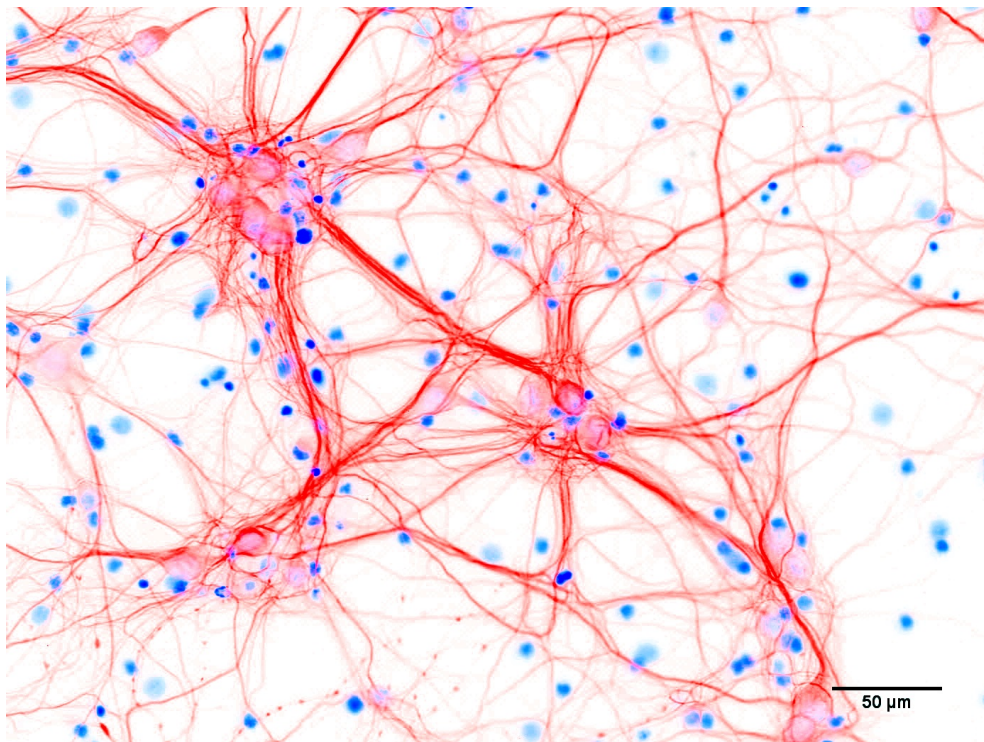


Figure 2.2. – Biological neural network *in vitro*:

A fluorescence image of a neuronal *in vitro* culture was taken, with blue coloured cell bodies and red coloured dendrites. Origin picture taken by Margot Mayer at UAS Aschaffenburg.

2.2. Types of connectivity

Connectivity provides knowledge of how a network is connected. Like every kind of network also neuronal networks are based on nodes and connections. In this context, the nodes are nerve cells and, like mentioned before, the connections consist basically of axons, synapses and dendrites. There are three different types of connectivity [16, 17] which are often used to describe the topology of neuronal networks:

- Structural connectivity, the pure existence of connections (see Figure 2.3.a)
- Functional connectivity, the knowledge about used connections (see Figure 2.3.b)
- Effective connectivity, the detailed knowledge about used connections (see Figure 2.3.c)

In addition to the illustration, their similarities, differences and characteristics are explained in the following.

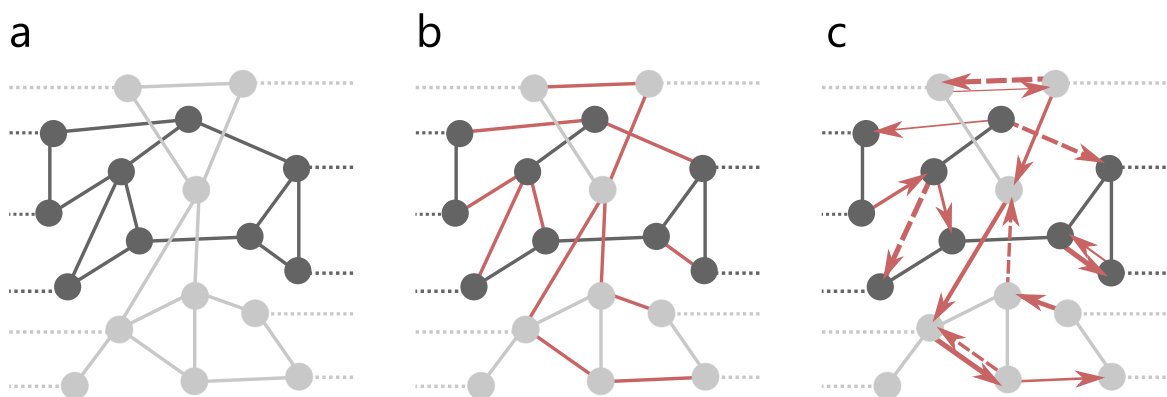


Figure 2.3. – Types of connectivity: (a) Structural connectivity, connections and neurons are marked with same color. Two unconnected networks have no anatomical connection to each other. (b) Functional connectivity, used connections are marked with red. Information was transferred over these connections. (c) Effective connectivity, used connections are marked with red, bigger connection widths denotes stronger influences and arrows label causality. Dashed connections indicates inhibitory behaviour, while normal ones stays for excitatory behaviour. Detailed knowledge about transferred information is possible. (a), (b) and (c) illustrate the same network in different perspectives in the form of connection types. Figure inspired by [17].

2.2.1. Structural connectivity

A structural or anatomical connection refers to physical interactions. In this particular case, it is an electrical or biochemical link between two neurons known as synapse. Thus, structural connectivity is the ability to communicate which does not mean connections are necessarily used for observed network activity. For example, the connectome can be seen as a structural network map of the human brain [18]. All synaptic connections are time- or activity-dependent [19]. Since short timescale investigations showed static morphological connections, the structural connectivity is manifest over a short time. Over longer terms anatomical connections are able to grow or fully degenerate [20]. Knowledge about this type of connectivity does not offer us to understand real functions of a network but about the ability of a function which could be possible. It is similar to the knowledge about existing streets of a motorway network without knowing anything about the traffic.

2.2.2. Functional connectivity

As the name indicates functional connectivity allows statements about functions of a neuronal network. Such a functional connection exists if the activity of two neurons is correlated somehow. This interaction is not described in more detail, since each functional connection is just defined as an activity correlation. In contrast to structural connectivity, the functional one can not be detected by using optical methods without genetic modifications (e.g. sequences of fluorescent calcium indicator proteins are incorporated into the genome for so-called calcium imaging methods) [21]. On the contrary, there would still be attained knowledge using normal imaging, since functional connections are a subset of structural connections [22]. The ability of synapses to strengthen or weaken over time is called synaptic plasticity and leads to an even greater time-dependency of functional connectivity, due to more direct influences of activity and the fact that structural connectivity is just manifest for a specific time [23].

2.2.3. Effective connectivity

By knowing the third and final type of connectivity we are able to describe effects of each interaction in detail. The amount of influence between neurons offers to distinguish weak connections from strong connections. Investigations can also differ between inhibitory or excitatory behaviour of a synaptic connection. Effective connectivity makes it even possible to answer causality questions of synapses [17]. For instance, which neuron is source and which is target? By knowing all these details, a neuronal network can be fully reconstructed in its characteristics. Since the observed effects are defined by the used model, effective connectivity is not model free like the other types of connectivity [24].

As one may already noticed, effective connectivity is a subset of functional connectivity and in order of that also a subset of structural connectivity. Like functional connectivity, the same impact of synaptic plasticity appeals effective connectivity. Thus, it changes its properties with time fast.

2.3. Spike train data *in vitro*

Since information transfer is decisive, estimation of functional or effective connectivity is only possible by observing the communication events between neurons, which are action potentials as mentioned. Therefore, these communication events are required to be recorded. The neuronal raw data then has to be preprocessed for a demanded format, which is based on detected action potential peak times, so-called spikes. The history of these spikes is called spike train data. In this section the way of signals from neuronal cultures *in vitro* to connectivity estimation algorithms will be explained.

2.3.1. Measurement of neuronal raw data *in vitro*

To measure signals of *in vitro* cultures various methods exist. These techniques are divided into two subgroups: Intracellular and extracellular. While intracellular measurements require at least one electrode inside the neuron or axon and destroy them afterwards, extracellular methods try to measure at the surface of cells without damaging them [2]. In this project non-implantable MEAs are used. MEA chips are capable of simultaneously recording multiple electrical signals from investigated objects such as cardiac muscle cells, neuronal cultures, hippocampal slices or stem cells extracellularly with a dense array of biocompatible electrodes. Common MEA chips (see Figure 2.4.a) of Multi Channel Systems (MCS) (Reutlingen, Germany, <http://www.multichannelsystems.com>) consist of 60 electrodes distributed on an area size of about $1.4 \times 1.4 \text{ mm}^2$, but there are also chips with 120 electrodes.

New technologies like High Density Microelectrode Arrays (HDMEAs) make it possible to improve our measurements by recording a culture with more electrodes which are closer to each other. Instead of 60 channels an HDMEA chip (see Figure 2.4.c) by 3brain (Wädenswil, Switzerland, <http://www.3brain.com/>) is able to record signals from up to 4096 (64×64) channels on an area size of

about $2.67 \times 2.67 \text{ mm}^2$. This also means a reduction of inter-electrode-distance from 200 to $21 \mu\text{m}$. Electrodes are sampled simultaneously at a frequency up to a maximum of 18 kHz, that is enabled by using a special Active Pixel Sensor (APS) based on Complementary Metal-Oxide Semiconductor (CMOS) technology [25]. In Figure 2.5 layouts of MEA and HDMEA are comparably visualized.

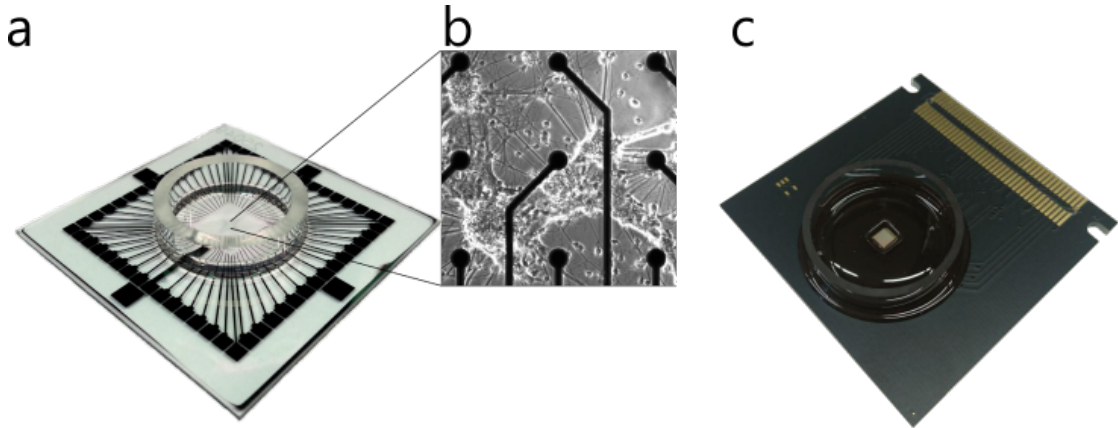


Figure 2.4. – MEA and HDMEA chip: (a) 60 electrode MEA chip by MCS with an electrode diameter of $30 \mu\text{m}$ and spacing of $200 \mu\text{m}$. (b) An enlargement of some electrodes (black dots) and a neuronal culture whose signals can be measured at the electrodes and transmitted via trace (black lines). (c) 4096 electrode HDMEA chip by 3brain with an electrode length of $21 \mu\text{m}$ and spacing of $21 \mu\text{m}$.

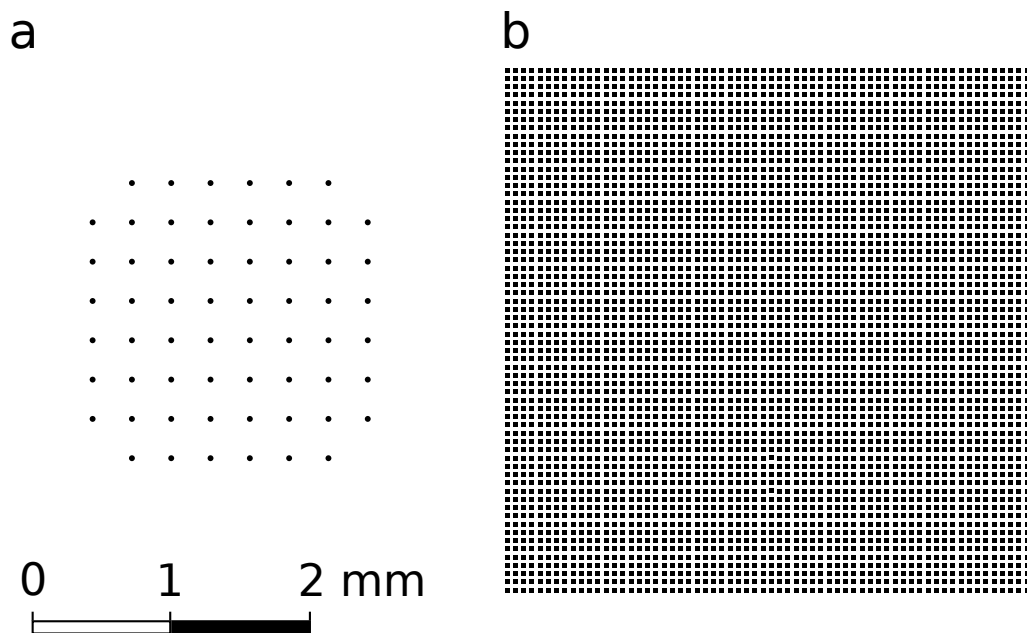


Figure 2.5. – Layout of MEA and HDMEA: (a) On the left a drawn to scale 60 electrodes MEA: Electrodes have a diameter of $30 \mu\text{m}$, the electrode distance is $200 \mu\text{m}$ and working area is about $1.4 \times 1.4 \text{ mm}^2$. (b) On the right a drawn to scale 4096 electrode HDMEA by 3brain: Electrodes have a size of $21 \times 21 \mu\text{m}^2$, each electrode distance is $21 \mu\text{m}$ and the working area is about $2.67 \times 2.67 \text{ mm}^2$. Figures taken at UAS Aschaffenburg

The improvement of electrode density is obvious. Consequently, HDMEA chips are able to help us understanding how neuronal networks work even better by increasing the percentage of recorded neurons in a network [2]. However, with smaller spaces between electrodes also some disadvantages in signal processing are produced, which will be explained in the next step.

2.3.2. Signal preprocessing

After a successful measurement neuronal raw data is noisy because of externally coupled signals and neurons, which are too far away from the electrode to be measured but near enough to take influence in form of background noise. Furthermore, recorded neuronal signals have broad frequency spectra. Since spikes are short voltage pulses (see Figure 2.6), digital filters can be used to improve the detection of spikes. At UAS Aschaffenburg the standard procedure is a reduction of low-frequency portions by using a high-pass Finite Impulse Response (FIR) filter.

The next crucial step is spike detection, which determines the peaks of network activity. Especially in context with HDMEAs it is still an up-to-date topic [26]. The easiest and fastest spike detection is simple Hard Threshold (HT), which is widely used [27, 28]. Since a low signal-to-noise ratio can be problematic, there are several different methods to detect spikes with adaptive thresholds [29]. By using stationary wavelet transform or time-frequency based algorithms a better performance is also possible [30]. In Figure 2.6 the basic function of spike detection is illustrated. The preprocessing software for HDMEA chips of 3brain *BrainWave* provides some spike detection methods like Precise Timing Spike Detection (PTSD), Sliding Window Differential Threshold (SWDT), HT or Quantile Based Detection (QBD). In Aschaffenburg, for standard 60 channel MEA chips the *MATLAB* based software *DrCell* is used and comes also with tools like filtering and spike detection [31]. The result of spike detection for a signal is then the spike train, which is the binary history of spike times: One for spikes or zero for no spiking at a sampling time.

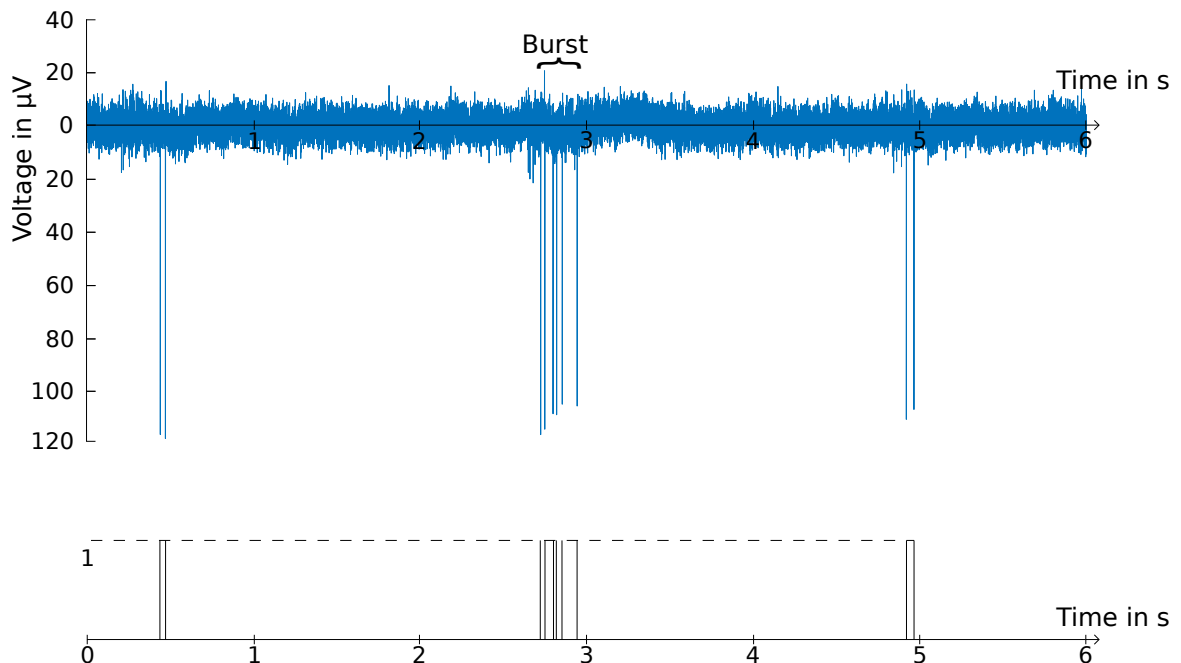


Figure 2.6. – Spike detection: Recorded raw data of neuronal cells is converted into a binary spike train via filtering and a spike detection algorithm. Multiple spikes in a short time window define a burst.

Since the signals from more than just one cell are able to be measured with an electrode, some researchers try to separate and assign the detected action potential to a specific cell. This step is called Spike Sorting [32].

However, many connectivity estimation algorithms require to use binned spike trains for improving their performance in terms of quality and speed. Selecting a bin size the spike train is divided into equal pieces of that size. For each bin, the spikes are added together in this time window. Basically there are two types of binning:

- Binary binning, in which the exact amount of spikes in a bin is irrelevant (see Figure 2.7.a)
- Multistage binning, in which the exact amount of spikes in a bin is relevant (see Figure 2.7.b)

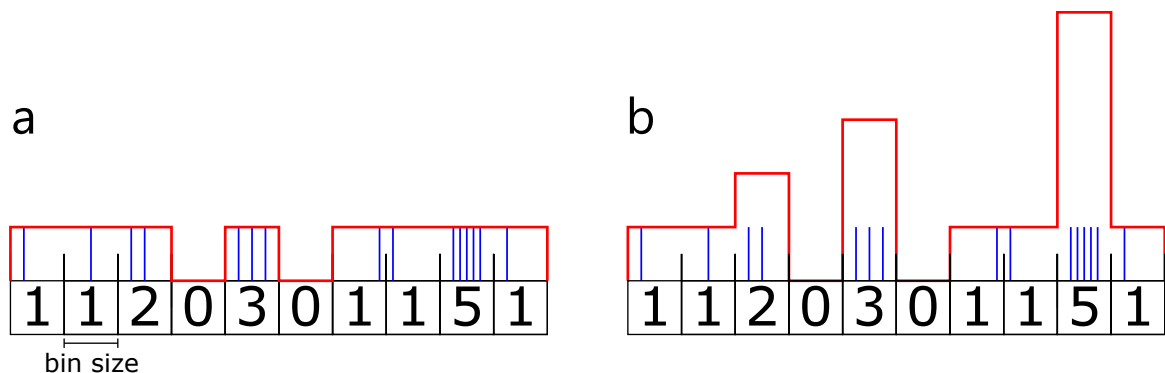


Figure 2.7. – Binning types: A spike train (blue-colored) is binned (red-colored) by select a bin size and sum up all underlying spikes (numbers in boxes). Binary binning (a) compromises sum values to binary states: One for each sum value bigger than zero else zero. The second, also widely used method is multi-stage binning (b), which directly uses the sum values for each bin.

In addition to the choice of a binning type, the choice of a bin size also influences the performance of an algorithm. Moreover, spike sorting algorithms are used to assign spikes to specific neurons. Since it is possible for an electrode to have contact with more than one cell, these algorithms try to discriminate between shapes of spikes in order to identify which spike is emitted by which neuron [33]. Especially for HDMEA chips, it can also be a problem if a neuron is recorded multiple times by adjacent electrodes.

3.

Simulation framework for evaluation applications

In contrast to real neuronal data (see Section 2.3), simulations are able to produce datasets with a known network connectivity. These datasets play a major role to quantify how accurate the results of connectivity estimation methods are. As biological neural networks - even *in vitro* - are far too complex (see Figure. 2.2) to reveal connections between single neurons, *in silico* neural networks with known topology are typically modelled. These simulated networks should be biophysically representative for a meaningful evaluation of neurocomputational algorithms, like connectivity estimation.

As the topology of an *in silico* network can affect the results and accuracy of algorithms [34], it is essential to evaluate these methods with realistic topologies. In the following, known *in silico* models are compared with respect to their applicability in large-scale simulations for biological neural networks. Implementations for different topologies are analysed in terms of biological plausibility. Based on these findings, an evaluation framework for the evaluation of connectivity estimation algorithms is developed. Parts of this section have already been published during the work on the project [35].

3.1. Selection of a neuron model

Like mentioned in Section 2.2 a neuronal network consists of somata (nodes) and axons, synapses and dendrites (connections). There are many types of neuron models with different strengths and weaknesses. We considered three well known types and rated them for the sensuous usage for testing connectivity algorithms. First, the Hodgkin–Huxley (HH) model takes experimentally measured ion channels and pumps into account but is too complex for large network simulations, due to its high number of needed differential equations [36] (see Appendix A for further information). Second, the Integrate-and-Fire (IF) model handles just essential functions of a neuron to be simulated in large quantities [37]. Since many observed processes are not captured by the IF model, it is too simplified for a meaningful evaluation (see Appendix B for further information). Several models, also HH and IF, were compared in computing complexity and biological plausibility by investigate their possible features [38]. The Izhikevich model is a simplification of the HH model by using two-differential equations. This model was chosen because of its good trade-off and its good reputation for biological simulations. In Appendix C further information can be found.

Izhikevich model

The Izhikevich model is especially designed for so-called large-scale simulations, which means up to tens of thousands of neurons. By combining the biological plausibility of HH model with the computational efficiency of IF model the Izhikevich model is able to reproduce spiking and bursting of cortical neurons in real time [39]. The operating principle is based on the variable v , which represents the membrane potential while u handles a slower recovery. For this reason u is also called recovery variable and takes the inactivation of sodium Na^+ and activation of potassium K^+

channels into account. Both variables obey the dynamics (3.1) and (3.2). Impacts driven by synaptic currents are realized with variable I .

$$\dot{v} = 0.04v^2 + 5v + 140 - u + I \quad (3.1)$$

$$\dot{u} = a \cdot (b \cdot v - u) \quad (3.2)$$

By reaching the threshold of $v \geq 30$ mV, the neuron emits an action potential and the auxiliary after-spike resetting is activated. In that case variables v and u are changed obeying the rule,

$$\text{if } v \geq 30 \text{ mV, then } \begin{cases} v = c \\ u = u + d. \end{cases} \quad (3.3)$$

Parameters adapt the model for different types of neurons. a is a time scale parameter for recovery variable u . Small values will lead to a slow recovery. For excitatory neurons 0.02 is chosen for a , while inhibitory ones use 0.1 normally. Thus, excitatory neurons recover faster than inhibitory cells. b describes the sensitivity of u to the subthreshold fluctuations of v . Great values of b will enable a strong coupling of v and u . This could end up in low-threshold spiking behaviour or subthreshold oscillations. A typical value for b is 0.2. c is the reset potential after each spike. Typically -65 mV is used for both, excitatory and inhibitory neurons. Finally parameter d describes the reset value of the recovery variable u after each spike. While inhibitory neurons use 2 for d , excitatory ones are enabled with 8 usually. Users of the Izhikevich model are able to select between several neuron types by configure the parameters a , b , c and d . The published combinations [39] are mentioned in Table 3.1.

Table 3.1. – Configuration of neuron types: Options of the Izhikevich model to define different types of neurons only by using parameter combinations. Three excitatory (exc.) and two inhibitory (inh.) types are provided as well as a thalamo-cortical type. Information by Izhikevich [39].

Neuron type		a	b	c	d
Exc.	Regular Spiking (RS)	0.02	0.20	-65	8.00
	Intrinsically Bursting (IB)	0.02	0.20	-55	4.00
	Chattering (CH)	0.02	0.20	-50	2.00
Inh.	Fast Spiking (FS)	0.10	0.20	-65	2.00
	Low-Threshold Spiking (LTS)	0.02	0.25	-65	2.00
	Thalamo-Cortical (TC)	0.02	0.25	-65	0.05

3.2. Modeling of networks

Besides defining neuron types by using parameter combinations (see Table 3.1), there are also synaptic properties to adjust for a neuronal network *in silico*. Therefore, two matrices will be introduced which handle the construction of networks: Synaptic Weight Matrix (SWM) and Delay Matrix (DM).

3.2.1. Synaptic Weight Matrix

Strengths of connections are stored in a square symmetric matrix with size N , which is the number of neurons. This parameterizable matrix is known as SWM. Each row represents targets of one neuron. The column index of the SWM then indicates source neurons of these targets. Thus, for

instance, element (4, 8) of the SWM stays for the synaptic weight of a connection from neuron 4 to neuron 8. Value ranges depends on the used model while the sign indicates types of connections and value 0 means no connection. Weights of the Izhikevich model are chosen for a maximum of 10 for excitatory and a minimum of -5 for inhibitory synapses. Adjusting the SWM we are able to design any topologies.

3.2.2. Delay Matrix

Structured like the SWM a second matrix stores durations for each signal transfer taken place. In a realistic picture long axons could lead to longer transmission time. Times are randomly distributed over a value range of 1 to 20 ms. Since reported, these range is realistic for monosynaptic delay times in mammalian cortex [40, 41]. By knowing DM and SWM it would be possible to reconstruct the network topology in an geometric formation: Connection existences depend on the SWM and their lengths depend on the DM.

3.3. Network types

All kinds of networks are able to manage certain goods in very different ways. Therefore, the topology depends on its application. For example, a motorway network is simpler constructed than the World Wide Web. In particular, sums of all incoming and outgoing connections of nodes can be very different. Such a sum is also called degree in graph theory. By investigating these degrees in the whole network and using a histogram, the so-called degree distribution is a common tool to characterize the network. Basically in network theory there are four subgroups of networks to distinguish. This section will briefly introduce these network types. For further information the book *Network Science* by Barabasi is recommended [42].

3.3.1. Regular networks

Regular networks are defined with a fixed number of connections for each node, which means a constant degree k for the whole network and a standard deviation for degree distribution of zero [17]. The connection probability is one for degree k and else zero,

$$P(deg = k) = 1. \quad (3.4)$$

Mostly, the regularity is ensured with connections between neighbours. Since such networks are not found in nature, uniform grid structure can only be artificially created for biological neuronal networks.

3.3.2. Random networks

A *random network* is constructed by using a constant connection probability following a Poisson distribution,

$$P(deg = k) = e^{-Np} \cdot \frac{(N \cdot p)^k}{k!}. \quad (3.5)$$

Nodes with significantly higher or lower numbers of connections are very rare, but unlike the *regular network*, they exist [43]. A clearly identifiable mean degree can be recognized for $N \cdot p$, where N is the number of neurons and p is the connection probability. All nodes are connected to the same number of other nodes on average, but there is a standard deviation. For the illustrated *random network* in Figure 3.1, mean degree would be around five, which is the maximum of degree distribution.

3.3.3. Small-world networks

The combination of *random* and *regular networks* is called *small-world network*. By slowly decreasing regularity of a *regular network* small-worlds will arise: Most nodes are connected in their own neighbourhood, but also some long range connections are existing [44]. In addition, the standard deviation of connection distribution increases and some outliers in form of high degree nodes emerge.

3.3.4. Scale-free networks

In *scale-free networks* some nodes, so-called hubs, have an immense number of connections to other nodes [43]. As some nodes are barely connected while hubs are able to have 100 times more connections, the *scale-free networks* could also be called ultrasmall-world networks: Some nodes are almost isolated of other groups [45]. *Scale-free* and also *small-world networks* find usage in many applications of nature like the brain. Furthermore, hub neurons were already detected in regions of the brain and characterised [46, 47]. In Figure 3.1 an exemplary *scale-free network* is illustrated with seven red marked hub neurons, resulting in a fundamentally different distribution of node degrees. This kind of log normal distribution can be described by a power law function with free parameter γ ,

$$P(deg = k) \propto k^{-\gamma}. \quad (3.6)$$

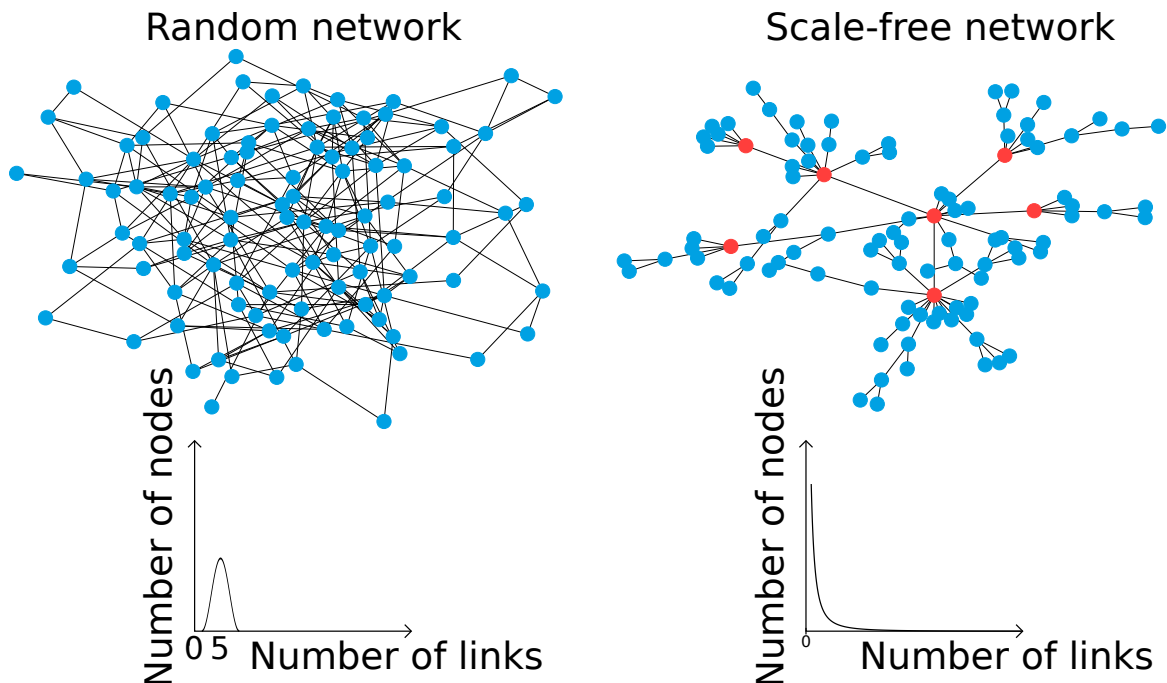


Figure 3.1. – Difference between *random* and *scale-free* neuronal networks: A *random network* is constructed by a constant connection probability. All neurons have approximately a same number of connections. The distribution of node linkages for *random networks* is bell shaped. The most neurons for the illustrated *random network* would be connected with about five synapses, which is the number of links at the maximum of degree distribution. A *scale-free network* is constructed by special methods [48]. Hub neurons are red marked and have an immense number of connections to average. The distribution of node degrees is formed like a power law function. Thus, there are many nodes which are sparsely connected while some hubs are able to have lots of links.

3.4. Neuronal network simulations

Simulated networks will contain 1000 neurons (like the original model [39]), which will be connected randomly for specific network types. Thus, each simulation will deliver different datasets. As software *MATLAB* of MathWorks is chosen because of its modifiability (for details see Appendix D). Since MEA chips usually do not measure signals from each neuron only a randomly chosen subset of 100 neurons is recorded (see Figure 3.2). For all subsets the ratio of excitatory to inhibitory neurons is just like for the whole network chosen to be 4 to 1. In these networks model, parameters for RS ($a = 0.02; b = 0.2; c = -65; d = 8$) are selected for excitatory neurons and FS ($a = 0.1; b = 0.2; c = -65; d = 2$) for inhibitory respectively (see Table 3.1). While excitatory synapses contribute to the membrane potential of the receiving neuron, inhibitory ones counteract.

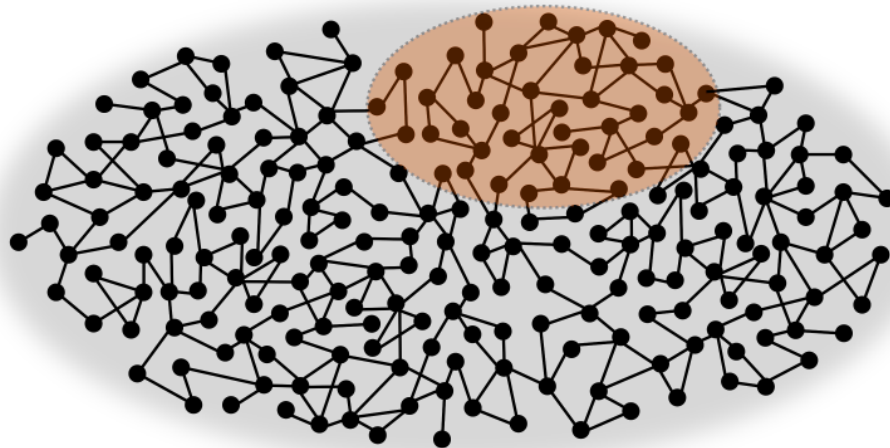


Figure 3.2. – Neuronal network *in silico*: 1000 Izhikevich neurons will be simulated and a subset (orange marked) is randomly chosen. It contains 80 excitatory and 20 inhibitory neurons.

As reported in [41], synaptic transmission times of 1 to 20 ms are realistic in mammalian cortex. However, the original Izhikevich model simulation of [39] uses uniform delay times of 1 ms for all connections. To increase the biological plausibility, here implemented simulations are based on the code by Izhikevich in 2006 [49], which is an advanced version with plasticity obeying the Hebbian theory and axonal conduction delays. The ability of plasticity is called Spike-Timing Dependent Plasticity (STDP), where synchrony dramatically decreases after seconds and realistic network bursts do not appear any more (see Figure 3.3). In this approach a static topology is more desirable. Therefore STDP is not used, but transmission times randomly distributed with values between 1 and 20 ms.

For comparison of possible network topologies, their characteristics are described in Table 3.2. The *regular network* was not used for simulation because of its unrealistic construction in nature. The Standard Implementation of Izhikevich (SII) [49] for *random networks* was constructed with randomly chosen 100 of outgoing synapses for each neuron, where no inhibitory-to-inhibitory connections are allowed. In this way, for a network of 1000 neurons, the resulting connection probability of outgoing synapses is set to $\frac{100}{1000} = 0.1$ without standard deviation. For incoming synapses, the probability is also 0.1 with standard deviation. Furthermore, a second *random network* will be evaluated in form of an implemented Erdos–Renyi (ER) network topology [50] with a connection probability of 0.1, following a Poisson distribution for input- and output-degrees. Another difference to the SII *random network* is the possibility of connections between inhibitory neurons. Thus, both *random networks* have a theoretical mean degree of 200 synapses: 100 inputs and 100 outputs.

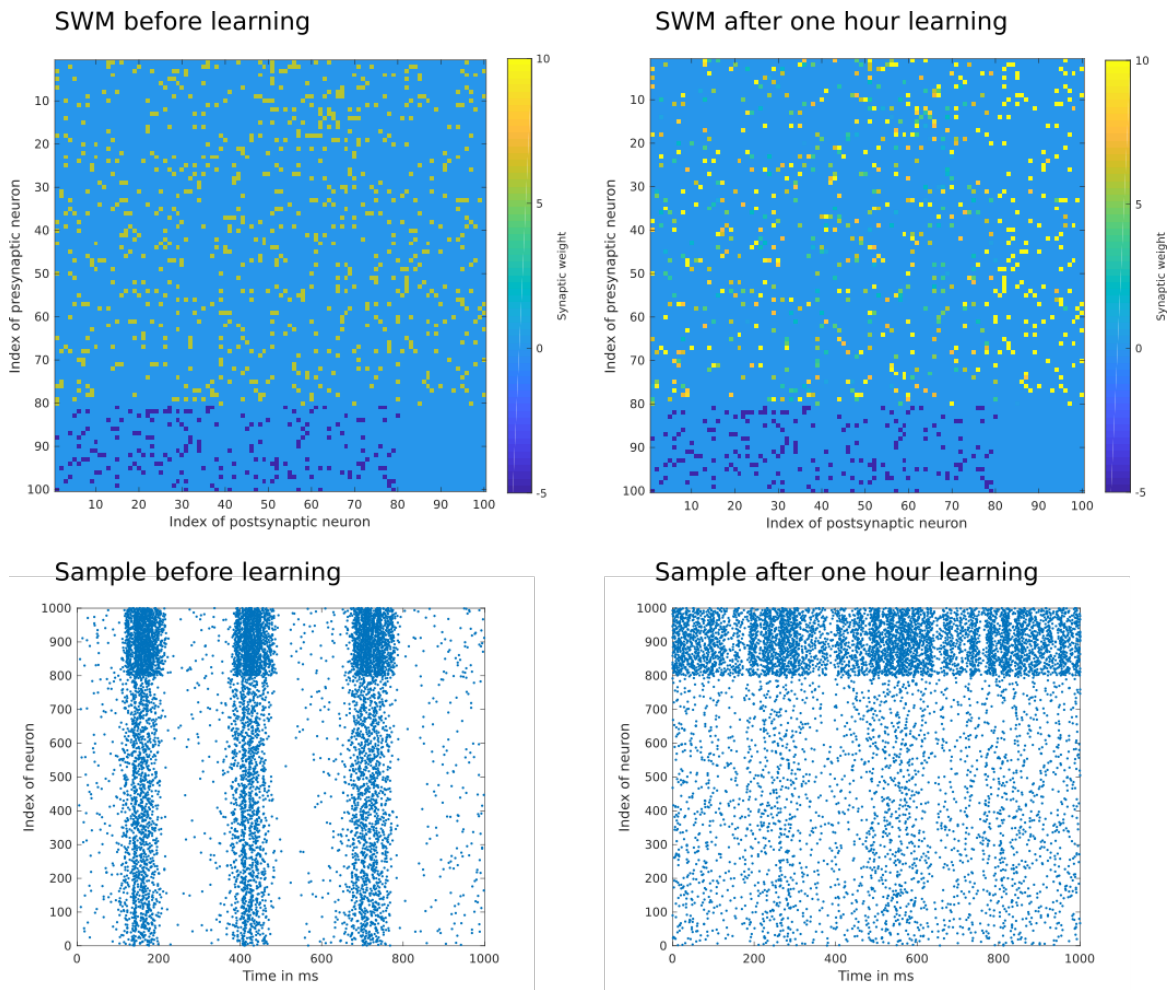


Figure 3.3. – Effects of STDP: At the beginning all excitatory synapses have a weight of 6 and all inhibitory ones -5. After one hour learning with STDP (only allowed for excitatory connections) some excitatory synapses expand to their maximum of 10 while others shrink to nearly 0. For the purposes of illustration both SWMs only show a subset for 100 neurons (representatively 80 excitatory and 20 inhibitory neurons). These changes of the SWM have a massive impact on spike trains, which can be seen in both samples. Before learning there is a much higher synchrony.

Table 3.2. – Summery of network type characteristics:

Different network types are characterized by the existence of hubs, the distribution of input- and output-degree.

	In-degrees	Out-degrees	Hubs
<i>Regular network</i>	constant	constant	no
<i>SII random network</i> [49]	Poisson	constant	very unlikely
<i>ER random network</i> [50]	Poisson	Poisson	unlikely
<i>IC scale-free network</i> [48]	power-law	power-law	yes
<i>BA scale-free network</i> [43]	power-law	power-law	yes

Moreover, two ways of *scale-free* construction are investigated. First, the Implementation of Catanzaro (IC) [48] for uncorrelated random *scale-free networks* uses a connection probability function in form of formula (3.6). The parameters applied are a minimum degree of 10 and $\gamma = 2.0$. Second, the Barabasi–Albert (BA) [43] network, which is also a form of *scale-free network*, with 24 connections, 12 input- and 12 output-synapses, per each growing step were constructed. Thus, the minimum degree of BA networks is 24. Inhibitory to inhibitory connections are permitted for both *scale-free network* types.

For all networks, self-connections and parallel synapses are prohibited, while antiparallel synapses are allowed. Binary masks for respective SWMs were constructed by modified implementations of the *Python* complex network package *NetworkX* [51]. SWMs were filled up with log-normal distributed synaptic weights with a maximum of 10. The mean synaptic weight is chosen for each simulation in such a way that network bursts appear. It was found that a higher density of connections required a lower average synaptic weight for regular network bursts.

3.5. Results and discussion of simulation

Samples of the simulated spike train data are shown in Figure 3.4. Network bursts were ensured for all simulations with manual regulation of synaptic weights. In this way, all samples of the explored network types show similar patterns, even if the spiking density varies in network bursts.

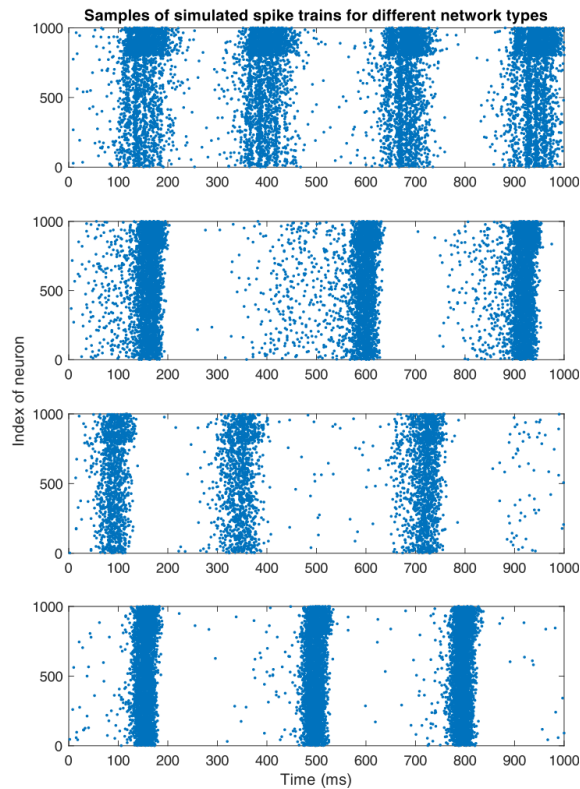


Figure 3.4. – Samples of simulated spike trains:

Each dot represents an emitted action potential of the neuron with index of respective y-coordinate. The networks with overall 1000 neurons each produced three or four network bursts in the shown second of simulation. The samples are sorted for network types from top to bottom: SII *random network*, ER *random network*, IC *scale-free network* and BA network.

The resulting distributions for input-, output- and total-degree (sum of input- and output-degree), separated into excitatory and inhibitory neurons, are analysed. Furthermore, respective Mean Firing Rates (MFRs) are measured by counting all spikes of neuron i , whose history is called spike train $S_i(t)$, and dividing the number by the considered time range,

$$MFR_i = \frac{\sum_{t=t_{start}}^{t_{end}} S_i(t)}{t_{end} - t_{start}}. \quad (3.7)$$

Due to the constant output-degrees of 100 for SII *random networks*, the difference between its normal distributions of total-degree and input-degree is an offset by 100. Since every fifth neuron is an inhibitory neuron and inhibitory-to-inhibitory connections are not allowed for SII, the offset between input-degrees of both neuron types is theoretically $\frac{100}{5} = 20$, which is same for the total-degrees. The theoretical assumption can be confirmed by the results, see Figure 3.5, as the mean values of the total degree distributions differ by about 22. It is also the reason for a separation of normal distributed MFRs for both neuron types. The inhibitory effects lead to inhibited MFRs of excitatory neurons, while MFRs of inhibitory neurons are not inhibited. Knowing the effects, in the upper plot of Figure 3.4 the inhibitory neurons can be identified easily at indexes 801 to 1000.

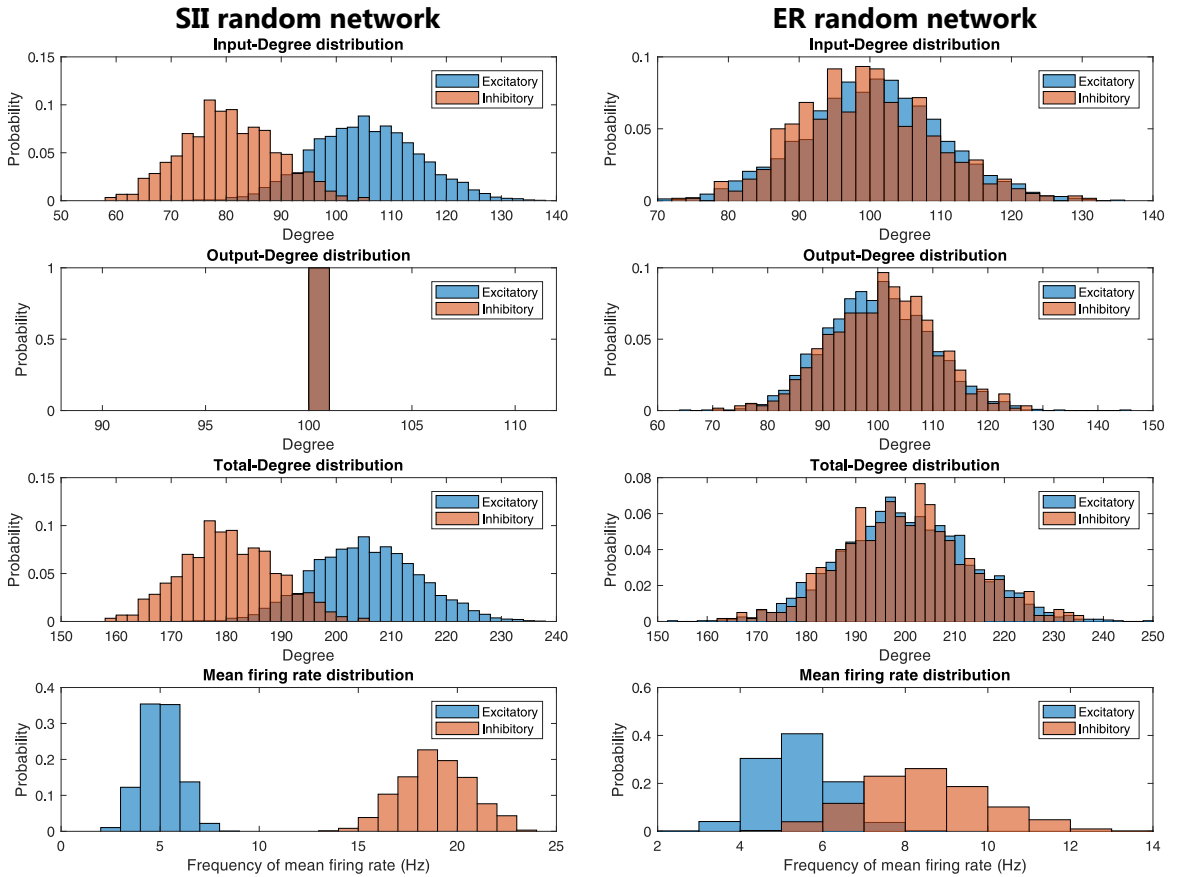


Figure 3.5. – Analysis of SII and ER *random network*:

A lower mean degree of inhibitory neurons is the result of prohibited inhibitory-to-inhibitory connections. The inhibitory effects lead to lower MFRs of excitatory neurons, while inhibitory neurons will not be inhibited. In contrast to SII *random network*, the distribution of MFRs for both neuron types of ER *random network* have a super-imposed area.

The ER model reduces this separation with a non-constant output-degree and the permission for inhibitory-to-inhibitory connections (see Figure 3.5). Its normal distributions of input-degree and output-degree are similar to each other with a mean value of 100. In this way the normal distribution of total-degrees has a $\sqrt{2}$ higher standard deviation. Despite superimposed area for MFRs of both neuron types, the distribution of MFRs of inhibitory neurons still has a higher mean value with higher standard deviation.

Both *scale-free* implementations lead to intersections of inhibitory and excitatory MFRs. For the IC networks, log normal distributions of input- and output-degree are similar with a maximal probability at low degrees and outliers can be found at up to 400 connections (see Figure 3.6). Thus, total-degrees are also log-normal distributed. Resulting MFR distributions of excitatory and inhibitory neurons are similar and can be fitted by a power law function. For the BA networks, log normal distributions of input-, output- and total-degree are almost identical for inhibitory and excitatory neurons. The minimum input- and output-degrees are added up to minimum total-degrees. The BA network leads to a larger deviation in the distribution of inhibitory MFRs than that of excitatory MFRs (see Figure 3.6). Respective outliers can be identified at up to 300 inputs or outputs. The total-degree for hub neurons are up to 600. Even with a big superimposed area, the log normal distribution of MFRs for inhibitory neurons has a higher standard deviation than the one for excitatory neurons.

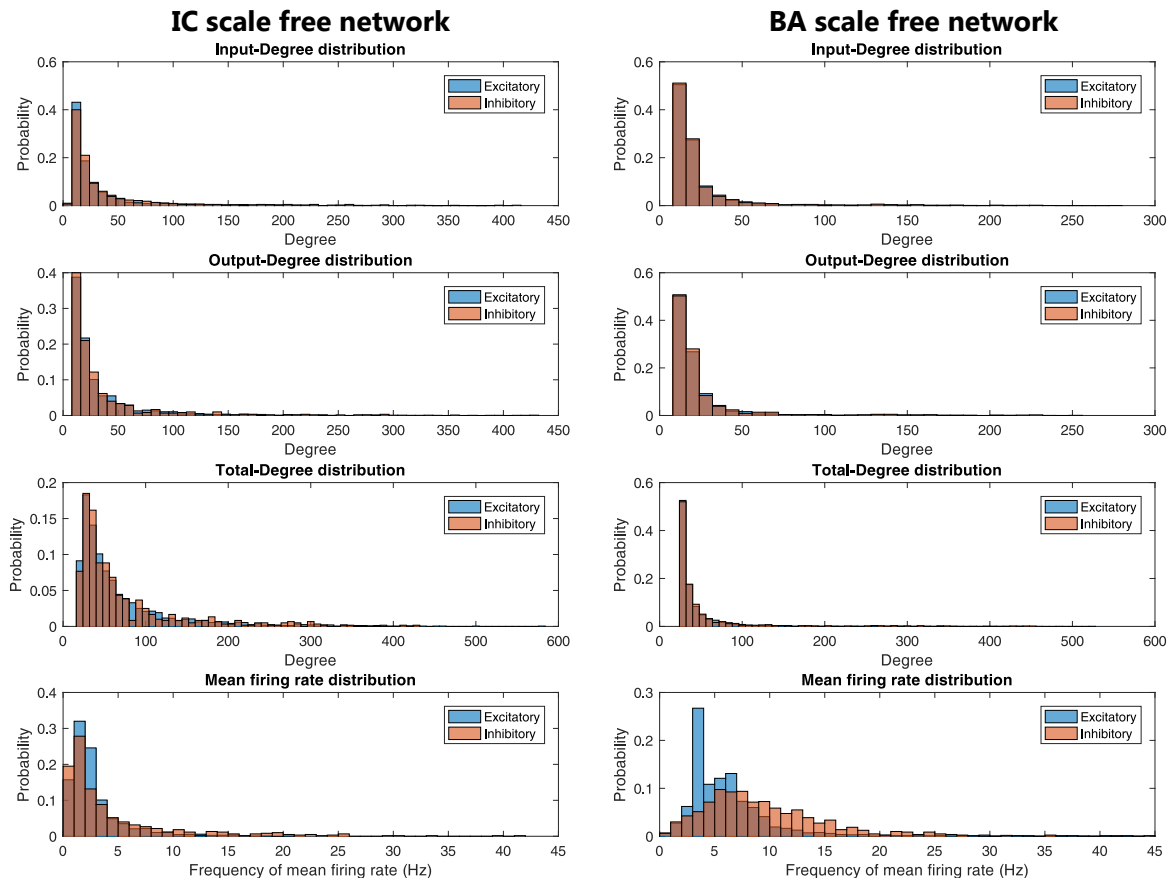


Figure 3.6. – Analysis of generated IC and BA *scale-free* network:

Resulting MFR distributions of excitatory and inhibitory neurons are similar and can be fitted by a power law function. For BA *scale-free* networks, log normal distributed MFRs have different standard deviations for both neuron types.

Summarizing, the distribution of MFRs can be immensely influenced by modelling different network topologies. Since a log normal distribution for intracortical spontaneous MFRs was already demonstrated [52], many neurons fire far above network average in biological *in vitro* cultures. One can conclude that more realistic MFRs can be measured by using *scale-free* topologies for large scale neural network simulations.

3.6. Conclusion of simulation

For a meaningful evaluation of neurocomputational algorithms analysing large neuro datasets, *in silico* neural networks shall be employed with good biological relevance. However, the complexity and topology of commonly used *in silico* neural networks and thus the evaluation results can vary. The result is indeed that the implemented neural network topology immensely influences the distribution of the MFRs and thus the meaningfulness of evaluation results. Whereas SII topologies are used in many evaluations, e.g. without delay times [53], with delay times, and with different use of STDP [54, 55], more realistic *scale-free* topologies are rarely used for connectivity estimation evaluations [34]. One can conclude that searching for the best algorithms can be confusing, since apparently better results are not synonymous with physiologic relevance for real biological neural networks.

For future evaluations, a standardised method improves an effective research of neurocomputational algorithms. Widely used and uniform benchmarking also makes it easier to compare newly developed methods with previous methods. Moreover, the further development and improvement of intergroup research is possible in a simpler way. To ensure topology independent algorithms, a multiple model evaluation is used. Usage of at least one *scale-free network* implementation is necessary for good, sufficient biological plausibility. Furthermore, to strengthen the significance repeated simulations are required. Since electrophysiological recording methods do not measure all signals of a neuronal culture, it is recommended to use spike train data of a small subset, e.g. 100 spike trains of a simulated network with 1000 neurons.

4.

Methods of connectivity estimation

The goal of effective and functional connectivity estimation algorithms is gaining knowledge about the SWM. Thus, the result of these methods is also a matrix of same size, a so-called Connectivity Matrix (CM). The definition of CM is very similar to SWM: While SWM stores real synaptic weights the CM is filled up with estimated values, which describe connection strengths. Since CMs are just results of algorithms, their value ranges strongly depend on the used method:

- Functional connectivity estimation algorithms do not indicate connection types and causality. However, some algorithms are able to extract a few characteristics of effective connectivity.
- Effective connectivity estimation algorithms indicate connection types (e.g. inhibitory synapses with negative and excitatory ones with positive values) and causality.

Because value ranges of CM also strongly depend on the measured signal, there is no information to know what connection strength corresponds to a real synapse. Since values of CM should ideally be proportional to real synaptic weights of SWM, the need of a threshold selection is given to distinguish between a true connection and just statistical correlation. The result of this step is then called Thresholded Connectivity Matrix (TCM). The general workflow is illustrated in Figure 4.1.

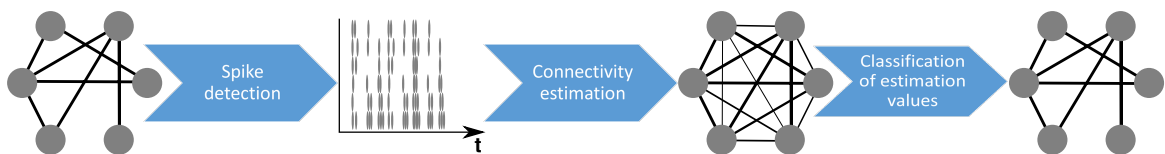


Figure 4.1. – Workflow of connectivity estimation: Signals of a considered neuronal network (left side) are measured. After applying a spike detection algorithm spike trains are obtained. The result of connectivity estimation algorithms is the CM, which describes a graph with values for each possible connection. A classification of these estimation values leads to a TCM, which describes the final graph (right side). Ideally this graph should be identical to the considered neuronal network.

To estimate the functional or effective connectivity different methods based on information theory [53, 56], pattern recognition [57, 58], model fitting [59–61] or data mining [62] have been developed and applied. The quality of the results is strongly dependent on datasets gained from *in vivo* or *in vitro* neuronal networks.

Some methods are not developed for large and complex networks, for example estimating the connectivity by modeling *in silico* neuronal networks [59–61] or by using data mining methods [62]. Another method is Partial Correlation, which is able to distinguish between direct and indirect connections by considering linear contributions. Partial Correlation estimates connectivity precisely for *in silico* with a small amount of neurons, e.g. 130 neurons [34]. However, Partial Correlation is inaccurate for large scale network models [63] because of the complex amount of possibilities for considered indirect contributions. Therefore, in this work we focus on a scenario measuring signals of a small subset of a large scale neuronal network, which is more realistic for most *in vitro* and *in vivo* applications.

As the number of electrodes in electrophysiological recordings have increased up to several thousands accompanied with huge datasets, used algorithms for connectivity analysis have to be highly computationally effective.

All chosen algorithms investigate pairwise a source spike train X for effects on a target spike train Y . Thus, statements about causality are possible, which is a characteristic of effective connectivity. Furthermore, only algorithms with a higher potential of good performances are considered. For example, Granger Causality [64] was often used to estimate connectivity [65–67] and is available as *MATLAB* based toolbox [68]. Since Granger Causality is insensitive to nonlinear correlations [69], more promising methods were chosen, which will be introduced in the following.

4.1. Cross Correlation

Cross Correlation (CC) is similar to normal convolution and a classic tool to recognize a pattern. In 1967 CC was already used to measure relations between spike trains [57]. By multiplication of a time-shifted signal $x(i - d)$ element-wise with another non-shifted signal $y(i)$, similarity can be recognized as a function of time shift d . Ideally, the greatest similarity should be at the delay, where the result of CC has its largest peak staying for the greatest correlation. The essential idea of CC can be expressed as

$$CC_{XY}(d) = \sum_{i=-\infty}^{\infty} y(i) \cdot x(i - d). \quad (4.1)$$

Since the binary spike trains X and Y only add up values in formula (4.1) and MFR of a spike train can vary, this form has problems with its value range. Thus, to solve this problem and enable comparability between results normalizations are used. This means a variable division of formula (4.1) depending on X and Y . Using different types of normalization can strongly influence results. While some implementations have trouble detecting inhibitory connections [58], other methods of CC are even able to distinguish between inhibitory (negative peak of CC) and excitatory (positive peak of CC) connections [70].

4.1.1. Normalized Cross Correlation Histogram

The most common method is Normalized Cross Correlation Histogram (NCCH), which normalizes results with the geometric mean of total spiking times n_x and n_y of both spike trains [17, 55, 71–77],

$$NCCH_{XY}(d) = \frac{1}{\sqrt{n_x \cdot n_y}} \sum_{i=-\infty}^{\infty} y(i) \cdot x(i - d) \quad (4.2)$$

4.1.2. Normalized Cross Correlation

Another method of normalization is the usage of Standard Deviations (SDs) $\sigma_x \cdot \sigma_y$ and the recording length N stated in bins. In addition, subtracting the mean values \bar{x} and \bar{y} of the respective spike trains before multiplying them is recommended for binary binned spike trains. The mean of all results should now be zero and inhibitory correlations will lead to negative peaks while excitatory connections produce positive peaks [78] (see Figure 4.2). The so defined type of CC is called Normalized Cross Correlation (NCC) in the following,

$$NCC_{XY}(d) = \frac{1}{N} \sum_{i=-\infty}^{\infty} \frac{(y(i) - \bar{y}) \cdot (x(i - d) - \bar{x})}{\sigma_x \cdot \sigma_y}. \quad (4.3)$$

For sparse spike trains NCC and NCCH lead to similar results. However, the performance of NCC increases with increasing spike train length [55]. Thus, here only NCC is used for evaluation. Since the resulting matrix for the pairwise comparison of all combinations of spike trains is symmetric (see

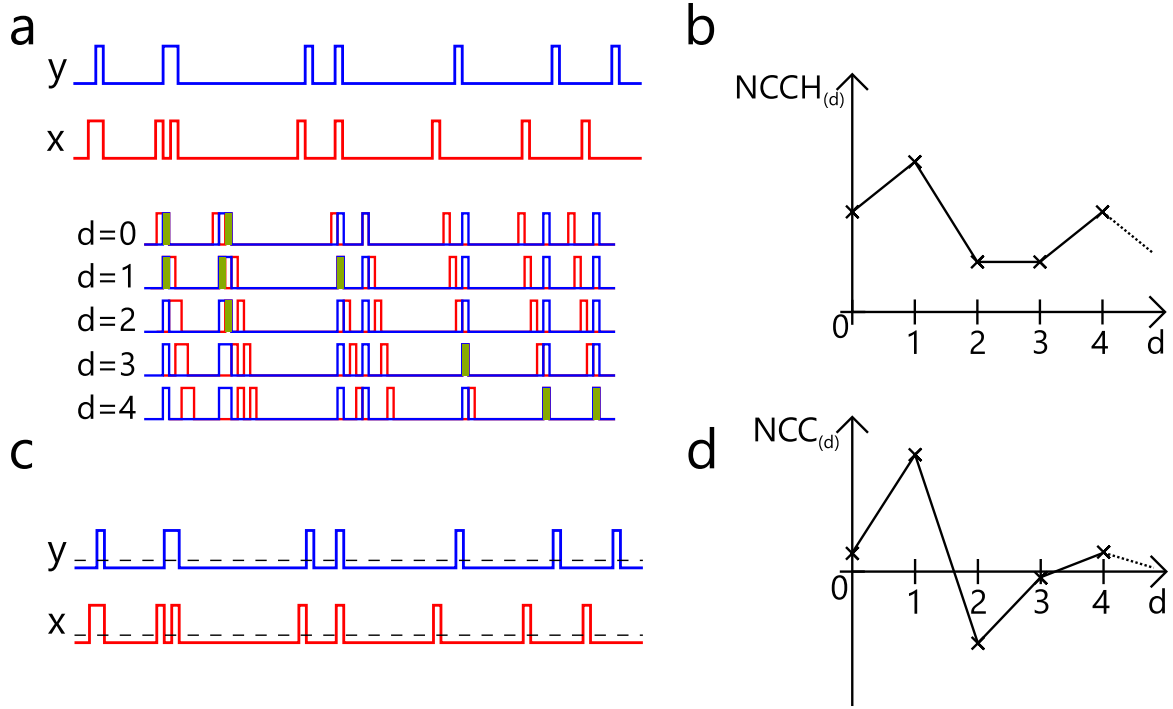


Figure 4.2. – Cross Correlation: (a) Two spike trains are illustrated. The blue spike train y is target while the red one x is source spike train of the investigated connection $X \rightarrow Y$. The binary spike trains are shifted for delay times d in range of 0 to 4. The green spots are summed up for their respective delay time. (b) After normalization the NCCH is obtained. The peak at delay $d = 1$ would be the maximal correlation. By subtracting the mean values of respective spike trains the mean of them is zero. (c) The changed spike trains for NCC are illustrated. The dashed lines indicate their zero levels. Thus, in a sparse spike train most values are slightly negative. (d) The normalization of NCC leads to a different result. The total mean of this function should be zero, where negative values indicates an inhibitory effect. Finding the maximum of absolute values would support the assumption of an excitatory connection of $X \rightarrow Y$ at $d = 1$.

formula (4.4)), the number of independent calculations for NCCs is $\frac{K^2 - K}{2}$, where K is the number of spike trains.

$$NCC_{XY}(d) = NCC_{YX}(-d) \quad (4.4)$$

Coincidence Index

A delay-dependent function $M(d)$ is normally analysed by looking for its peak value, like $NCC_{XY}(d)$ for example. In order to further improve the results of an analysis qualitatively, a widely used tool is introduced: The Coincidence Index (CI) [55, 79–81],

$$CI = \frac{\sum_{d=d_p - \frac{\tau}{2}}^{d_p + \frac{\tau}{2}} M(d)}{\sum_{d=d_{\min}}^{d_{\max}} M(d)}. \quad (4.5)$$

The CI algorithm integrates values in a range of τ around the maximum peak value and normalizes that integral (see Figure 4.3 for an illustration of its function). In this context, for $M(d)$ $NCC_{XY}(d)$ was chosen, which improves the results. For reasons of overview, suffix $-CI$ will indicate the use of CI, e.g. Normalized Cross Correlation Coincidence Index (NCCCI) for the CI of NCC.

However, CI normally handles only positive values, which is the reason to use the absolute values of NCC for NCCCI. The maximum correlation would now correspond to a value of one. An improvement of performance achieved with this modification was reported in an evaluation of connectivity estimation algorithms [55].

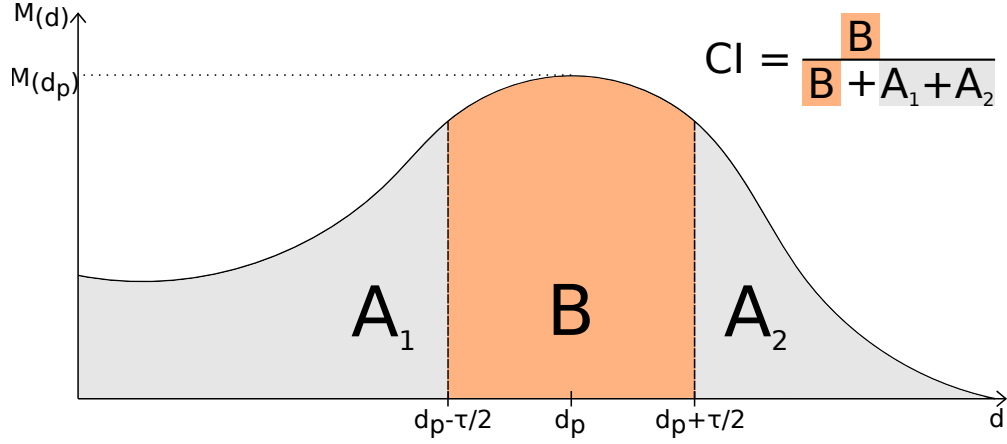


Figure 4.3. – Principle of Coincidence Index: A delay-dependent function $M(d)$ (e.g. $NCC_{XY}(d)$ or also $NCC_{XY}(d)$) has a peak value $M(d_p)$. The integral B between $d_p - \frac{\tau}{2}$ and $d_p + \frac{\tau}{2}$ (orange area) will be divided by the total area under curve (orange plus grey areas). The result value is called CI. An equation illustrates this function by using colors for respective integral values A_1 , A_2 and B.

4.2. Transfer Entropy

Information theory provides many tools for potentially estimate connectivity. One of the simplest tools is Mutual Information (MI), which measures statistical dependency of two random processes, e.g. spike trains (further information can be found in Appendix E). By upgrading MI with a third process under investigation the so-called Transfer Entropy (TE) is introduced. Since this universal tool can be implemented and used in different ways, some relevant implementations are explained in this section beginning with its most common one.

4.2.1. Delay One Transfer Entropy

The source spike train is just like the target spike train one of the three observed processes for the TE. The third process is chosen as the future bin of the target spike train. Therefore, spike trains are usually delayed by one bin,

$$TE_{X \rightarrow Y} = \sum_{x_i \in X} \sum_{y_i \in Y} \sum_{y_{i+1} \in Y} p(y_{i+1}, y_i, x_i) \cdot \log_2 \frac{p(y_{i+1} | y_i, x_i)}{p(y_{i+1} | y_i)}. \quad (4.6)$$

This form of TE is called Delay One Transfer Entropy (D1TE) and known as the original definition [82]. In Figure 4.4 the original TE and its considered bins are illustrated. TE measures information flow by testing all possible patterns for any kind of dependency. Therefore, for each process there is a sum used in formula (4.6) running through all combinations (e.g. for binary spike trains only spiking or non-spiking). If a combination occurs significantly more frequently than others, the information flow increases. For instance, the binary pattern $x_i = 1, y_i = 0, y_{i+1} = 1$ means all cases where neuron X emitted at least one spike and neuron Y did not, which then led to spiking of Y in the

next time bin. So discovered statistical dependency would support the assumption of an excitatory synapse $X \rightarrow Y$, because of its change from non-spiking to spiking.

The required probabilities in formula (4.6) are normally calculated by counting the number of occurred patterns and divide it by the maximal possible number of existences. Thus, $p(y_{i+1}, y_i, x_i)$ is just the likelihood of occurrence for a given pattern $y_{i+1}y_ix_i$. TE makes also use of conditional probabilities, which are probabilities of occurrence for a pattern whenever a special condition is giving. For example, observing for a pattern $x_i = 1$ and $y_i = 1$, $p(x_i|y_i)$ is the likelihood of occurrence of $x_i = 1$ whenever $y_i = 1$ is given. This can be calculated by using the probability that $x_i = 1$ and $y_i = 1$ occur together, divided by the likelihood of an occurring $y_i = 1$,

$$p(x_i|y_i) = \frac{p(x_i, y_i)}{p(y_i)}. \quad (4.7)$$

It is a similar calculation for the conditional probability of three processes. Taking this third process in account is the only variation,

$$p(x_i|y_i, z_i) = \frac{p(x_i, y_i, z_i)}{p(y_i, z_i)}. \quad (4.8)$$

Like MI also TE is able to detect linear and nonlinear correlations [53, 56]. The advantage of TE taking own history into account is tremendous for neuronal data because of refractory periods after spiking and causality statements [55]. The formula (4.6) of D1TE takes for signals with base n (e.g. binary spike trains have the base two) n^3 independent calculations. Thus, by increasing the base of spike train data from binary to a higher base n computing time will increase exponential just like the number of patterns. Using logarithms with base two leads to bits as result unit in the CM. Higher values indicate a stronger information flow from source to target neuron.

D1TE was often able to show good results for *in silico* evaluations [53, 63, 74]. Unfortunately, these models did not take variable delay times of axonal conductions into account, which is reason for an easy but unrealistic selection of optimal bin sizes (e.g. in their studies 1 ms). In contrast, for an *in silico* evaluation with variable delay times by [55] the best performance of D1TE was reached with a bin size of approximately 15 ms. Thus, in reality, it is a problematic issue to choose, rather guess a good value because it depends on each pair of spike trains.

4.2.2. Higher Order Transfer Entropy

Normally TE is used with an order of one bin for both spike trains [53, 63, 74, 83]. However, D1TE can be extended to an Higher Order Transfer Entropy (HOTE) by increasing its temporal range [84]. [55] studied different combinations from one bin variable up to five bins to improve its performance. To understand the modification it is recommended to study Figure 4.4 combined with formula (4.9).

$$HOTE_{X \rightarrow Y} = \sum_{x_i^{(l)} \in X} \sum_{y_i^{(k)} \in Y} \sum_{y_{i+1} \in Y} p(y_{i+1}, y_i^{(k)}, x_i^{(l)}) \cdot \log_2 \frac{p(y_{i+1}|y_i^{(k)}, x_i^{(l)})}{p(y_{i+1}|y_i^{(k)})} \quad (4.9)$$

Parameters k and l are the orders of history bins of target and source spike train taken into account. For $k = 1$ and $l = 1$ HOTE would be equal to D1TE. The number of patterns is 2^{1+k+l} and rises with the chosen order exponentially. Thus, HOTE can be computationally intensive compared with D1TE which can be uncomfortable in context with an increasing amount of recorded neurons.

4.2.3. Delayed Higher Order Transfer Entropy

Besides HOTE another modification of TE was introduced to neuroscience [55], which was already used in other fields of research [85]. By shifting the source spike train with a delay d in the past,

it is possible to consider effects in a variable time window. This shifting process is similar to CC. Therefore, the formula of HOTE (4.9) is further extended to

$$DHOTE_{X \rightarrow Y(d)} = \sum_{x_i^{(l)} \in X} \sum_{y_i^{(k)} \in Y} \sum_{y_{i+1} \in Y} p(y_{i+1}, y_i^{(k)}, x_{i+1-d}^{(l)}) \cdot \log_2 \frac{p(y_{i+1} | y_i^{(k)}, x_{i+1-d}^{(l)})}{p(y_{i+1} | y_i^{(k)})}. \quad (4.10)$$

In Figure 4.4 Delayed Transfer Entropy (DTE) for $d = 3$ and Delayed Higher Order Transfer Entropy (DHOTE) for $d = 2$ are exemplary comparable with their normal forms TE and HOTE. DHOTE with $d = 1$ is equal to the normal HOTE. For varied delay times (e.g. 1 to 25 ms in 1 ms steps) DHOTE can now be calculated. Investigating of so stored result values enable locating a maximum of flown information. This single peak value is then taken for the resulting CM value of the examined connection $X \rightarrow Y$.

Thus, in contrast to normal TE or HOTE, the information flow is observed for variable impact times. Since it is no longer necessary to guess a good bin size in order to take into account as many influences as possible, the selection of a small bin size in combination of a wide shifting range should always be able to process all relevant effects. Nevertheless, selecting the smallest possible bin size, which would be limited by the sampling frequency, leads to a longer computing time because of the increasing signal length for probability calculations.

However, besides the increased computing time of DHOTE, there is another disadvantage of small bin sizes, which is even able to affect the quality of results negatively. This is due to the information flow function of delay times getting sensitive for outliers. Selecting always just the peak could be misleading. Therefore, the CI is turned into account, which can be used for all delay-dependent functions like explained. Since the results of DTE and DHOTE are such functions, Delayed Transfer Entropy Coincidence Index (DTECI) and Delayed Higher Order Transfer Entropy Coincidence Index (DHOTECI) are introduced.

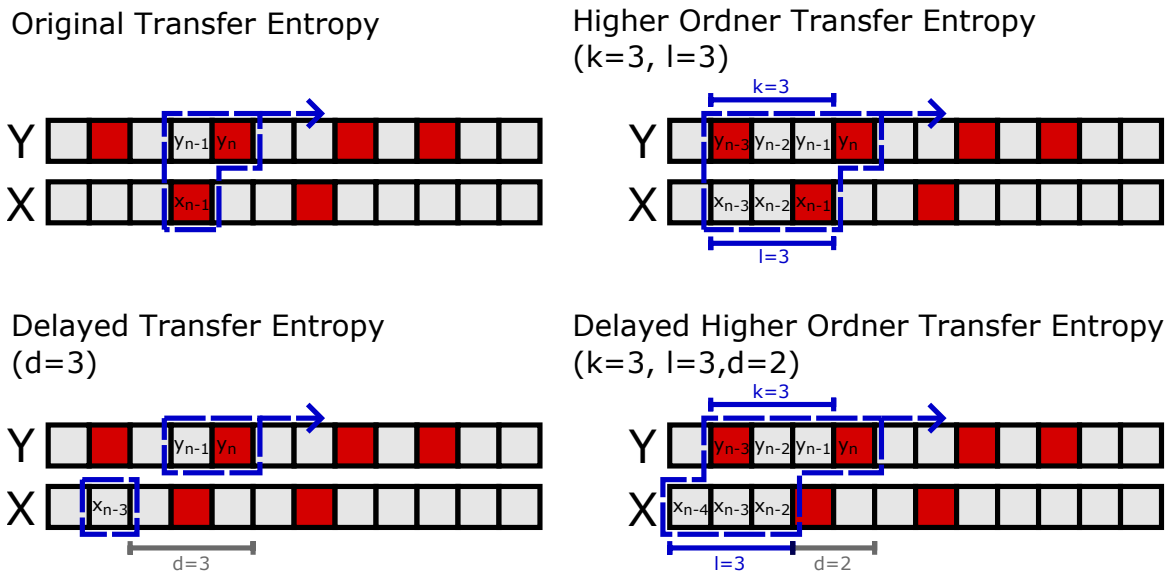


Figure 4.4. – Principle of Delayed Transfer Entropy: Two binary binned spike trains Y and X are illustrated. Red bins mean spiking while gray bins mean no spiking. The patterns (dashed blue lines) for TE are shifted over the whole spike trains. These patterns can have many forms like shown for four cases: Normal D1TE, HOTE, DTE and DHOTE. By calculating TE for shifted spike trains of X with different delays d a function of d can be created. Its peak is the maximum of information transfer. Figure inspired by [55].

4.2.4. Combined Higher Order Transfer Entropy

By combining the results of connectivity estimation algorithms, it is possible to get a different accuracy. Based on the idea of establishing the significance of DHOTE [86], an approach of Combined Delayed Higher Order Transfer Entropy (CDHOTE) is implemented by plotting DHOTECI values against DHOTE values (see Figure 4.5). In this plot the value pair M ($\max(\text{DHOTE})$; $\max(\text{DHOTECI})$) is assumed as the place with highest possibility for a connection. The two dimensional euclidean distances between two points P and Q can be calculated by

$$d(P, Q) = \sqrt{(P_1 - Q_1)^2 + (P_2 - Q_2)^2}. \quad (4.11)$$

Calculating the euclidean distance from the point of interest M to each value pair V with coordinates (DHOTE; DHOTECI), a new CM can be formed. Low values of formula (4.12) (distances to M) are more likely to indicate connections and the threshold is the Euclidean distance starting from 0.

$$CDHOTE_{X \rightarrow Y} = d(V_{X \rightarrow Y}, M) \quad (4.12)$$

In this way the nearest result pair to M is the most likely connection and points near to (0;0) are very unlikely.

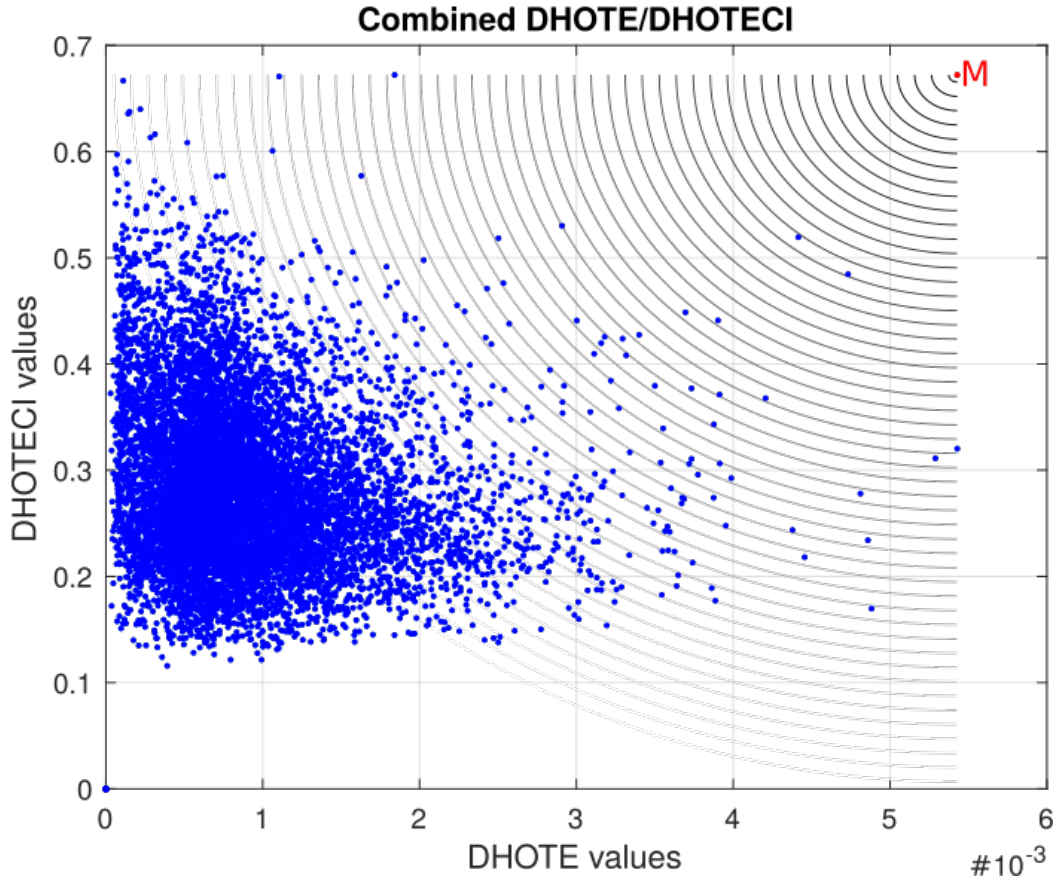


Figure 4.5. – Principle of CDHOTE: The DHOTECI values are plotted against DHOTE values. Each blue dot is a result pair. The coordinates of the red point M are ($\max(\text{DHOTE})$; $\max(\text{DHOTECI})$), whereas euclidean distance from M is indicated as gray quarter circles. The radius can be seen as threshold, which leads to encircled result pairs identified as connections. The nearest result pair to M is the most likely connection.

4.3. Total Spiking Probability Edges

A novel effective connectivity estimation method, called Total Spiking Probability Edges (TSPE) [87], is based on the following assumptions:

- If the spike rate of a neuron increases after it has received an input signal, the connection is considered excitatory. Due to refractory times of the receiving neuron, the spike rate drops again after the excitatory input signal. The resulting cross-correlogram of emitting and receiving spike train shows a maximum (excitatory input) followed by low values (refractory time).
- If the spike rate of a neuron decreases after receiving an incoming action potential, the connection is considered inhibitory. The resulting cross-correlogram of emitting and receiving spike train shows a minimum (inhibitory input) surrounded by high values (activity before and after the inhibitory input). In this way inhibitory stimulation can only be identified if the receiving neuron is active before the stimulation.

In order to capture these local maximum and minimum of the cross-correlogram, an edge filter is applied to the cross-correlogram. More precisely, the cross-correlation between spike train X and spike train Y (see Figure 4.6.(c)) is calculated (see NCC in the attachment) to obtain the cross-correlogram $NCC_{XY}(d)$, where d is the temporal displacement (see Figure 4.6.(d)). Next, the filter is applied by convolving $NCC_{XY}(d)$ with 1D edge filter $g(i)$ (Figure 4.6), resulting in Spiking Probability Edges (SPE)

$$SPE_{X \rightarrow Y}(d) = NCC_{XY}(d) * g(i). \quad (4.13)$$

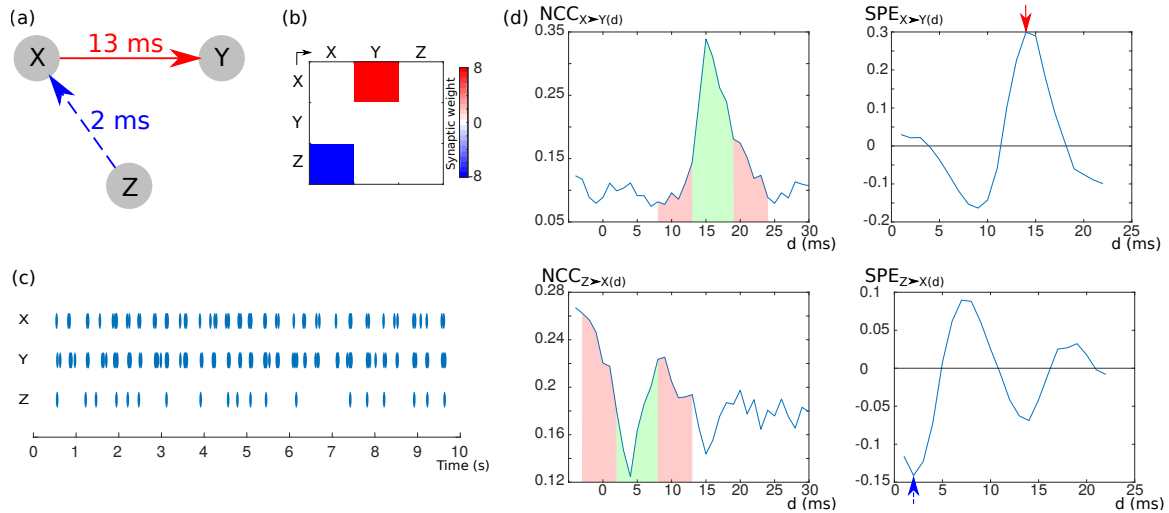


Figure 4.6. – Principle of SPE: An exemplary network of three neurons (a) with a SWM (b). Neuron X has an excitatory impact on Y with a latency of 13 ms after activation, while X is influenced by an inhibitory input of Z with a latency of 2 ms. (c) Spike trains of the three neurons X , Y and Z . (d) NCC of neuron pair $X \rightarrow Y$ and $Z \rightarrow X$ (left column). The convolution of the NCC with an edge filter $g(i)$ results in the respective SPE (right). Global maxima (excitatory) and minima (inhibitory) are indicated by red and blue arrows, respectively. The latency can be seen on the abscissa. Areas in the left column show the corresponding areas for the calculation of the maximum and minimum (green: addition, red: subtraction).

The edge filters are defined as a function $g(i)$ with window size parameters a , b , c (in sampling periods, see Figure 4.7 (a)). In our simulation, sampling frequency is set to 1 kHz.

$$g(i) = \begin{cases} -\frac{1}{a} & \text{if } 0 < i \leq a \\ \frac{2}{b} & \text{if } a + c < i \leq a + b + c \\ -\frac{1}{a} & \text{if } a + b + 2c < i \leq 2a + b + 2c \\ 0 & \text{else.} \end{cases} \quad (4.14)$$

a is the window size for the surrounding area of the point of interest which is used to calculate the local spiking probability average. b is the window size of the observed area. Small values for b increase the sensitivity for single outliers at the cross-correlogram. To avoid the including of overlapped spiking probabilities of interest with the local spiking probability average a soft crossover parameter c can be used. For an *in silico* evaluation with constant transmission times and a simple neuron model the usage of c is not necessary. Note that without using c the spiking probability edges of complex networks (*in vitro* or *in vivo*) can be smoothed, which is disadvantageous for an edge detection.

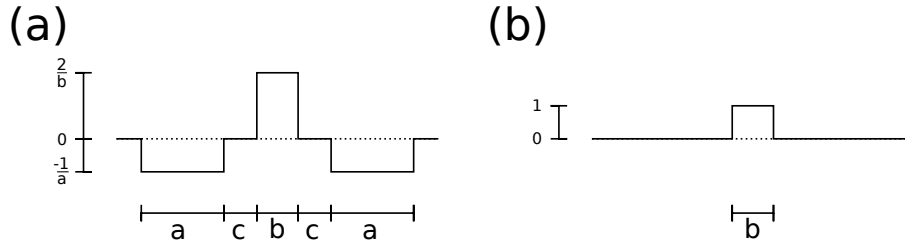


Figure 4.7. – Design of edge filter $g(i)$ and running total filter $h(i)$: (a) The designed edge filters have an arithmetic mean of zero and are applied to the cross-correlogram. (b) The running total filters are designed by the same parameter b of the corresponding edge filter.

If the mean of function $g(i)$ is zero, the calculation results in an arithmetic mean of zero for $SPE(d)$, which prevents an offset for the resulting value range of $SPE(d)$. If $NCC_{X \rightarrow Y}(d)$ shows a local maximum, $SPE_{X \rightarrow Y}(d)$ leads to a positive peak, while a local minimum for $NCC_{X \rightarrow Y}(d)$ results in a negative peak, see Fig 4.6.(d). Thus, negative peaks of $SPE_{X \rightarrow Y}(d)$ indicate an inhibitory effect of neuron X to neuron Y while positive peaks correspond to excitatory effects. By considering the highest absolute value of $SPE_{X \rightarrow Y}(d)$, the synaptic relation $X \rightarrow Y$ is obtained.

Since the network activity is significantly higher at periods of network bursts, this leads to a local offset of $SPE_{X \rightarrow Y}(d)$ and distort the calculation by overestimating the influences on receiving neurons. Normalization can reduce this unwanted impact. For this purpose, each $SPE(d)$ is divided by the sum over all neuron pair results for the delay d ,

$$SPE'_{X \rightarrow Y}(d) = \frac{SPE_{X \rightarrow Y}(d)}{\sum_{X=1}^{X=N} \sum_{Y=1}^{Y=N} SPE_{X \rightarrow Y}(d)}. \quad (4.15)$$

Parameter values $a = 5$, $b = 4$, and $c = 0$ (no smoothing) provided the best results to our simulated data. Thus, this combination captures the time constant of the used neural model. For more realistic applications different time scales should be considered because neurons are able to emit action potentials in several firing patterns.

To cover multiple spiking behaviours of neurons $SPE_{X \rightarrow Y}(d)$ is extended by the integration of many combinations of filter parameters. $a = [3, 4, 5, 6, 7, 8]$, $b = [2, 3, 4, 5, 6]$, $c = [0, 1]$ with vector length N_a , N_b , N_c were chosen. Low values of a and b increase the sensitivity to noise whereas high values do not affect results.

Further $N_a \cdot N_b \cdot N_c$ combinations were taken into account. This introduces different lengths of convolution results $SPE_{X \rightarrow Y}(d)^{(n)}$ (n is the index of the used edge filter). To obtain result vectors with same length 1D running total filters $h(i)^{(n)}$ (see Figure 4.7.(b)) are applied to $SPE_{X \rightarrow Y}(d)^{(n)}$. For each edge filter $g(i)^{(n)}$ a corresponding running total filter is designed (4.16) by using the same parameter b from (4.14).

$$h(i) = \begin{cases} 1 & \text{if } 0 < i \leq b \\ 0 & \text{else.} \end{cases} \quad (4.16)$$

As all $SPE_{X \rightarrow Y}(d)^{(n)}$ have the same length, a matrix is obtained by introducing a row for each calculated $SPE_{X \rightarrow Y}(d)^{(n)}$ (see Figure 4.8.(d)). A vertically addition of this matrix enables the consideration of different time scales.

$$TSPE_{X \rightarrow Y}(d) = \sum_{n=1}^{N_a \cdot N_b \cdot N_c} SPE_{X \rightarrow Y}(d)^{(n)} * h(i)^{(n)} \quad (4.17)$$

The resulting $TSPE_{X \rightarrow Y}(d)$ values are interpreted as described before for $SPE'_{X \rightarrow Y}(d)$. The sign of $TSPE_{X \rightarrow Y}(d)$ with d at the absolute extreme value allows a discrimination between inhibitory from excitatory effects.

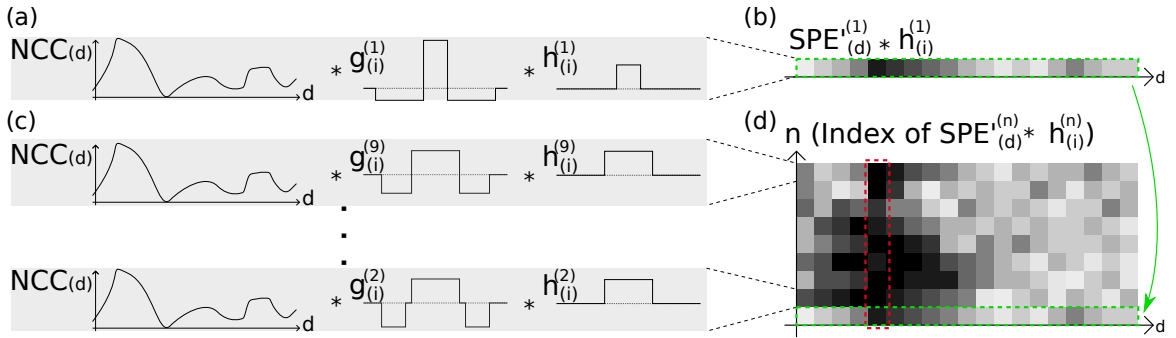


Figure 4.8. – Principle of TSPE: (a) After the $SPE(d)$ is calculated by a convolution of $NCC(d)$ with an edge filter $g(i)^{(1)}$ (see Figure 4.6), a second convolution with a 1D running total filter $h(i)^{(1)}$ is performed. (b) The result of the second convolution $SPE(d)^{(1)} * h(i)^{(1)}$ is plotted with a gray scale plot. Dark color indicates a high value at a certain delay time d . (c) In order to capture the variance of time constants of the neurons, n edge filters $g(i)$ are calculated for different window parameters. By $n = 9$ filtering operations, a three dimensional representation is obtained (d). The abscissa is the delay time and the ordinate is the index of calculated $SPE(d)^{(n)} * h(i)^{(n)}$, while the gray scale indicates the resulting value. The green marked convolution (b) can be found in function (d) as first row, which is also marked green. The resulting $TSPE(d)$ can be obtained by adding the values vertically. The absolute maximum is the most likely point of effect, which is marked red.

4.4. Threshold calculation methods

The resulting CMs of connectivity estimation algorithms contain values depending on the chosen method. These values have to be classified in order to distinguish between a 'real connection' and a 'statistical correlation'. There are different approaches to select a threshold, which are presented below.

4.4.1. Easy threshold calculation

In some studies [54] the distribution of the resulting CM is used to calculate the threshold. By obtaining the mean value and the SD of all CM values a threshold for the whole CM is calculated. For example, a threshold is selected at $\overline{CM} + 4 \cdot \sigma_{CM}$ [54]. Here, the computing time is negligible.

4.4.2. Threshold calculation with surrogate data

To generate surrogate data spike dithering (also known as jittering) [88] is used. The method of Date is a classic tool of neuroscience [89–92] for testing the significance of results. In a defined time window each spike of an original spike train will be individual and randomly displaced in order to generate spike trains with similar characteristics (see Figure 4.9). The distribution of shifting times is chosen uniform. In this way a set of slightly different spike trains is obtained.

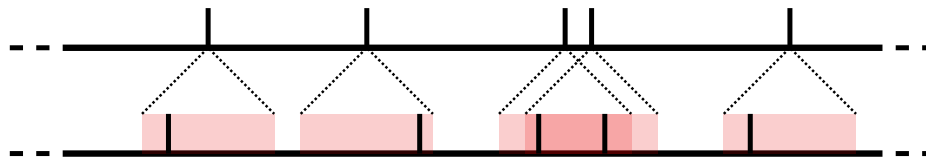


Figure 4.9. – Spike dithering for generate surrogate data: Every detected spike of an original spike train will be shifted by a random time in a specific time window (shaded areas). The upper spike train is original and was used to generate the lower surrogate spike train. Close spikes (e.g., at bursting) can even be switched.

Since the focus is on paired-wise examinations of connectivity, the threshold should be calculated for each pair of spike trains. Considering two spike trains X and Y , which are both used for the generation of surrogate data several times (here n is between 100 and 1000). A distribution of connectivity estimation results is obtained for this potential link between the neurons. The threshold is selected at values calculated with the surrogate value distribution. This single threshold is only used for the classification of the relation between the two spike trains. For each relation of spike trains the generation of surrogate data and calculation of threshold is necessary. Thus, the computation time of this classification step is about n times the time required by the estimation algorithm for connectivity.

4.5. Implementations

For DTE, DHOTE, DTECI and DHOTECI the toolbox described in [55] is used, which is a MATLAB executable (MEX) application. CDHOTE is based on the calculations of DTECI and DHOTECI. The implementation of NCC, NCCCI and TSPE are realized with sparse matrices multiplications (unbinned simulation data, approx. 0.2% filled). All spike trains are stored in a common sparse matrix with the length that equals the sampling number. This matrix is multiplied with the transposed and time shifted matrix. The normalization matrix is calculated by multiplying the SD vector with the its transposed version. For a faster calculation of TSPE the mean values of spike trains (0.005 to 0.04 at bin size of 1 ms) were omitted, because they did not affect the accuracy.

5.

Evaluation of connectivity estimation

Based on the findings of Chapter 3 an evaluation framework was used to evaluate the connectivity estimation methods of Chapter 4. First, the necessary tools for an appropriate comparison of estimation accuracy are presented as well as the results of the evaluation. Furthermore, the calculation time of each method were measured and compared with each other. The issue of interpreting the result values of the tested methods is analysed with multiple methods. At the end of this chapter, the results are concluded and summarized.

5.1. Evaluation tools

5.1.1. Simulation

All simulations were performed in *2017a MATLAB*, MathWorks, with a modified version of the published code described in [49]. Each network type was generated and simulated ten times with different seed values for the random number generator of our simulation. The *in silico* networks were designed according the guide described in [35] for evaluation applications in neuroscience. The spike train subset of 100 neurons was recorded for 60 minutes, while studies were performed also for shorter time frames to analyse the impact of this parameter. It was demonstrated that long recording times improve the estimation results [55].

5.1.2. ROC Curve

The accuracy of a connectivity estimation algorithm is evaluated by comparing the results with the properties of the simulated network, described in the SWM. Since value ranges of CM are strongly dependent on the measured signal, these values are not directly comparable. In the best case, values of CM should be proportional to real synaptic weights of SWM. A threshold to distinguish between a 'real connection' and a 'statistical correlation' is used to calculate the TCM. This binary pattern of connection or non-connection will be used for the comparison with the SWM. The matches and mismatches between TCM and SWM are stored in four groups. Matches of connections are True Positive (TP), mismatches are False Positive (FP), matches for non existing synapses are True Negative (TN), and mismatches are FP. A standard method to evaluate the performance of classifiers is the Receiver Operating Characteristic (ROC) curve, which is a plot of True Positive Rate (TPR)

$$TPR = \frac{TP}{TP + FN} \quad (5.1)$$

depending on the False Positive Rate (FPR)

$$FPR = \frac{FP}{FP + TN}. \quad (5.2)$$

A perfect reconstruction of the SWM is indicated by a TPR of 1 and a FPR of 0. In case of equality of both rates classification is a random guess.

Because of the sparse SWM a low FPR means a larger amount of wrongly estimated connections than correctly estimated connections even with large TPRs. To prevent this misleading impression, the evaluation focuses on the TPR values at 1% FPR.

5.1.3. Confusion matrix

A widely used visualization tool for the classification performance is the confusion matrix, or error matrix. It is a specific table layout that allows visualization of the performance of an algorithm. Each column of the matrix represents the labels while each row represents the predicted class. This visualization allows to see easily which classes are classified with high or low accuracy and which classes are often confused. In this study, inhibitory, excitatory, and no connection were used as class labels. The columns of a 2D confusion matrix are real labels obtained by the SWM. The rows contain the predicted classes of the classification algorithm. On the very right column the percentage of correctly classified connections of the output class is shown, at the bottom the percentage of correctly classified connections of the target classes is displayed. The general classification accuracy can be found in the lower right box. The classification ability of TSPE for distinguishing inhibitory from excitatory synapses is evaluated at a 1% FPR level.

5.2. Accuracy of functional connectivity estimation

Generally, spike raster plots of all simulated topologies show spikes and network bursts with varying rate (see Figure 5.1 left). For *random networks* the spike density within network bursts increases with connection probability p . For *scale-free networks*, spike density within network bursts is lower for the IC version than for the BA version.

The accuracy of the connectivity estimation methods TSPE, NCC, NCCCI, DHOTE, DHOTECI, DTE, DTECI and CDHOTE was calculated for signals generated with *random* and *scale-free networks* and compared. The results of all tested algorithms are depicted in Figure 5.1 and better than random guessing (grey dashed line). The accuracy strongly depends on network topologies. For spike raster plots generated with *random networks*, the performances of the tested algorithms deteriorates with higher connection probability p . Methods based on a coincidence index (NCCCI, DHOTECI, DTECI) perform significantly better than their corresponding basic algorithms (NCC, DHOTE, DTE). The results of the TSPE algorithm shows a ROC curve with a TPR up to 99.5% for $p = 0.05$ and $p = 0.1$. For $p = 0.15$ the performance accuracy decreased. The CDHOTE algorithm was inferior to NCCCI, DHOTECI, and DTECI. In contrast, for *scale-free network* topologies CDHOTE was superior. The SD of the results varied depending on topology. For *random networks*, the SD was lower than for *scale-free networks*. At a FPR of 1% TSPE estimated the connectivity more precisely than any other tested algorithms. For both *scale-free networks* the accuracy of TSPE is inferior to the performance for random networks.

To study the performance dependency on the recording duration of spike train data, the TPR was measured at FPR of 1% for simulation durations of 1 min, 5 min, 10 min, 30 min and 60 min (see Figure 5.2). The results show that accuracy increases with recording time. In case of *random networks*, TSPE is able to reach almost a TPR of 100% for a simulation duration of 60 min ($p = 0.05$ and $p = 0.1$). Connectivity estimation saturates and therefore no accuracy increase is assumed for simulation durations longer than 60 minutes which is also true for *scale-free networks*.

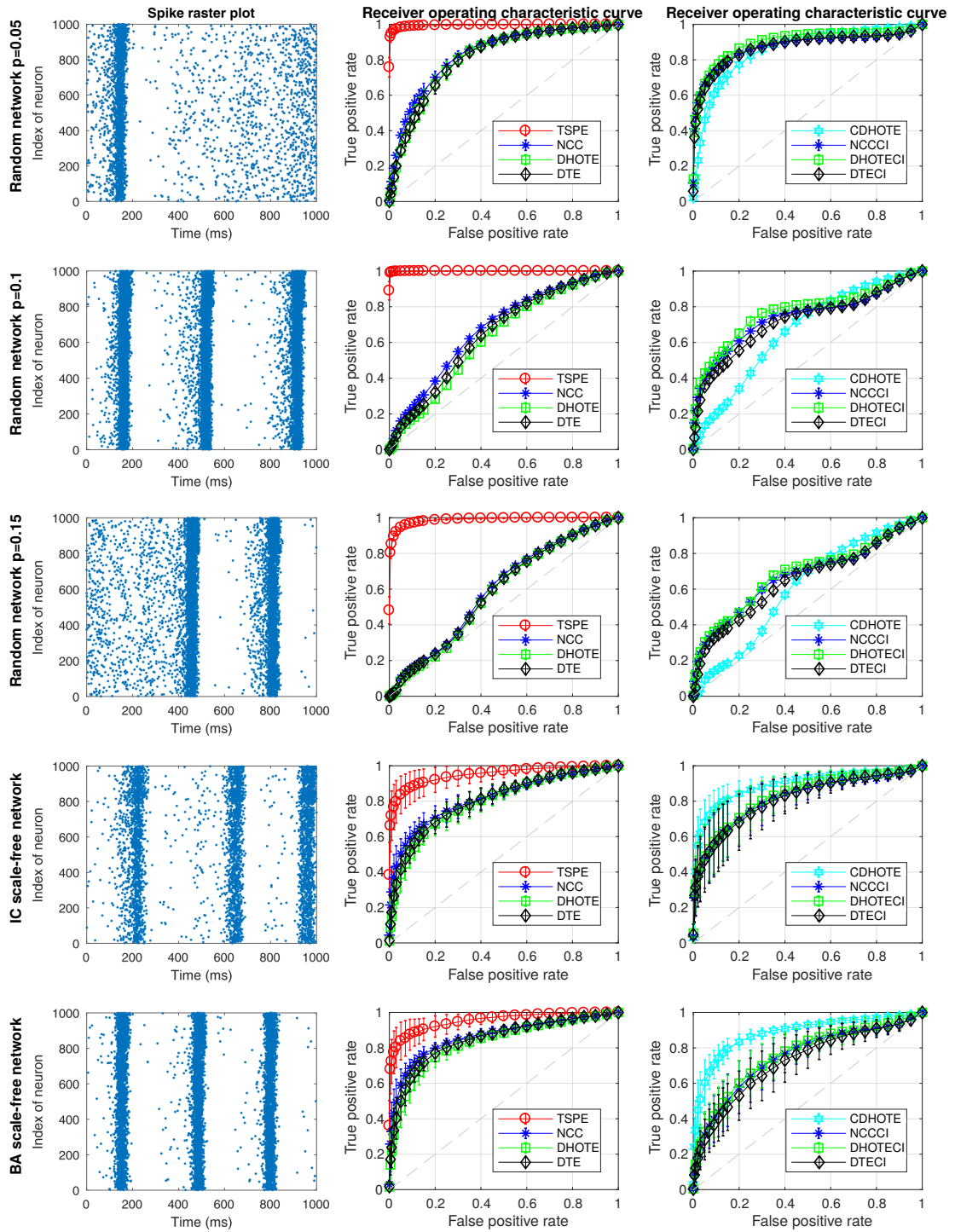


Figure 5.1. – Evaluation of connectivity estimation algorithms for different network topologies: **Left column:** Spike trains of the simulated networks. For the evaluation a subset of only 100 spike trains with a simulation duration of 30 minutes were used. Network bursts appeared for all network topologies. **Middle and right column:** ROC curves of all tested algorithms for $n = 10$ simulations per network topology. With increased complexity of the *random networks* the accuracy of all algorithms decreased. TSPE outperformed all evaluated algorithms.

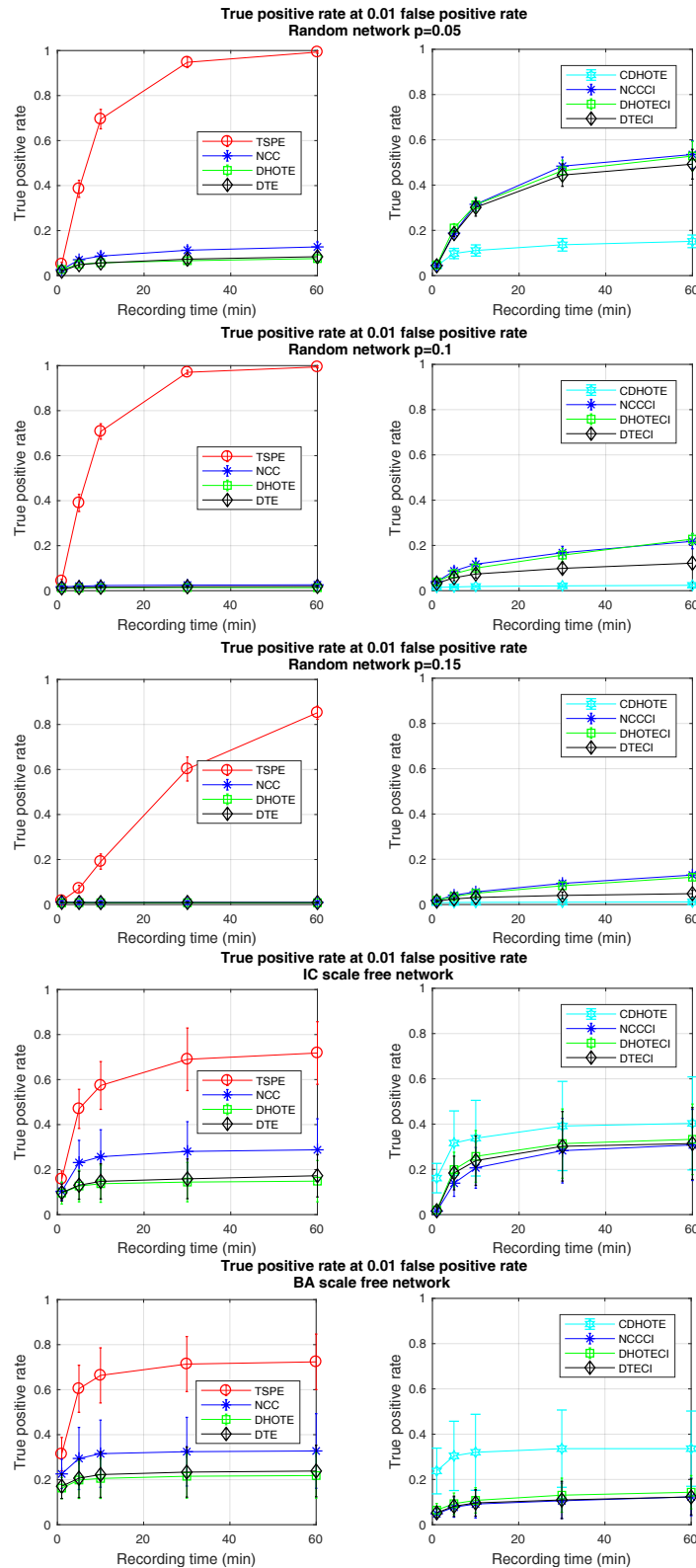


Figure 5.2. – Effects of the recording time on the accuracy of the connectivity estimation. Accuracy estimation increases until a saturation is reached. Within the first ten minutes, the increase is strongest which is prominent for the TSPE algorithm.

5.3. Accuracy of effective connectivity estimation by TSPE

For effective connectivity not just connection strength but also information about causality and the synaptic effect is required. In contrast to the other tested algorithms, TSPE offers information about excitation and inhibition. In Figure 5.3, the confusion matrices are plotted for TSPE at a FPR threshold level of 1%.

For *random networks* with $p = 0.05$, the total classification accuracy was 98.9%, which is 0.1% below the maximal achievable classification accuracy. By increasing the complexity of *random networks* to $p = 0.1$, the total accuracy decreased by 0.2% (see blue boxes in Figure 5.3). The classification accuracy of excitatory connections decreased and the detection rate of inhibitory effects increased. Further increase of complexity to $p = 0.15$ resulted in a collapse of the classification performance and many effects were not detected instead of classified as a synaptic connection.

For both *scale-free network* types, the accuracy was 98.2 and 98.4% (78.4% and 76.9% for excitatory effects). However, about 70% of all inhibitory effects were not classified correctly (see Figure 5.3 dark grey, bottom-center boxes).

To summarize, the estimation accuracy for excitatory synapses was between 64.8 and 99.5%, for inhibitory effects it was between 28.2 and 83.8%.

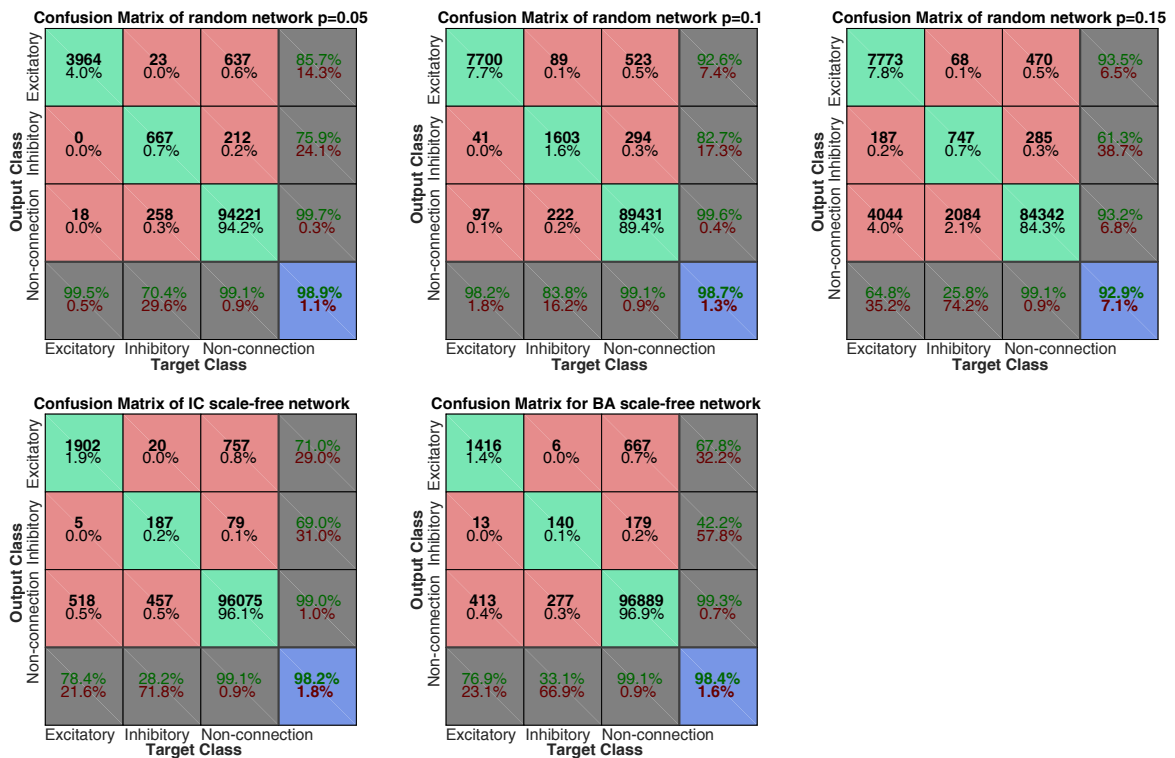


Figure 5.3. – Confusion matrices for connection types classified by TSPE: Green (red) fields: correct (incorrect) classification (upper number: absolute, lower number: in percentage). Bottom row (grey): estimated connections to actual connections; Right column (grey): correctly estimated connections to all estimated connections. Blue field: total accuracy of classification. Grey and blue fields: green number percentage of correctness; red number percentage of incorrectness.

5.4. Calculation time

For a comparison of calculation efficiency, the processing time was measured for the calculation of connectivity estimation for IC *scale-free* networks with different number of spike trains (between 2 and 1000) and different simulation durations (between 1 and 60 minutes, see Figure 5.4). Calculations were conducted using *MATLAB Distributed Computing Server* toolbox on a high-performance computer, which is equipped with 2 Intel Xeon 'Broadwell' E5-2680v4 processors, 8x32 GB DDR4 2400 MHz RAM, SSD and 4 SXM-2 P100 GPUs.

The results show that the calculation time increased linearly with recording time (visible in Fig 5.4). Due to the pairwise comparison of spike trains, the computing time increased exponentially (power of two) with the number of spike trains. For large numbers of recorded spike trains, the calculation of TE based algorithms, like DTE or DHOTE, was longer than the calculation of CC based algorithms. NCC and TSPE were parallelized (matrix operation based algorithms). For example, the calculation time for a IC *scale-free* network with 1000 recorded spike trains and a simulation duration of 10 minutes was approx. 25 seconds for NCC or NCCCI, 45 seconds for TSPE, 16 minutes for DTE or DTECI, and 51 minutes for DHOTE or DHOTECI.

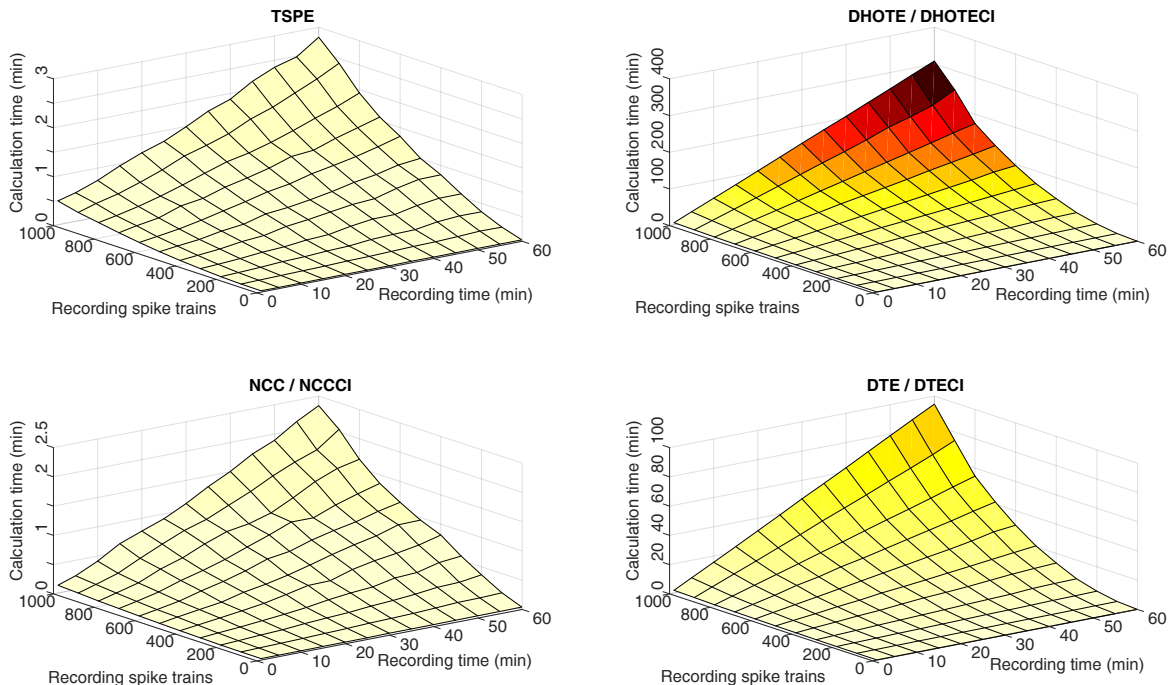


Figure 5.4. – Comparison of calculation times of tested algorithms: The connectivity estimation algorithms were evaluated using data generated by IC *scale-free networks* for different lengths of recording and a variable number of spike trains. Red colored areas indicated long and light areas indicated small calculation times. Calculation time increased linearly with duration but exponentially with number of spike trains. Calculation time was in the following ascending order for algorithm groups: 1) NCC, NCCCI, TSPE 2) DTE, DTECI 3) DHOTE, DHOTECI.

5.5. Evaluation of threshold calculation

Since resulting CMs of connectivity estimation algorithms have different value ranges, different thresholds have to be calculated in order to obtain a TCM with the best combination of TPR and FPR (optimal case: $\text{TPR} = 1$ at $\text{FPR} = 0$). This is a crucial step in connectivity estimation because even the best connectivity estimation method have two random guess points: $\text{TPR} = 0$ at $\text{FPR} = 0$ (no estimated connection) and $\text{TPR} = 1$ at $\text{FPR} = 1$ (all estimation values are identified as connection). In the following the threshold calculation methods are evaluated.

5.5.1. Easy threshold calculation

The TPRs and FPRs are illustrated for TSPE and DHOTE with easy threshold calculation with $4 \cdot \sigma_{CM}$ in Table 5.1. To keep clarity other connectivity estimation methods are not mentioned here. All FPR are smaller than 1 percent. For TSPE it is even zero in all examined cases. However, the result is not satisfying because of the low TPRs. At least for ER *random networks* with $p = 0.05$ and the *scale-free networks* TSPE is able to archive mean TPRs between 0.357 and 0.448. This means the selected threshold is too large. For DHOTE the easy threshold calculation with $\overline{CM} + 4 \cdot \sigma_{CM}$ works fine in order to set the FPR at one percent (with low TPRs because its ROC).

Table 5.1. – Evaluation of easy threshold calculation (four times SD):

For TSPE and DHOTE FPRs is low with easy threshold calculation ($\overline{CM} + 4 \cdot \sigma_{CM}$). Especially for *random networks* with connection probability larger than 0.05, TPRs are also low. FPRs of DHOTE are around one percent.

Network type	TPR of TSPE	FPR of TSPE	TPR of DHOTE	FPR of DHOTE
ER <i>random network</i> $p=0.05$	0.392 ± 0.028	0.000 ± 0.000	0.045 ± 0.011	0.007 ± 0.001
ER <i>random network</i> $p=0.1$	0.104 ± 0.012	0.000 ± 0.000	0.001 ± 0.003	0.007 ± 0.001
ER <i>random network</i> $p=0.15$	0.030 ± 0.005	0.000 ± 0.000	0.009 ± 0.002	0.011 ± 0.001
IC <i>scale-free network</i>	0.357 ± 0.075	0.000 ± 0.000	0.110 ± 0.055	0.008 ± 0.002
BA <i>scale-free network</i>	0.448 ± 0.109	0.000 ± 0.000	0.149 ± 0.056	0.006 ± 0.002

By decreasing the threshold to $\overline{CM} + 3 \cdot \sigma_{CM}$ the probability of increasing FPRs is larger. Since FPRs of TSPE were small in Table 5.1, larger FPRs can be allowed in order to archive better TPRs. In Table 5.2 the results for $\overline{CM} + 3 \cdot \sigma_{CM}$ are illustrated. While FPRs of DHOTE are here already too large, FPRs of TSPE are still low. In this way the estimation accuracy of TSPE was able to be further increase by up to 25.3 percent.

Table 5.2. – Evaluation of easy threshold calculation (three times SD):

While FPRs of DHOTE strongly increased, FPRs of TSPE are still low with easy threshold calculation ($\overline{CM} + 3 \cdot \sigma_{CM}$).

Network type	TPR of TSPE	FPR of TSPE	TPR of DHOTE	FPR of DHOTE
ER <i>random network</i> $p=0.05$	0.645 ± 0.017	0.000 ± 0.000	0.115 ± 0.002	0.017 ± 0.001
ER <i>random network</i> $p=0.1$	0.349 ± 0.020	0.000 ± 0.000	0.032 ± 0.005	0.019 ± 0.002
ER <i>random network</i> $p=0.15$	0.130 ± 0.014	0.000 ± 0.000	0.021 ± 0.001	0.025 ± 0.002
IC <i>scale-free network</i>	0.469 ± 0.079	0.001 ± 0.002	0.173 ± 0.079	0.013 ± 0.002
BA <i>scale-free network</i>	0.581 ± 0.095	0.002 ± 0.001	0.240 ± 0.078	0.013 ± 0.003

For $\overline{CM} + 2 \cdot \sigma_{CM}$, all TPRs increase even further. Like before DHOTE gains too large FPRs. Results of Table 5.3 substantiate that each method the optimal multiplication factor of SD can be different. Even lower thresholds increase the FPRs of TSPE too much.

In summary, the optimal easy calculation threshold for TSPE is $\overline{CM} + 2 \cdot \sigma_{CM}$ and for DHOTE $\overline{CM} + 4 \cdot \sigma_{CM}$. By using one threshold for the whole CM the resulting estimation accuracy will always be a point of the ROC function.

Table 5.3. – Evaluation of easy threshold calculation (two times SD):

While FPRs of DHOTE strongly increased, FPRs of TSPE are still low with easy threshold calculation.

Network type	TPR of TSPE	FPR of TSPE	TPR of DHOTE	FPR of DHOTE
ER <i>random network</i> $p=0.05$	0.828 ± 0.020	0.000 ± 0.000	0.224 ± 0.022	0.037 ± 0.002
ER <i>random network</i> $p=0.1$	0.700 ± 0.019	0.000 ± 0.000	0.090 ± 0.008	0.039 ± 0.003
ER <i>random network</i> $p=0.15$	0.372 ± 0.021	0.001 ± 0.000	0.057 ± 0.008	0.039 ± 0.001
IC <i>scale-free network</i>	0.604 ± 0.074	0.005 ± 0.007	0.272 ± 0.095	0.027 ± 0.004
BA <i>scale-free network</i>	0.718 ± 0.088	0.013 ± 0.008	0.376 ± 0.102	0.032 ± 0.006

5.5.2. Threshold calculation with surrogate data

Referencing to the long computing time of DHOTE and the high number of iterations (between 100 and 1000), this part of evaluation is only done for TSPE. The calculation was tested for three different thresholds:

- The mean value +/- four times SD (Table 5.4)
- The minimum/maximum value (Table 5.5)
- The minimum/maximum value +/- SD (Table 5.6)

These mean, minimum and maximum values refer to the generated surrogate data of the examined pairwise correlation. The accuracy of minimum and maximum based threshold calculation varies even with high numbers of iterations due to the randomly increasing thresholds. Even if the evaluation results of these methods are promising, the reproducibility of the results in the experimental environment may be negatively affected. This is the reason for recommending the first method 'mean value +/- four times SD'. Here, the reproducibility of results is good.

Table 5.4. – Evaluation of surrogate threshold calculation (mean value +/- 4 SD) with window size 2 ms: For 100 iterations, FPRs are fine for all cases except BA *scale-free networks*. Here, the FPR of 1.9% was able to be improved only slightly to 1.7% by increasing the number of iterations.

Network type	TPR of TSPE	FPR of TSPE	Number of iterations
ER <i>random network</i> $p=0.05$	0.329 ± 0.072	0.000 ± 0.000	100
ER <i>random network</i> $p=0.1$	0.643 ± 0.066	0.000 ± 0.000	100
ER <i>random network</i> $p=0.15$	0.045 ± 0.018	0.000 ± 0.000	100
IC <i>scale-free network</i>	0.623 ± 0.101	0.001 ± 0.003	100
BA <i>scale-free network</i>	0.918 ± 0.030	0.019 ± 0.020	100
	0.929 ± 0.029	0.017 ± 0.018	500

Table 5.5. – Evaluation of surrogate threshold calculation (minimum/maximum) with window size 2 ms: In contrast to all previous threshold selection methods, the TPRs are improved with the minimum/maximum version. The FPRs of all *scale-free networks* are too large – even with 1000 iterations.

Network type	TPR of TSPE	FPR of TSPE	Number of iterations
ER <i>random network</i> $p=0.05$	0.770 ± 0.049	0.003 ± 0.000	100
ER <i>random network</i> $p=0.1$	0.959 ± 0.027	0.010 ± 0.003	100
ER <i>random network</i> $p=0.15$	0.354 ± 0.078	0.004 ± 0.000	100
IC <i>scale-free network</i>	0.818 ± 0.066	0.026 ± 0.037	100
	0.786 ± 0.076	0.016 ± 0.027	200
BA <i>scale-free network</i>	0.954 ± 0.019	0.052 ± 0.044	1000

Table 5.6. – Evaluation of surrogate threshold calculation (minimum/maximum \pm SD) with window size 2 ms: Except for *random network* $p=0.05$, the TPRs are larger than for the easy threshold calculation methods. With 1000 iterations low FPRs are even ensured for BA *scale-free networks*.

Network type	TPR of TSPE	FPR of TSPE	Number of iterations
ER <i>random network</i> $p=0.05$	0.463 ± 0.059	0.000 ± 0.000	100
ER <i>random network</i> $p=0.1$	0.818 ± 0.090	0.000 ± 0.000	100
ER <i>random network</i> $p=0.15$	0.130 ± 0.035	0.000 ± 0.000	100
IC <i>scale-free network</i>	0.677 ± 0.107	0.001 ± 0.001	100
BA <i>scale-free network</i>	0.948 ± 0.034	0.045 ± 0.043	100
	0.909 ± 0.041	0.005 ± 0.005	1000

5.6. Conclusion of evaluation

A large framework of *in silico* networks with different topologies was used to benchmark the performance of the connectivity estimation methods TSPE, NCC, NCCCI, DHOTE, DHOTECI, DTE, DTECI and CDHOTE. Influences of recording time on estimation accuracy and calculation time were analysed. Furthermore, the classification ability in terms of inhibitory and excitatory effects of TSPE was evaluated.

The novel method TSPE is able to outperform the accuracy of other connectivity estimation algorithms when applied on simulated neuronal network data with different topologies. Especially for spike trains with a long recording duration like 30 minutes TSPE was outperforming. With TSPE, it was possible to discriminate between estimated excitatory and inhibitory connections, which is characteristic for effective connectivity. The total classification accuracy varied between 92.9 and 98.9%, depending on complexity of network topology.

Although these results are very promising, there are some critical aspects. TSPE is not able to detect effects of self-connections. Thus, the diagonal values of the CM have to be neglected or set to zero. Like for all other evaluated algorithms, the current implementation does not take multiple effects, e.g. driven by parallel connections, for a causal relation into account. Further, inhibition is more difficult to identify and to classify than excitation with estimation algorithms [55, 58] which is one aim of further improvements of TSPE.

TSPE is easy to implement and fast for large spike train datasets. Since new technologies of electrophysiological recording are able to record from thousands of electrodes, e.g. HDMEA chips with 4096 electrodes [25], it is crucial to minimize the computation time for large numbers of recorded spike trains. In our studies, TSPE, NCC and NCCCI were computed for 1000 spike trains (30 min-

utes duration) in less than 2 minutes, while Transfer Entropy based methods needed more than 45 minutes. Nevertheless, also the Transfer Entropy based methods take less than 3 minutes for 30 minutes of 60 channel recordings (standard MEA chip), which is considered acceptable for this application. The *in silico* model for evaluation was sampled at 1 kHz. It was also simulated for 10 kHz (data not shown) but no difference in accuracy for the evaluated algorithms with the unbinned or binary binned (1 ms bin size) spike trains were found. The binning for preprocessing is recommended because of the linearly increasing computing time for evaluated connectivity estimation algorithms with smaller bin sizes. The gradient of computing time is smaller for cross correlation based connectivity estimation algorithms than for the TE based algorithms. Thus, long term experiments will benefit by applying TSPE or NCC.

The activity dependent plasticity of connectivity should be considered for long term recordings of *in vitro* or *in vivo* neuronal networks. Since a long duration of recording improves the performance of connectivity estimation algorithms, a compromise between recording time and plasticity of connectivity has to be found. Our research will be continued with the development of innovative threshold selection methods for connectivity estimation and the application of SPE and TSPE for spike trains of *in vitro* experiments. The ability of TSPE to distinguish between excitatory and inhibitory effects could improve the meaningfulness of these experiments.

The determination of an accurate threshold was evaluated as well. This is a crucial step of connectivity estimation because it is not possible to select a threshold at 1% FPR for real spike trains without knowing the connectivity of biological *in vitro* network, which is generally true for all reviewed algorithms. For TSPE the easy threshold calculation with 3 times SD obtain good results with small FPRs. Using some surrogate based methods can improve the TPRs at still small FPRs. However, these methods require a multiplication of the computation time for the connectivity estimation.

To summarize, the evaluation results show that the accuracy of connectivity estimation of large scale neuronal networks has been enhanced by the novel algorithm TSPE. This advantage combined with the ability to distinguish between excitatory and inhibitory effects will help to improve the accuracy of future experiments. The used simulation framework for large scale neural networks with different topologies is available as well as the *MATLAB* based TSPE toolbox, which has the potential of parallelization, on the attached DVD. The *MATLAB* code of TSPE is also attached to this thesis (see Appendix F).

6.

Graph theory

The resulting network of connectivity estimation methods (see Chapter 4) is a structure of correlated neurons, a so-called graph of neurons. Since graphs can be very complex depending on the analysed network, specific analysis methods were developed. These methods are not only used for the analysis of neuronal networks, but also for many graphs such as social networks or power grids. The study of graphs is called graph theory.

To compare experimental network properties, the graph obtained is mathematical analysed. In this way quantitative metrics are gained [17]. The first introduced graph theory parameter is the Mean Path Length (MPL), which is defined as the average distance between nodes in the whole network. A low MPL means a high density of connections in the network. In that case quick communication between neurons is more likely. For the unweighted graphs each given connection has a distance of one. The distance between two nodes i and j (here neurons) is given by the function $d(i, j)$, which counts how many nodes must be passed through to reach the target node. The MPL is calculated by the knowledge about all distances,

$$MPL = \frac{2}{N \cdot (N - 1)} \sum_{i \neq j} d(i, j). \quad (6.1)$$

In graph theory, a clique is a subset of the graph in which all nodes are connected to each other, also called a full graph. The local clustering coefficient for undirected graphs is a parameter quantifying the closeness of neighbour nodes to a clique. This coefficient is calculated by

$$C^{ws} = \frac{2E}{k \cdot (k - 1)}. \quad (6.2)$$

Where E is the number of edges between neighbours and k is the number of connections. To quantify the network communication of the neuronal network, the local clustering coefficient and the MPL are calculated for a *random network* with the same number of nodes and connections like the observed network: MPL_{rand} and C_{rand}^{ws} . The generated *random network* is then compared with the observed network in terms of graph theory. The so-called small-world-ness [93] is expressed by

$$S^{ws} = \frac{\gamma_g^{ws}}{\lambda_g} = \frac{C_g^{ws} / C_{rand}^{ws}}{MPL_g / MPL_{rand}}. \quad (6.3)$$

While a S^{ws} below 1 means that the observed network has *random network* character, a network is identified as a *small-world network* if S^{ws} is larger than one. In this way a quantitative metric can be used to characterize a network or a network change.

Since the focus of this work is on connectivity estimation, no further parameters are explained in detail. However, subsequent research work could include additional parameters like efficiency, hubs, centrality or robustness [11].

7.

Application of connectivity estimation

Since the evaluation results of TSPE are promising, the connectivity estimation method is applied to *in vitro* experiments. Here, measured signals of neuronal cultures were obtained with MEA chips. Due to setup difficulties no HDMEA experiments could be performed. The work described in this chapter is based on a collaboration between University of California Irvine (UCI) and UAS Aschaffenburg. This collaboration was founded by the Bavaria California Technology Center (BaCaTeC) project *Estimation of Effective Connectivity in Neuronal Networks*.

7.1. Setup of the experiment

To analyse neuronal networks of the hippocampus and associated brain regions involved in the learning and memory of an 120-channel MEA chip of MCS (Reutlingen, Germany, <http://www.multichannelsystems.com>) is used. Entorhinal Cortex (EC), Dentate Gyrus (DG), Cornu Ammonis 3 (CA3) and Cornu Ammonis 1 (CA1) sub-regions of the brain were cultured in a four-chamber system interconnected with micro-tunnels [94]. The micro-tunnels enabled passages of neurites but not somata and communication between sub-regions [94, 95] (see Figure 7.1). To obtain these chambers a Polydimethylsiloxane (PDMS) device was used (see Figure 7.2).

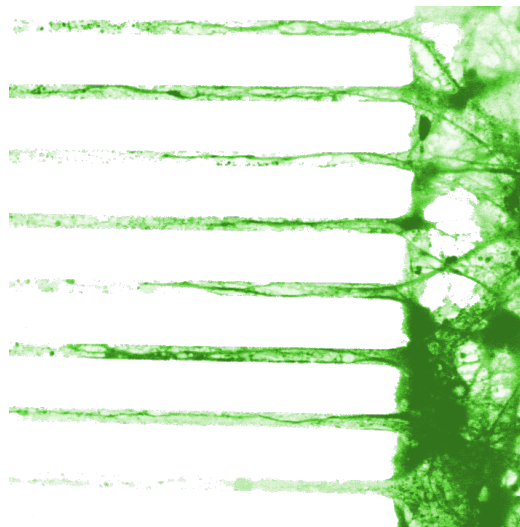


Figure 7.1. – Neurites in a micro-tunnel device: The micro-tunnel device prevents that neuronal cells of the chamber (right-hand side) enter the area on the left-hand side. Only axonal connections and dendrites are able to pass the tunnels. Origin picture taken by Udit Narula in 2016 at UCI.

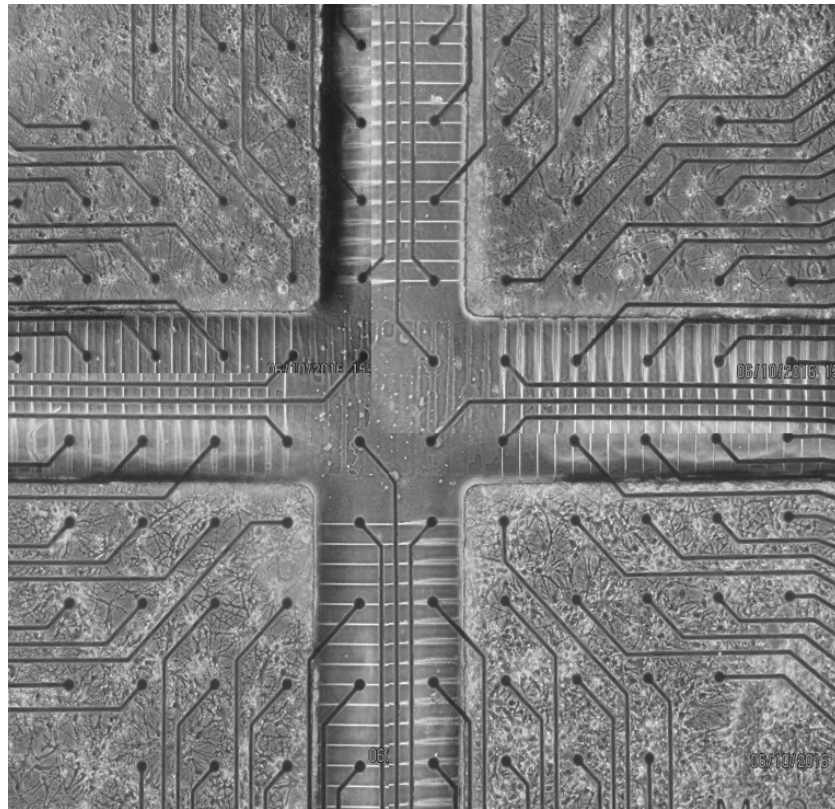


Figure 7.2. – Experiment with four cultures: The micro-tunnel device connects four subcultures EC, DG, CA3 and CA1 with each other. Black dots are electrodes and lines are conducting paths. For some micro-tunnels a pair of electrodes (all in all 120 electrodes) measured signals of axons in the tunnels (bright lines). Four electrodes in the middle of the MEA are covered and isolated by the tunnel device. Neuronal cultures can be recognized in the chambers. Picture taken by Daniele Poli at UCI.

The hippocampal cells were cultured at densities equal to 1000 cells/mm² for DG, 330 cells/mm² for CA3, 410 cells/mm² for CA1 and 330 cells/mm² for EC [96]. In this way a realistic ratios of neuronal densities *in vivo* (EC-DG 1:3, DG-CA3 3:1, CA3-CA1 1:1.25 and CA1-EC 1.25:1) is ensured [97]. For further information about the used devices and their fabrication see [98] and for information about the dissection process of the rat brain see [99]. The experiments were carried out at the Institute for Memory Impairments and Neurological Disorders (MIND) of UCI in 2015 and 2016. All datasets were recorded between 21 and 37 Days *in vitro* (DIV). For some experiments the order of cultures were changed. Clockwise (CW) means the order EC, DG, CA3, CA1 (starting from the left upper corner clockwise) and Counter Clockwise (CCW) means switched chambers CA1 and DG. For the experiments each chamber was stimulated at three electrodes with different stimulation protocol:

- Single stimulation
- Paired Pulse (PP) stimulation
- θ burst stimulation [100]
- 5 Hz θ burst stimulation
- High Frequency (HF) stimulation

For three experiments, Long Recordings (LRs) with a duration between 50 and 60 minutes were saved. Due to the complex datasets, it was previously not possible to estimate the connectivity with significant results. In Table 7.1 indicates which stimulation was applied to which experiment.

Table 7.1. – Description of experiment datasets: The first six digits of the experiment names is the used chip. The next six digits indicate the start date of the cultivation process and the last six digits indicate the date of the experiment with measurements.

Nr.	Experiment	DIV	Order	Spon.	Single	PP	θ	5θ	HF	HF (LR)
1	19908 160518 160610	22	CCW	✓	✓	✓	✓	✓	✓	
2	19914 160127 160217	21	CW	✓	✓	✓	✓		✓	
3	24574 160727 160818	22	CW	✓	✓	✓	✓	✓	✓	
4	19914 160127 160303	37	CW	✓					✓	✓
5	24088 160127 160302	36	CW	✓					✓	✓
6	19908 150729 150823	25	CCW	✓	✓	✓	✓			
7	19914 150805 150828	25	CCW	✓	✓	✓	✓			
8	24574 160127 160303	37	CW	✓					✓	✓

7.2. Spike detection and sorting

After filtering the measured raw data with a 500 Hz Butterworth high pass filter, spikes were detected at a threshold 5.5 times the estimated SD of the background noise for chamber electrodes. Since the Signal-to-Noise Ratio (SNR) for signals measured in the micro-tunnels is larger, here only 4.0 times the estimated SD were necessary. To distinguish between different neurons at a single electrode the spike sorting toolbox *FFMSpikeSorter* [101] was used with a 2 ms window size for the waveforms of detected spikes. Each cluster had to have at least 20 action potentials in order to be considered as identified neuron for postprocessing. In Figure 7.3 the results of spike sorting for one electrode in a tunnel is illustrated.

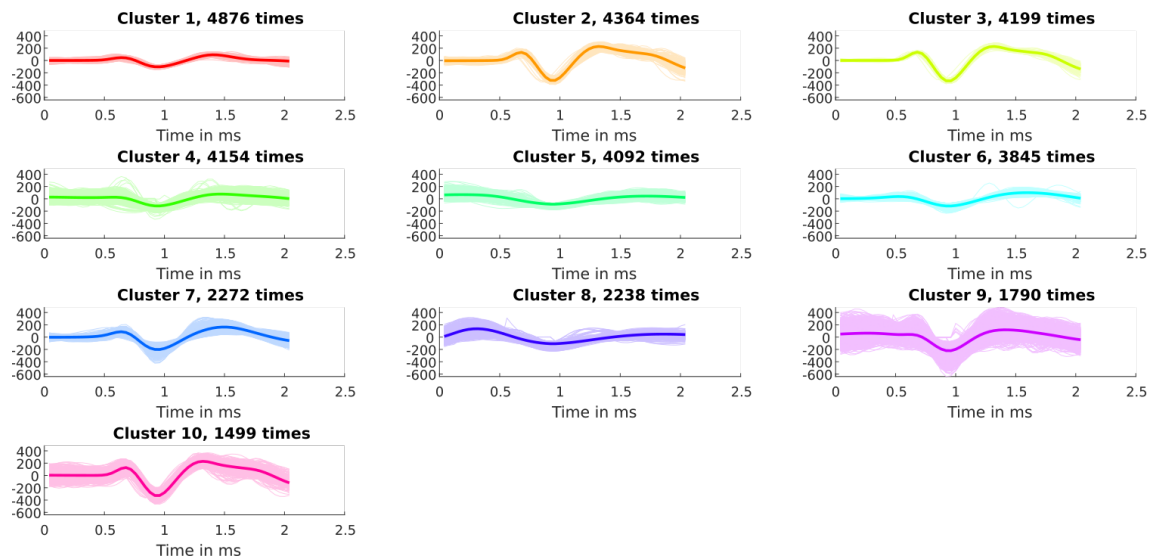


Figure 7.3. – Example of spike sorting: The measured signal in a micro-tunnel was filtered, spikes were detected and sorted. Ten different source neurons of these action potentials were identified. 4876 spikes were associated with cluster 1, which is the largest source of action potentials. The ordinates have normalized value ranges.

To compare the network dynamics the spontaneous datasets before and after stimulations of an experiment were merged. After applying spike sorting the results were separated again. The obtained raster-plot in Figure 7.4 illustrates different network behaviour in the chambers (each chamber marked with different colour). For example, chamber CA3 has a large abstinence of spikes in the last 18 seconds of the sample while all other chambers and the tunnels are still very active. The used spike detection and sorting identified over 700 neurons with the 120 electrode MEA. Especially in the tunnels many clusters were found because of the large SNR.

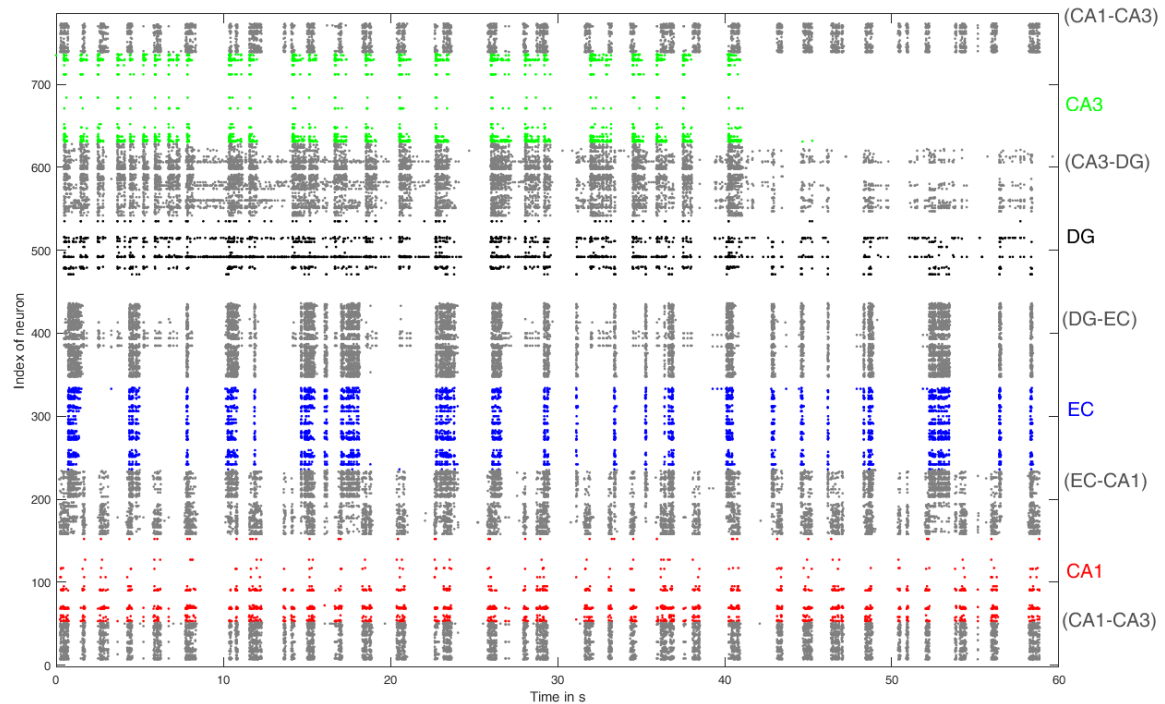


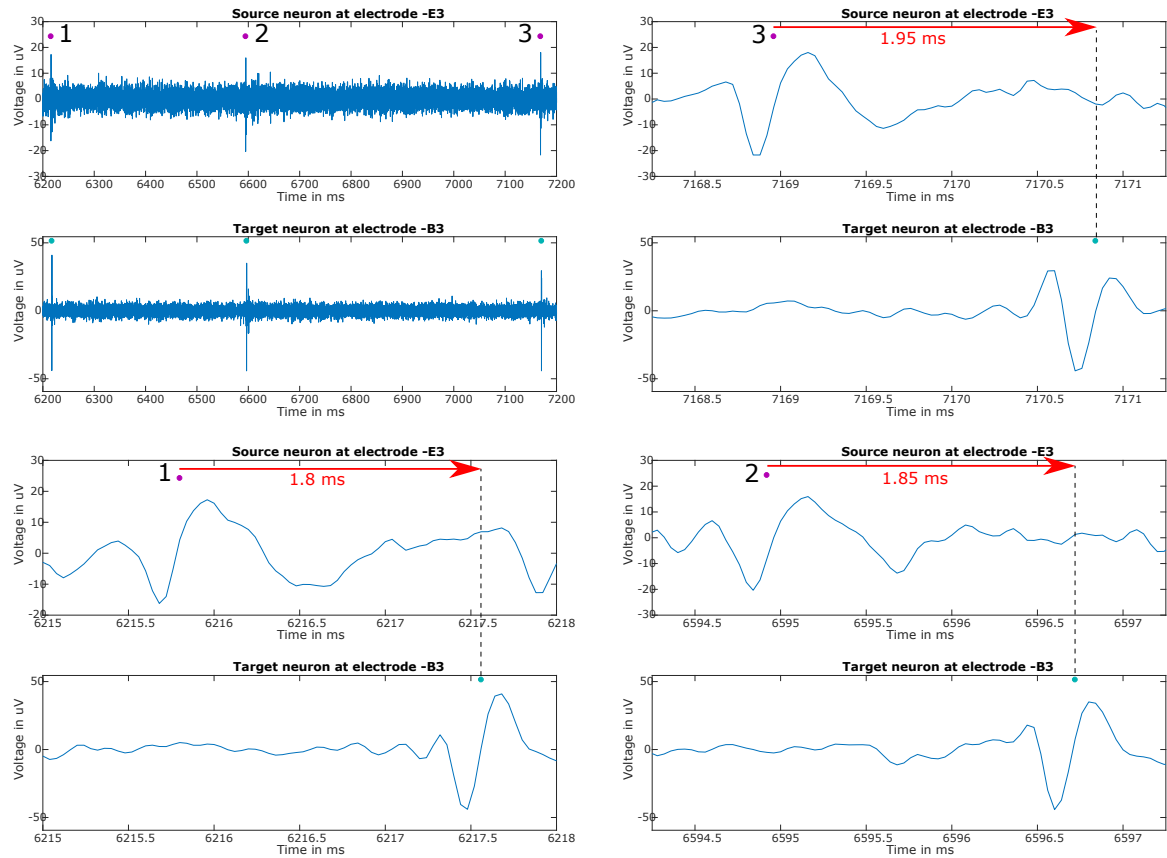
Figure 7.4. – Example of measured spike trains (1 min): Over 700 neurons were identified by the spike sorting algorithm. Subcultures and tunnels are illustrated in different colors (see right hand side).

Since some clusters seem to have similar waveforms (cluster 2 and 3 in Figure 7.3), the spike sorting algorithm could be too aggressive. As the focus of this work is on the estimation of connectivity, this topic has not been further investigated. For further research different spike sorting algorithms should be evaluated in order to gain the best accuracy of connectivity estimation.

7.3. Connectivity estimation with TSPE

The novel connectivity estimation method TSPE was applied to 5 minute recordings before and after the different stimulation types. For the operation parameters of TSPE the delay window was selected to be 30 ms, $a = [3, 4, 5, 6, 7, 8]$, $b = [2, 3, 4, 5, 6]$ and $c = [0]$ (all in ms). Optional scaling disabled because of different network bursts in each chamber. Estimated interchamber connections were only allowed between neighboured chambers. Furthermore, the four electrodes in the middle of the MEA were not considered for the estimation. Thresholds were calculated with 100 surrogate data generated with a 2 ms jittering window (threshold for inhibitory effects is the mean value of all negative values minus their SD and the mean value of all positive values plus their SD for excitatory effects). Each result value that passes these threshold calculation successfully is identified as connection. In Figure 7.5 an example is illustrated. A measured neuron at electrode -E3 excites another measured neuron at electrode -B3 with a transmission time of approx. 1.9 ms.

(a)



(b)

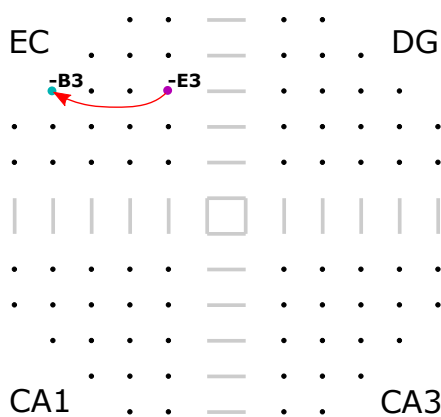


Figure 7.5. – Example of an estimated connection: The measured signals (a) of electrodes -E3 and -B3 is zoomed for the three action potential pairs. The action potentials of -E3 are marked with a purple dot and a green dot for -B3. After each action potential of -E3 it takes approx. 1.9 ms that an action potential at -B3 can be measured. This indicates an excitatory effect, which is illustrated at the MEA (b) with an red arrow.

7.4. Graph theory analysis

For each result, the estimated connectivity was analysed in terms of graph theory. The MPL was calculated as well as the small-world-ness. A toolbox was used for the calculation of latter (<https://github.com/mdhumphries/SmallWorldNess>). Figure 7.6 illustrates differences in the estimated connectivity between the experiments. Inhibitory effects are marked blue and excitatory effects red. Unfortunately, the differences in activity between the experiments made it impossible to use statistical groupings. Except for dataset 7 (bottom in Figure 7.6) all experiments have at least one very densely connected chamber.

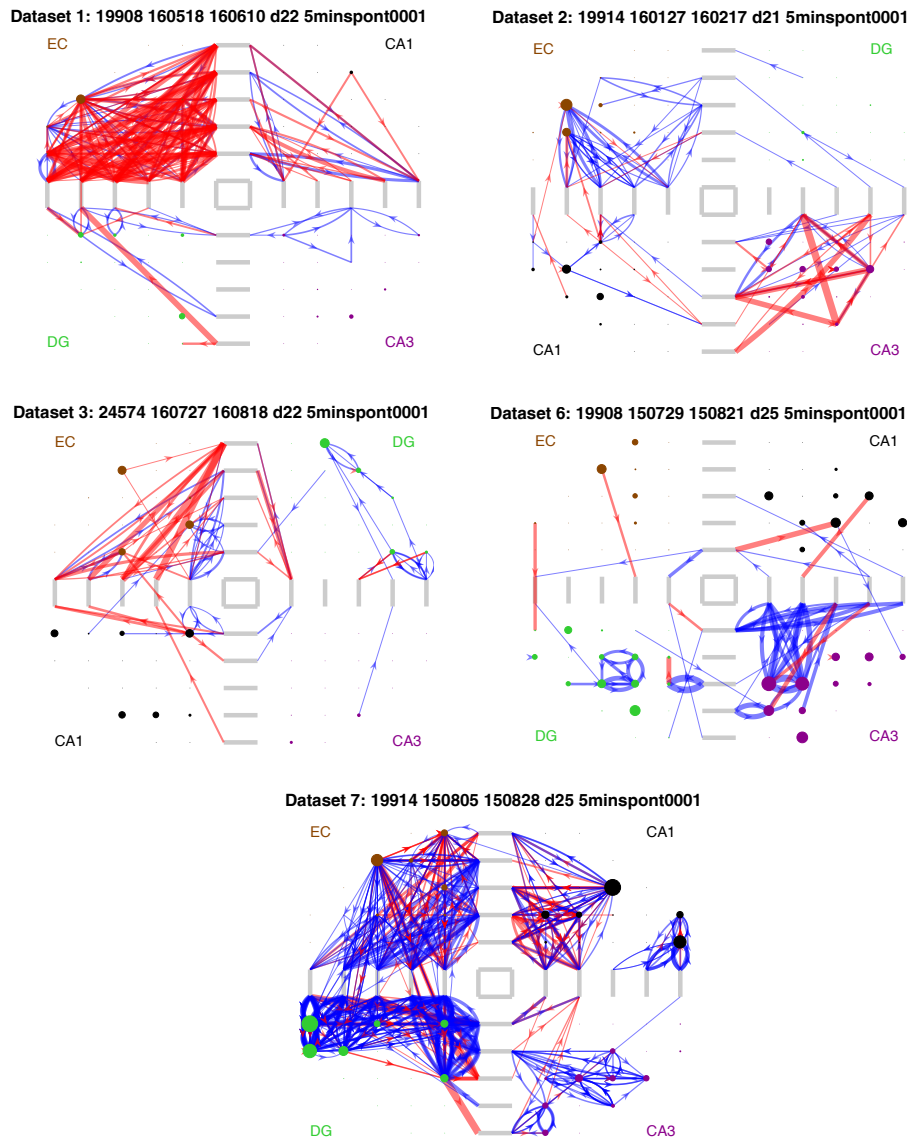


Figure 7.6. – Results of estimated graphs: The MEA is illustrated with different sizes of electrodes depending on the activity (large means more active). The width of a line indicates the strength of estimated correlation and the causality specified by arrowheads. Inhibitory effects are marked blue and excitatory effects red.

7.5. Network dynamics

As the analysis was not successful for the whole graph, individual identified connections were grouped and examined individually for each chamber. The observation of status changes of a network in time is called studying the network dynamics.

In order to gain more detailed knowledge about network dynamics, synaptic effects are divided into four groups: strong/weak inhibitory and strong/weak excitatory. Strong effects were defined through the 75% quantile of all appearing effects. The network activity changes due to the applied stimulus. Each group of effects is considered separately with percentage changes. There are five change possibilities:

- Gained effect – during the two recordings to be compared, this effect appeared new
- Stronger effect – during the two recordings to be compared, this effect became more powerful than before
- Same effect – during the two recordings to be compared, this effect did not change
- Weaker effect – during the two recordings to be compared, this effect became less powerful than before
- Lost effect – during the two recordings to be compared, this effect disappeared

To identify significant differences the Kolmogorov-Smirnov test (K-S test) was used ($\alpha = 0.05$). The null hypothesis is always that stimuli have no influence on the behaviour of effective connectivity in a neuronal network.

7.5.1. Comparison of different stimuli

This analysis focuses on influences of various stimuli (single stim, PP and θ burst). For the analysis, $n = 5$ (dataset 1, 2, 3, 6 and 7). Because of this low number, it is hard to disprove the null hypothesis that there is no correlation of stimuli on connectivity. However, in DG it was possible to successfully prove an influence on the behaviour (see Figure 7.7, cases marked red). The stimulation with PP reduced the generation of weak excitatory effects and simultaneously enhanced the lost of weak excitatory effects in contrast to single and θ burst stimulation.

7.5.2. Long recording based analysis

To increase the statistical power one considers longer recordings. The one hour recordings (dataset 4, 5 and 8) were divided into five minutes pieces to obtain a larger number of connectivity states. No overlap was used. In this way the network dynamics without influences can be studied and compared with the dynamics after a stimulation protocol. With the three LR experiments it is possible to gain $n_{\text{before}} = 31$, $n_{\text{stim}} = 3$ and $n_{\text{after}} = 31$. In the following the observations are listed and sorted by chamber.

Dynamics in DG

In DG, strong synaptic effects rarely appeared. However, after the HF stimulation the strong and weak excitatory effects were less stable than before. The effective connectivity of excitatory synapses was then more dynamic. Shortly after stimulation, less weak excitatory synaptic effects appeared new than before stimulation or later.

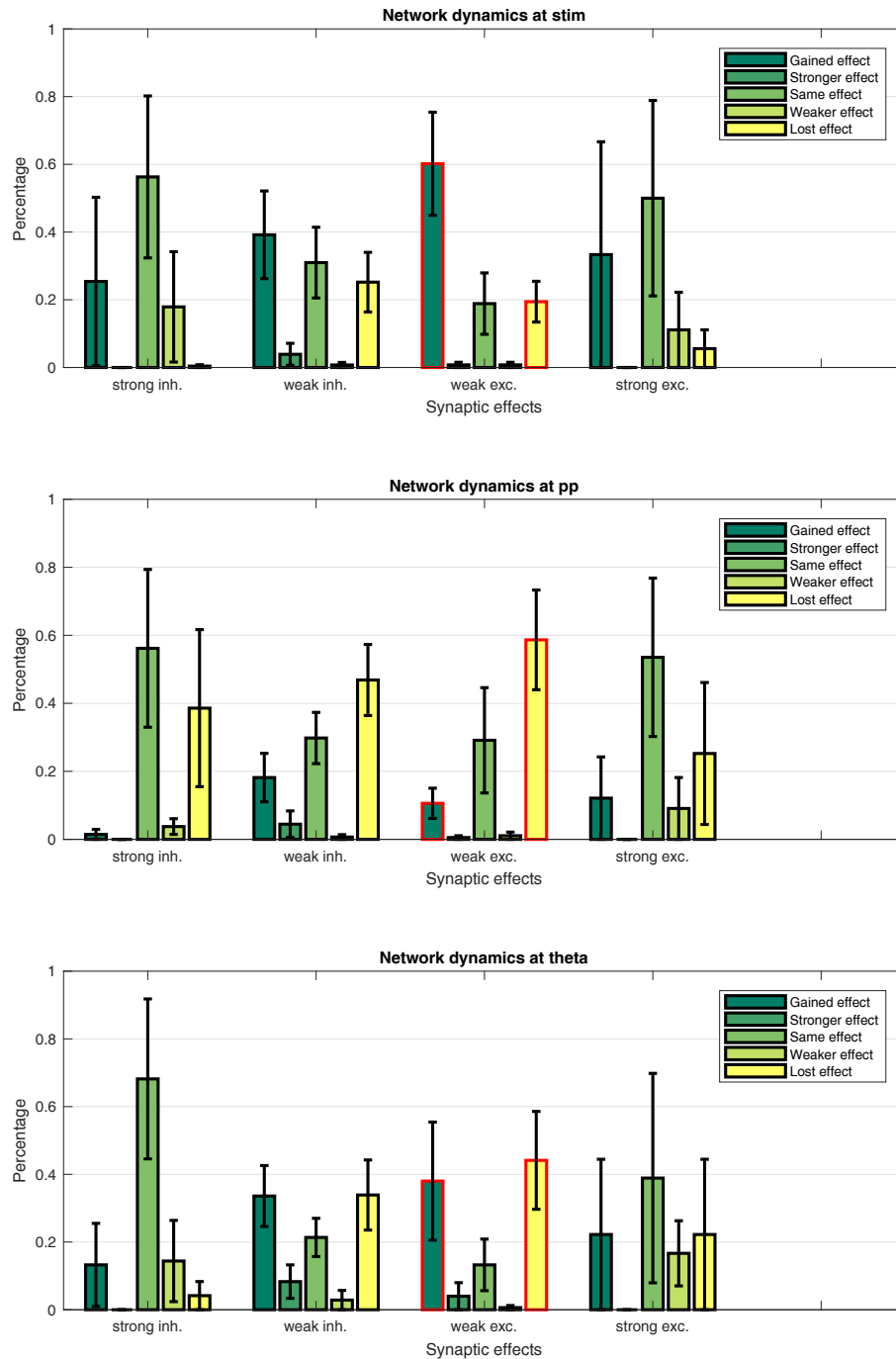


Figure 7.7. – Network dynamics for different stimuli at DG: The representation with standard error bars is based on five experiments. Synaptic effects are divided into four groups: strong/weak inhibitory and strong/weak excitatory. The network activity changes due to the applied stimulus. Each group of effects is considered separately with percentage changes. There are five change possibilities for each appeared effect. Significant differences are marked in red.

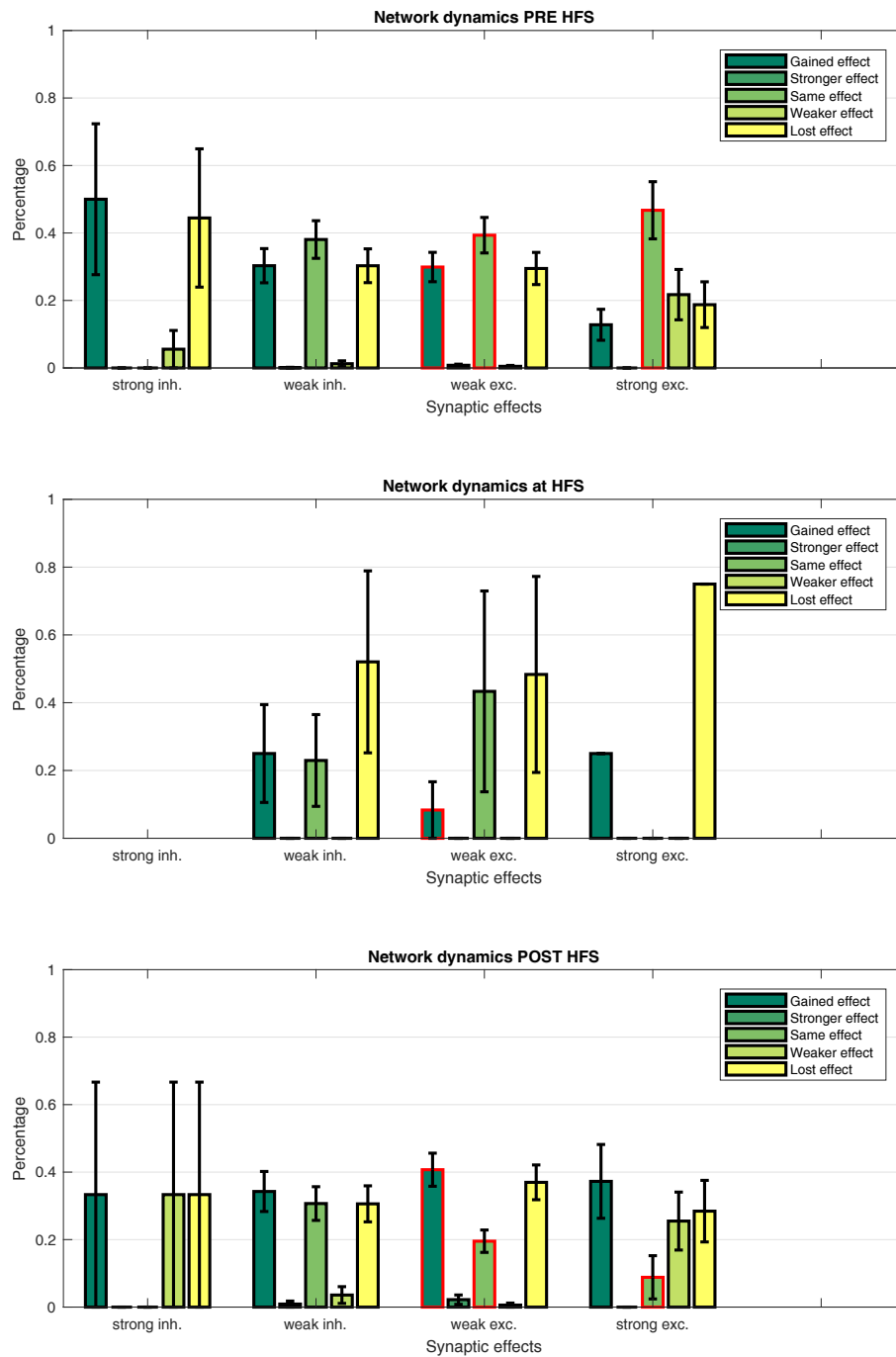


Figure 7.8. – Network dynamics for HF stimulation at DG with long recordings: The representation with standard error bars is based on three experiments. Significant differences are marked in red.

Dynamics in CA1

In CA1, more weak inhibitory effects disappeared with HF stimulation than before and after stimulation. It is also interesting that the dynamics before and after the stimulation are very similar. If the neural network is not externally influenced, the behaviour of dynamics is predictable.

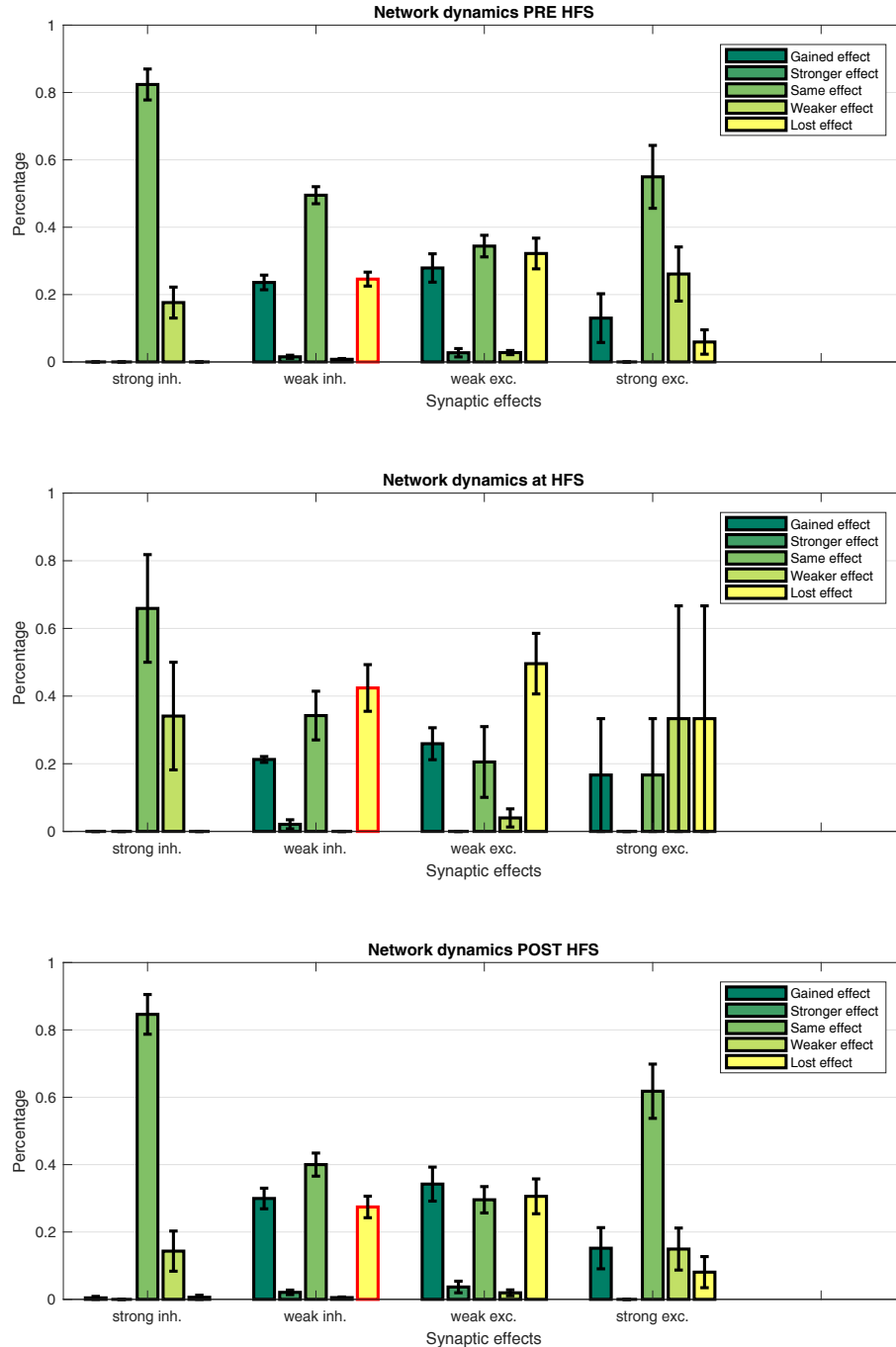


Figure 7.9. – Network dynamics for HF stimulation at CA1 with long recordings: The representation with standard error bars is based on three experiments. Significant differences are marked in red.

Dynamics in CA3

In CA3, strong synaptic effects rarely appeared. For weak synaptic effects, CA3 generally is more flexible than EC, DG and CA1. The effective connectivity became even more unstable thru the HF stimulation.

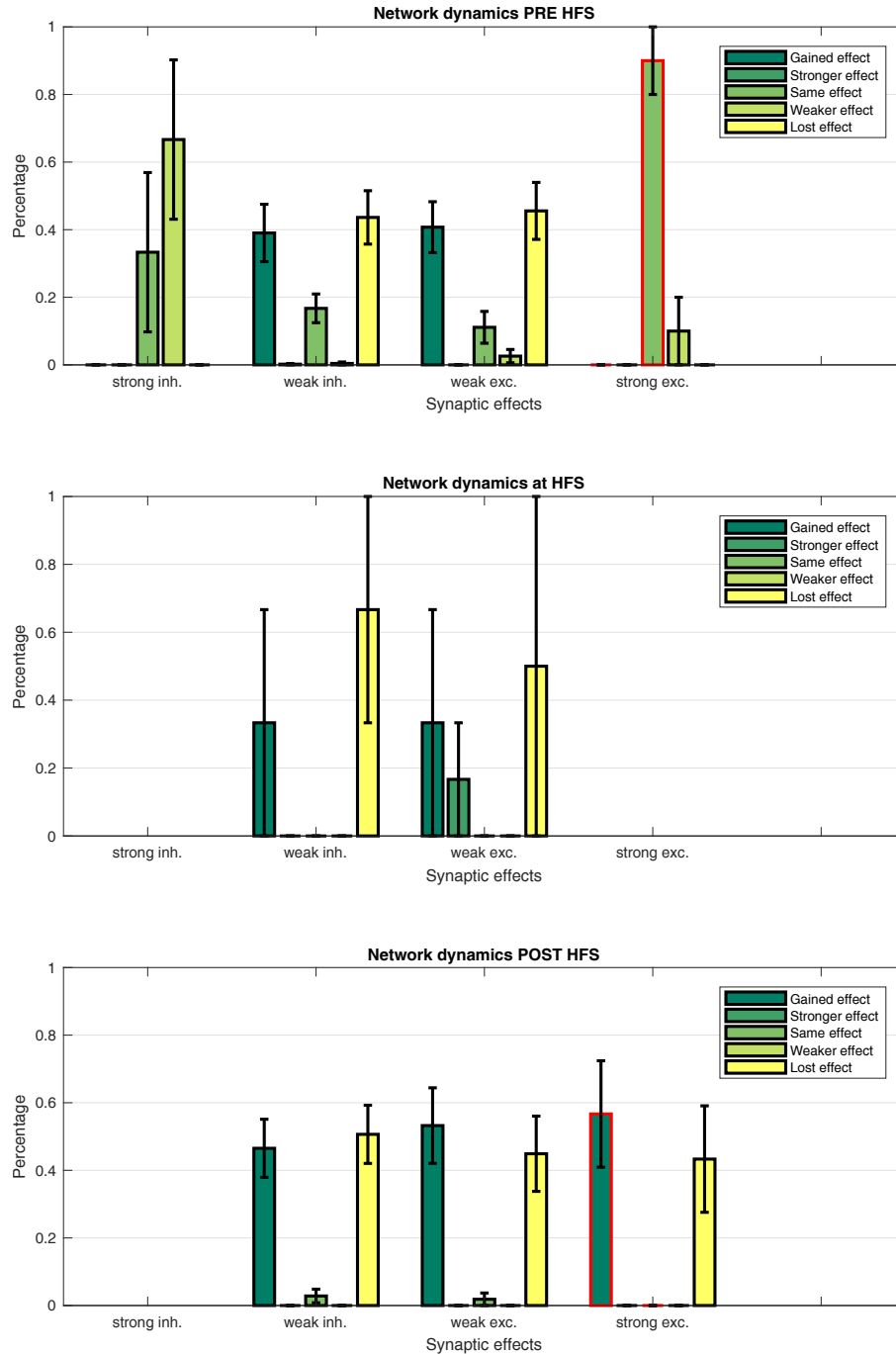


Figure 7.10. – Network dynamics for HF stimulation at CA3 with long recordings: The representation with standard error bars is based on three experiments. Significant differences are marked in red.

Dynamics in EC

In EC, strong inhibitory effects were rather lost during HF stimulation. However, after the stimulation weak inhibitory effects are more stable than before.

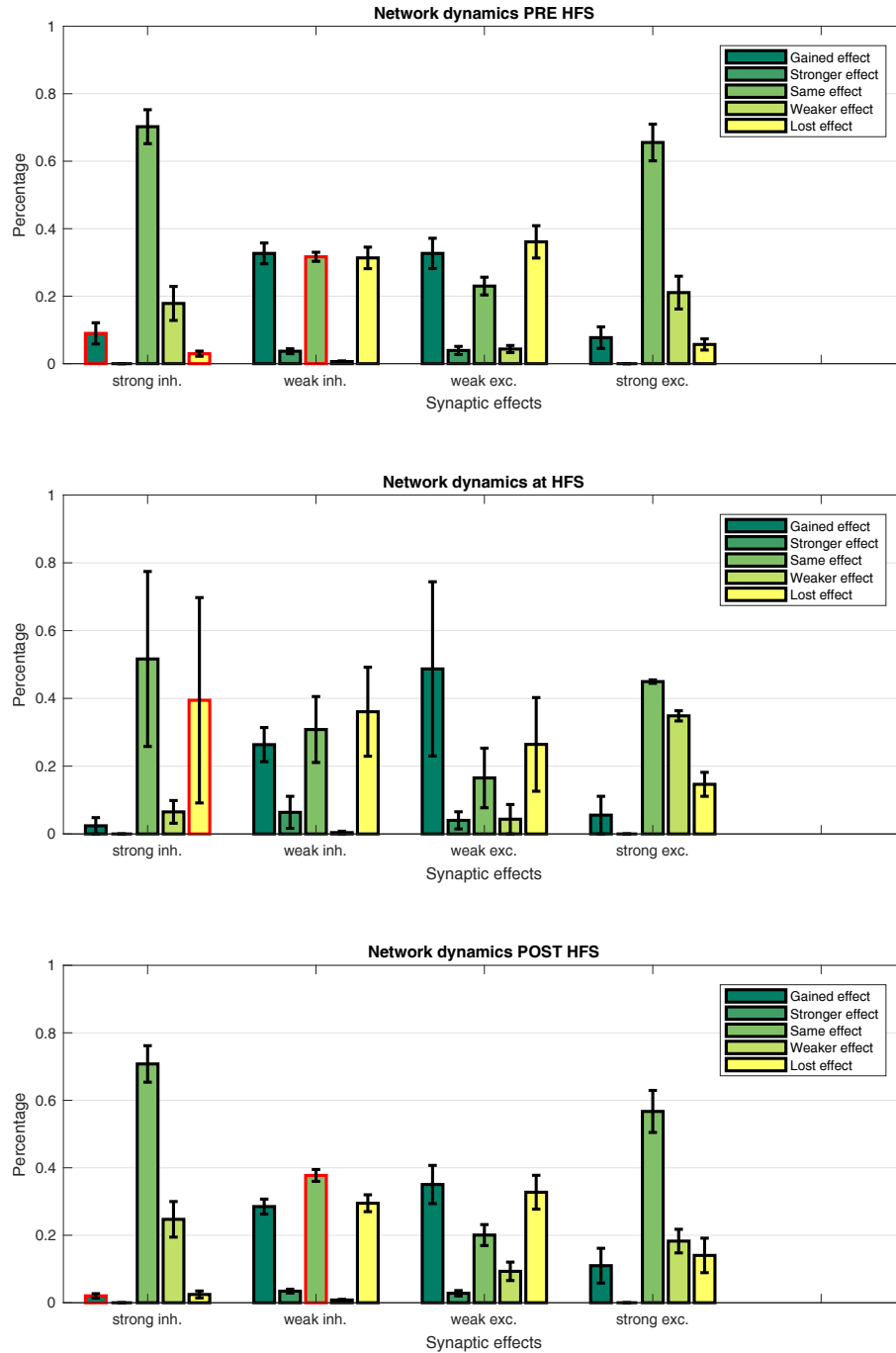


Figure 7.11. – Network dynamics for HF stimulation at EC with long recordings: The representation with standard error bars is based on three experiments. Significant differences are marked in red.

7.5.3. Interchamber comparison

To this point, the K-S tests have been applied to the comparison of states in each chamber. Another exciting aspect is the comparison between the chambers, the so-called interchamber comparison. Do the chambers generally behave differently? Does the stimulation influence the chambers in different ways?

To answer these questions, the K-S test is applied to the same states of different chambers ($\alpha = 0.05$). The analysis of recording datasets were used (for description see Section 7.5.2). In this way there were multiple significant statements obtained, which are listed below.

CA3

Weak inhibitory and excitatory effects were less stable in CA3 than in all other chambers. This observation was not changed for weak inhibitory effects by the HF stimulation. After 5 minutes also the weak excitatory effects were less stable again. In contrast, the strong excitatory effects were more stable in CA3 than in all other chambers before stimulation. This changed after HF stimulation, since strong excitatory effects were less stable in CA3 than EC and CA1. The instability of weak inhibitory effects is justified by the amount of gained effects in CA3 (larger than in EC and CA1) before stimulation and the amount of lost effects in CA3 (larger than in EC and CA1) after stimulation. Furthermore, after the stimulation there were more often weak inhibitory and strong excitatory effects gained in CA3 than CA1 and EC. Also weak excitatory effects were more often gained in CA3 (here in contrast to CA1 and DG).

CA3 and DG

Weak inhibitory effects became less often stronger in CA3 and DG than in EC and CA1 before the stimulation.

DG

Strong effects were less stable in DG than in EC and CA1 after stimulation.

EC

Strong inhibitory effects were gained more often in EC than in CA3 and CA1 before the stimulation. The stimulation affected the weak inhibitory effects, which became more often stronger in EC than in all other chambers after stimulation. Furthermore, these effects were gained less often in EC than in DG and CA3.

EC and CA1

Weak excitatory effects became more often weaker in EC and CA1 than in DG and CA3 before stimulation. This observation was not changed for EC by the HF stimulation.

CA1

Weak inhibitory effects were more stable in CA1 than in all other chambers before stimulation. The stimulation affected excitatory effects (weak and strong), which were more stable in CA1 than in DG and CA3 after stimulation.

7.6. Discussion

Within the scope of the research project of the biomems lab (UAS Aschaffenburg) and the MIND (UCI) TSPE was successfully used to estimate the connectivity of neuronal networks in complex experiments. These experiments were designed with a four-chamber system interconnected with micro-tunnels [94] for different sub-regions of the brain.

The workflow creating the connectivity graphs from raw data measured by 120 channel MEA chips from neuronal cells was explained and implemented. Eight experiments were analysed in terms of the influence on connectivity depending on stimulation with different protocols. Statistical methods were used to find and prove such influences.

Due to the complex experimental setup, it was not possible to use the estimated connectivity for statistically significant statements about graph theory. However, the changing of estimated connectivity with TSPE proved different behaviour for the chambers. In DG weak excitatory effects became unstable by the θ and HF stimulation, while the single stimulation gained new effects. Furthermore, the interchamber comparisons led to many statements. These could improve the understanding of the differences in brain regions. The continuation of this project would include the biological interpretation of these results.

8.

Conclusion and outlook

In this thesis the three types of neuronal network connectivity were presented as well as methods for estimating the functional connectivity according to the state of the art. Only algorithms with a higher potential of good performances are considered for a scenario measuring signals of a small subset of a large scale neuronal network, which is more realistic for most *in vitro* and *in vivo* applications. Furthermore, a novel estimation algorithm for effective connectivity was proposed called *Total Spiking Probability Edges* (TSPE). The new algorithm is based on cross-correlation and detects correlation by edge filtering on different time scales of the cross-correlogram. Since the number of recorded neurons can be tremendous with the usage of new technologies like the HDMEA chip, used algorithms have to be highly computationally effective.

A large framework of *in silico* networks was designed to benchmark the performance of all selected approaches. As the topology of an *in silico* network can affect the results and accuracy of algorithms [34], such a multi-topology evaluation is essential to evaluate the performance of connectivity estimation. Usage of at least one *scale-free network* implementation is necessary for good, sufficient biological plausibility due to more realistic MFR. The findings of the modelling of this framework were presented at the *POSTER 2018* on May 10, 2018 at Faculty of Electrical Engineering, Czech Technical University (CTU) Prague [35]. For future evaluations, a standardised method improves an effective research of neurocomputational algorithms. Widely used and uniform benchmarking makes it easier to compare newly developed methods with previous methods. Moreover, the further development and improvement of intergroup research is possible in a simpler way.

The novel method TSPE is able to outperform the accuracy of all tested state of the art connectivity estimation algorithms (NCC, NCCCI, DHOTE, DHOTECI, DTE, DTECI and CDHOTE) when applied to simulated neuronal network data with different topology complexity. In addition to improved accuracy, TSPE is able to distinguish between distinguish inhibitory and excitatory synaptic effects. This ability is one of the current challenges of connectivity estimation methods [102, 103]. In this way TSPE will help to understand neural communication. TSPE and the evaluation results were published at the *Journal of Neuroscience Methods* [87].

Different approaches to select the threshold for the resulting CM have been evaluated, which is the final step of the connectivity estimation. Depending on the topology and complexity of the network, different methods perform better. This makes it difficult to reach a general recommendation. The results of easy threshold calculation (absolute mean value + 2 SD) and the surrogate threshold calculation (mean value \pm 4 SD) were promising with reproducible results.

For the BaCaTeC project *Estimation of Effective Connectivity in Neuronal Networks*, TSPE was applied to complex experiments to understand the communication between brain regions. This application example was also used to explain the processing of the raw signals step by step up to the connectivity graphs. Graph theoretically based analyses were not successful due to quality differences between the cultures. However, by the connectivity estimation results of TSPE different network dynamics were observed. This contributes to a better understanding of how learning and memory are staged operations.

Experimental setups, which include HDMEA chips, enable measurements of thousands of neurons in a network [25] and thus improved graph-theoretical calculations. Repeating the experimental work with HDMEA chips could lead to further understanding with calculated MPL and small-world-ness for each chamber. Since the number of spike train comparisons and the associated computational effort will increase exponential, the use of a high performance computer is recommended.

All tested connectivity estimation methods are based on analysis of spike train data. The collection of additional data (f.e. optical data) in combination with the spike train data can be used to improve the methods. Since effective and functional connectivity is a subset of structural connectivity, optical methods can be used to discard connections that are not visible [104]. Furthermore, there are approaches to combine ROC based classifiers [105] that can further improve the connectivity estimation accuracy.

Experimental applications such as neurotoxicity measurements will benefit from connectivity estimation as a number of new parameters can be calculated to observe changes, e.g. MPL, connection density or cost, hubs, centrality or robustness [11].

Appendices

A.

Hudgkin-Huxley model

One of the most realistic mathematical descriptions of neurons is the HH model, which was introduced by Hodgkin and Huxley in 1952 [36] and honored with the Nobel Prize in 1963. They measured at a giant axon of a squid different influences of ion channels and pumps on the resulting membrane current I . In detail they took basically the ions sodium Na^+ and potassium K^+ into account. While these ions contribute to the membrane current directly in form of I_K and I_{Na} there are also other influences which are summarized to a leakage current I_l (mainly consists of Cl^- ions).

$$I = I_l + I_K + I_{Na} \quad (A.1)$$

This current passes through the channels but there is also a capacitive current I_C . The unknown membrane capacity C will then be charged or uncharged. This causes a membrane voltage change.

$$C \cdot \dot{u} = -I + I_C \quad (A.2)$$

Mathematically so called gating variables n , m and h define the activation and inactivation of ion channels. Together with experimentally defined conductances of ion channels \hat{g}_K and \hat{g}_{Na} influences are more precisely realized.

$$I_K = \hat{g}_K \cdot n^4 \cdot (u - u_K) \quad (A.3)$$

$$I_{Na} = \hat{g}_{Na} \cdot m^3 \cdot h \cdot (u - u_{Na}) \quad (A.4)$$

Each of the gating variables obeys its own dynamics which are described by a difference equation.

$$\dot{n} = \alpha_n(u) \cdot (1 - n) - \beta_n(u) \cdot n \quad (A.5)$$

$$\dot{m} = \alpha_m(u) \cdot (1 - m) - \beta_m(u) \cdot m \quad (A.6)$$

$$\dot{h} = \alpha_h(u) \cdot (1 - h) - \beta_h(u) \cdot h \quad (A.7)$$

The here used voltage-dependent transition rates $\alpha_n(u)$, $\alpha_m(u)$, $\alpha_h(u)$, $\beta_n(u)$, $\beta_m(u)$ and $\beta_h(u)$ are exponential functions of the membrane voltage u . Their definition was also part of the experimental work of Hodgkin and Huxley. This model is able to imitate and explain the function of a single neuron in many ways. Simulate a whole network of HH models leads to a realistic behaviour but for each neuron there would be the need of multidimensional difference equations. Especially taking the runtime of simulations into account the HH model seems to be inflated with its four difference equations. For this simple reason many researchers tried to decrease dimensions in order to simulate larger networks. For example, a famous two-dimensional simplification of the HH model is called FitzHugh-Nagumo model [106]. Since for this work only the spiking times are of interest, easier neuron models should work out and be less computationally intensive.

B.

Integrate-and-Fire model

The IF model is one of the most easiest neuron models to understand the main function of a single neuron. Every receiving spike of a neuron integrates the membrane voltage with specific weights until a threshold is reached, than the receiving neuron will also fire, which means it will emit a spike. Someone could imagine a neuron as simple repeater of neuronal signals. Basically there are two operating principles of IF models: Conductance-Based (COBA) and Current-Based (CUBA) impacts. One of the most famous IF models was designed to study the propagation of signals [37]. Let us concentrate on their COBA version. Excitatory and inhibitory neurons obeys the same dynamics with time $\tau = 20$ ms.

$$\tau \cdot \dot{v} = (V_{rest} - v) + g_{ex} \cdot (E_{ex} - V_{rest}) + g_{inh} \cdot (E_{inh} - V_{rest}) \quad (B.1)$$

It is also possible to make the equation B.1 easier by summarizing constant values and using a different factor for the effective synaptic conductances g_{ex} and g_{inh} .

$$\tau \cdot \dot{v} = (V_{rest} - v) + g_{ex} + g_{inh} \quad (B.2)$$

There are also used dynamics for both conductances with different time constants, where $\tau_{ex} = 5$ ms and $\tau_{inh} = 10$ ms.

$$\tau_{ex} \cdot \dot{g}_{ex} = -g_{ex} \quad (B.3)$$

$$\tau_{inh} \cdot \dot{g}_{inh} = -g_{inh} \quad (B.4)$$

Reversal potentials are chosen as $E_{ex} = 0$ mV and $E_{inh} = -80$ mV. After each spike the membrane potential of the firing neuron will be overwrite with these values. The original model does not use synaptic distances in form of delays. Thus, DM was introduced, which delivers a specific delay in range of 1 to 20 ms for each existing connection. Nevertheless, since network bursts can be measured at real data, non-existing of tonic spiking is a problem for realistic testing algorithms with this model.

C.

Comparison of neuronal models

Izhikevich reviewed eleven widely used neuron models for 20 neuro-computational features and biological plausibility. He also evaluated the implementation cost in form of Float Operations (FLOPs). In Figure C.1 the original summary of his studies is shown. Simulating HH models in a realistic number for networks is too computationally intensive. For thousands of simulated spiking neurons the IF model is most efficient. In contrast, the Izhikevich model is also efficient but even able to exhibit most firing patterns [38].

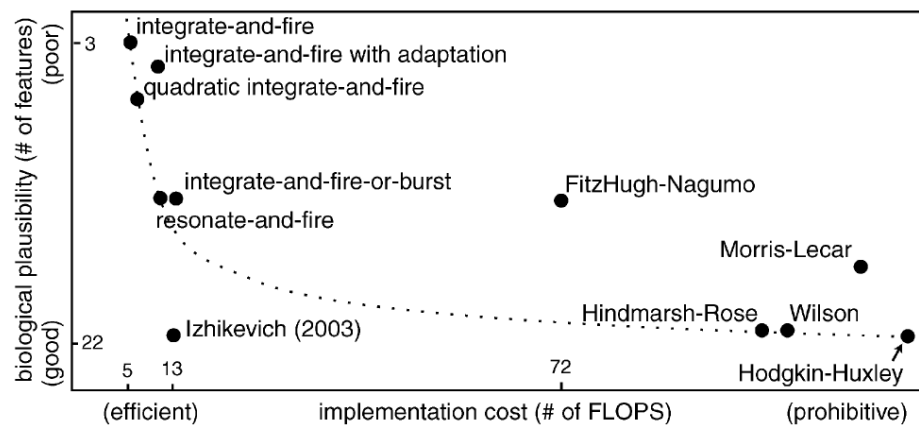


Figure C.1. – Comparison of neuronal models: Eleven neuronal models are evaluated taking into account the implementation cost in form of FLOPs and biological plausibility measured by the number of possible features (e.g. tonic spiking, tonic bursting or integrator). Figure and information by Izhikevich [38].

D.

Simulation software

Many research groups work with simulated biological neuronal networks or even try to improve them further. Over years lot of simulators were published and evaluated. For example, Vitay compared the most widely used simulators, see Figure D.1 [107]. Since *Brain 2* is implemented to be easy to use and learn, it is recommended for starter to build networks. Another reason is the fact *Auryn*, *ANNarchy* and *NEST* are not designed for Microsoft Windows, which is the most often used operation system on desktop computers in 2017. For *NEST* there exist workarounds with virtual machines or *Cygwin*. In that case the computer is not able to use its full resources. For professional long term simulation projects of complex neuronal networks with more than 5000 neurons and STDP for example C++ based *Auryn* on a Linux system is highly recommended. Since the used simulations are based on the Izhikevich model, there is also an option of using *MATLAB* of MathWorks. Easier modifying and debugging are possible and an optional visualization every second is noteworthy, while a longer runtime is a disadvantage. At this state of the project we use *MATLAB* because there is just the need of a few simulation runs. A future bachelor thesis by a colleague of mine will deal with further implementation ideas.

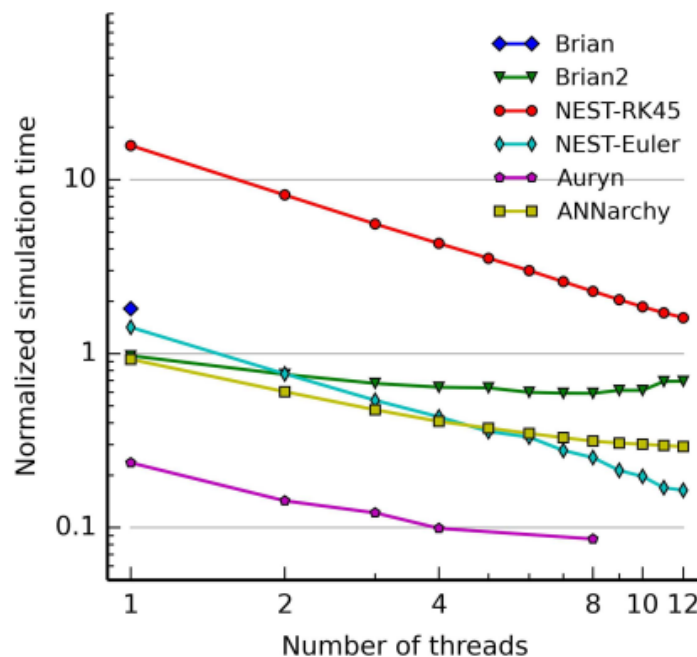


Figure D.1. – Comparison of simulation software: *Brian* (version 1.4.1), *Brian 2* (version 2.0b3), *NEST* (with *Python* bindings, version 2.4.2), *Auryn* (version 0.4.1) and *ANNarchy* (version 4.4.0) are compared in context of simulation times depending on threads of a shared-memory system. Simulation times are normalized: One runtime second per simulated second means one in normalized simulation time. Figure and information by Vitay [107].

E.

Mutual Information

MI is a classic tool of probability theory, which measures the dependence between two random processes, which are in this case spike trains [108]. The standard MI of formula (E.1) is able to detect also nonlinear correlations but does not provide any information of causality because of its symmetry, see formula (E.2). Thus, it is more often used to estimate the synchrony. Using two as base of the logarithm leads to bits as result unit.

$$MI_{XY} = \sum_{x \in X} \sum_{y \in Y} P(x, y) \cdot \log_2 \frac{P(x, y)}{P(x) \cdot P(y)} \quad (\text{E.1})$$

$$MI_{XY} = MI_{YX} \quad (\text{E.2})$$

However, by introducing a time shift for one spike train (E.3) and calculating MI for many delays, statements about causality are possible [65, 108]. Each peak value of $MI_{XY}(d)$ for all neuron pairs is stored in the resulting CM.

$$MI_{XY}(d) = \sum_{x \in X} \sum_{y \in Y} P(x_i, y_{i-d}) \cdot \log_2 \frac{P(x_i, y_{i-d})}{P(x) \cdot P(y_{i-d})} \quad (\text{E.3})$$

Binary or multistage binning is possible, but leads to an exponential gain of calculation operations. Garofalo evaluated MI with delay shifting in 2009 and came to the conclusion of a bad performance in comparison to CC and TE [53].

F.

TSPE MATLAB Code

```
1 function [CMres, DMres] = TSPE(sdf, d, neg_wins, co_wins, pos_wins, FLAG_NORM)
2 % Parameters:
3 %   sdf           – Time series in Spike Data Format (SDF)
4 %   d             – Maximal delay time (default 25)
5 %   neg_wins      – Windows for before and after area of interest (default [3, 4,
6 %   5, 6, 7, 8])
7 %   co_wins       – Cross-over window size (default 0)
8 %   pos_wins      – Sizes of area of interest (default [2, 3, 4, 5, 6])
9 %   jitt          – Jitter-Window-Size (default 4)
10 %   FLAG_NORM     – 0 – no usage of normalization (default)
11 %                – 1 – usage of normalization
12 % Returns:
13 %   CMres         – NxN matrix where N(i, j) is the total spiking probability
14 %                 edges (TSPE) i→j
15 %   DMres         – NxN matrix where N(i, j) is the transmission time with highest
16 %                 TSPE Value i→j
17 %
18 % Wrote by Stefano De Blasi, UAS Aschaffenburg in 2018
19
20 switch nargin
21   case 1
22     d = [];
23     neg_wins = [];
24     co_wins = [];
25     pos_wins = [];
26     FLAG_NORM = [];
27   case 2
28     neg_wins = [];
29     co_wins = [];
30     pos_wins = [];
31     FLAG_NORM = [];
32   case 3
33     co_wins = [];
34     pos_wins = [];
35     FLAG_NORM = [];
36   case 4
37     pos_wins = [];
38     FLAG_NORM = [];
39   case 5
40     FLAG_NORM = [];
41   case 6
42     % all parameters are already set
43   otherwise
44     error('Input error.')
```

```
44 if isempty(pos_wins)
45     pos_wins=[2, 3, 4, 5, 6];
46 end
47 if isempty(co_wins)
48     co_wins=0;
49 end
50 if isempty(neg_wins)
51     neg_wins=[3, 4, 5, 6, 7, 8];
52 end
53 if isempty(d)
54     d=25;
55 end
56 if isempty(FLAG_NORM)
57     FLAG_NORM=0;
58 end
59
60 %% Generation of sparse matrices
61 a=sdf{end};
62 NrC = a(1);
63 vec1=[];
64 vec2=[];
65 for i=1:NrC
66     vec1=[vec1 sdf{i}];
67     vec2=[vec2 i*ones(1,length(sdf{i}))];
68 end
69 mat=sparse(vec1(vec1>0 & vec1 <= a(2)),vec2(vec1>0 & vec1 <= a(2)),1,a(2),a
    (1));
70 NrS=a(2);
71
72 %% Calculation of std deviation and mean values
73 l=ones(1,NrS);
74 u_mean=l*mat/NrS;
75 u_0=mat-u_mean;
76 r=std(u_0);
77
78 %% Fast Cross-Correlation
79 ran=1-max(neg_wins)-max(co_wins):max(neg_wins)+d;
80 CM=zeros(length(ran),NrC,NrC);
81 ind=max(neg_wins)+max(co_wins);
82 if(ind <= 0)
83     ind=1;
84 end
85 for i=0:d+max(neg_wins)
86     CM(ind, :, :)=(mat(1+i:end, :)'*mat(1:end-i, :))./(r'*r)/NrS;
87
88     % Correct form:
89     % CM(ind, :, :)=(u_0(1+i:end, :)'*u_0(1:end-i, :))./(r'*r)/NrS;
90     % takes longer, no performance impact
91
92     ind=ind+1;
93 end
94
95 % Usage of symmetric construction of cross correlation for faster
96 % calculation:
97 if(max(neg_wins)+max(co_wins) > 0)
98     bufCM=zeros(NrC);
99     ind=0;
100     for j=max(neg_wins)+max(co_wins)-1:-1:1
```

```

101         bufCM(:)=CM(max(neg_wins)+max(co_wins)+j, :, :);
102         ind=ind+1;
103         CM(ind, :, :)=bufCM';
104     end
105 end
106
107 %% Additional scaling for reduction of network burst impacts:
108 if FLAG_NORM
109     s=zeros(length(ran),1);
110     for i=1:length(ran)
111         zwi=CM(i, ~ diag(ones(NrC,1)));
112         s(i)=sum(sum( zwi(~ isnan(CM(i, ~ diag(ones(NrC,1)))))));
113     end
114     CM=CM./s;
115 end
116
117 %% Generation of edge filters
118 WB=max(neg_wins)+max(co_wins);
119 sumWin=zeros(d+WB,NrC,NrC);
120 in=0;
121 for win_before=neg_wins
122     for win_p1=co_wins
123         for win_in=pos_wins
124             in=in+1;
125             win_p2=win_p1;
126             win_after=win_before;
127             windows{in}=[-1*ones(win_before,1)/win_before; zeros(win_p1,1);2/
                win_in*ones(win_in,1);zeros(win_p2,1);-1*ones(win_after,1)/
                win_after];
128             beginnings{in}=1+WB-win_before-win_p1;
129             win_inner{in}=win_in;
130         end
131     end
132 end
133 m=d+max(neg_wins)+max(co_wins)+max(pos_wins);
134
135 %% Usage of edge filters:
136 for j=1:in
137     CM3=convn(convn(CM(beginnings{j}:end, :, :),windows{j},'valid'),[
        ones(win_inner{j},1)], 'full');
138     m=min(m,length(CM3(:,1,1)));
139     sumWin(1:size(CM3,1), :, :)=CM3+sumWin(1:size(CM3,1), :, :);
140 end
141
142 %% Only look at valid window
143 sumWin=sumWin(1:m, :, :);
144
145 %% Adjustment and looking for maximum at each delay time
146 sumWin=permute(sumWin, [1 3 2]);
147 [~,index] = max(abs(sumWin));
148 CMres=zeros(NrC);
149 DMres=index;
150 for i=1:size(sumWin,2)
151     CMres(:,i)=sumWin(sub2ind(size(sumWin), index(1,1:size(sumWin,2),i), 1:
        size(sumWin,2), i * ones(1,size(sumWin,2))));
152 end
153
154 end

```



Content of DVD

The attached DVD contains several data related to the work during the candidature for a research degree at UAS Aschaffenburg:

- Documents
 - Thesis (PDF)
 - Submitted journal paper (PDF)
 - Presented conference poster (PDF)
 - Submitted conference paper (PDF)
 - Literature (PDF)
- Written functions and code
 - *MATLAB* code
 - *Python* code
 - *C++* code
- Data
 - Evaluation data
 - Experimental data

Bibliography

- [1] J. Olesen and M. Leonardi. "The burden of brain diseases in Europe". In: *European Journal of Neurology* 10.5 (2003), pp. 471–477. ISSN: 1351-5101. DOI: 10.1046/j.1468-1331.2003.00682.x.
- [2] A. Bhatti, K. H. Lee, and H. Garmestani. *Emerging Trends in Neuro Engineering and Neural Computation*. Series in BioEngineering. Springer Singapore, 2017. ISBN: 978-981-10-3957-7.
- [3] J. L. Pinyon et al. "Close-field electroporation gene delivery using the cochlear implant electrode array enhances the bionic ear". In: *Science translational medicine* 6.233 (2014), 233ra54. ISSN: 1946-6242. DOI: 10.1126/scitranslmed.3008177.
- [4] Y. H.-L. Luo and L. da Cruz. "A review and update on the current status of retinal prostheses (bionic eye)". In: *British medical bulletin* 109 (2014), pp. 31–44. ISSN: 1471-8391. DOI: 10.1093/bmb/1du002.
- [5] K. Deisseroth. "Optogenetics". In: *Nature methods* 8.1 (2011), pp. 26–29. ISSN: 1548-7105. DOI: 10.1038/nmeth.f.324.
- [6] O. Svendsen. "Ethics and animal welfare related to in vivo pharmacology and toxicology in laboratory animals". In: *Basic & clinical pharmacology & toxicology* 97.4 (2005), pp. 197–199, 197–199. ISSN: 1742-7835. DOI: 10.1111/j.1742-7843.2005.pto_letter_974.x.
- [7] G. M. Shepherd and K. M. Harris. "Three-dimensional structure and composition of CA3–CA1 axons in rat hippocampal slices: implications for presynaptic connectivity and compartmentalization". In: *The Journal of neuroscience : the official journal of the Society for Neuroscience* 18.20 (1998), pp. 8300–8310. ISSN: 1529-2401.
- [8] M. Mayer et al. "Human Embryonic Stem Cell Derived Neurospheres - A Novel Three Dimensional Model For Neurotoxicological Studies". In: *Frontiers in Neuroscience* 10 (2016). ISSN: 1662-453X. DOI: 10.3389/conf.fnins.2016.93.00081.
- [9] D. Flachs and M. Ciba. "Cell-Based Sensor Chip for Neurotoxicity Measurements in Drinking Water". In: *Lékař a technika - Clinician and Technology* 46.2 (2016), pp. 46–50. ISSN: 2336-5552.
- [10] T. Köhler et al. *TETRA specific long-term exposure of neuronal in vitro networks*. 2016.
- [11] E. Bullmore and O. Sporns. "Complex brain networks: graph theoretical analysis of structural and functional systems". In: *Nature reviews. Neuroscience* 10.3 (2009), pp. 186–198. ISSN: 1471-0048. DOI: 10.1038/nrn2575.
- [12] P. Dayan and L. F. Abbott. *Theoretical neuroscience: Computational and mathematical modeling of neural systems*. Computational neuroscience. Cambridge Mass. and London: MIT, 2005. ISBN: 0-262-54185-8.
- [13] Jarosz Quasar. *Creative Commons — Attribution-ShareAlike 3.0 Unported — CC BY-SA 3.0*.
- [14] W. Gerstner. *Neuronal dynamics: From single neurons to networks and models of cognition*. 1. publ. Cambridge: Cambridge Univ. Press, 2014. ISBN: 978-1-107-06083-8.
- [15] D. O. Hebb. *The organization of behavior a neuropsychological approach*. New York NY: John Wiley & Sons, 1949.

-
- [16] K. J. Friston. "Functional and effective connectivity in neuroimaging: A synthesis". In: *Human Brain Mapping* 2.1-2 (1994), pp. 56–78. ISSN: 10659471. DOI: 10.1002/hbm.460020107.
 - [17] D. Poli, V. P. Pastore, and P. Massobrio. "Functional connectivity in in vitro neuronal assemblies". In: *Frontiers in neural circuits* 9 (2015), p. 57. ISSN: 1662-5110. DOI: 10.3389/fncir.2015.00057.
 - [18] O. Sporns, G. Tononi, and R. Kötter. "The human connectome: A structural description of the human brain". In: *PLoS computational biology* 1.4 (2005), e42. ISSN: 1553-7358. DOI: 10.1371/journal.pcbi.0010042.
 - [19] T. Saneyoshi, D. A. Fortin, and T. R. Soderling. "Regulation of spine and synapse formation by activity-dependent intracellular signaling pathways". In: *Current opinion in neurobiology* 20.1 (2010), pp. 108–115. ISSN: 1873-6882. DOI: 10.1016/j.conb.2009.09.013.
 - [20] P. A. Buchs and D. Muller. "Induction of long-term potentiation is associated with major ultrastructural changes of activated synapses". In: *Proceedings of the National Academy of Sciences* 93.15 (1996), pp. 8040–8045. ISSN: 0027-8424. DOI: 10.1073/pnas.93.15.8040.
 - [21] R. Renault et al. "Combining microfluidics, optogenetics and calcium imaging to study neuronal communication in vitro". In: *PloS one* 10.4 (2015), e0120680. ISSN: 1932-6203. DOI: 10.1371/journal.pone.0120680.
 - [22] O. Sporns. "Network analysis, complexity, and brain function". In: *Complexity* 8.1 (2002), pp. 56–60. ISSN: 1076-2787. DOI: 10.1002/cplx.10047.
 - [23] L. F. Abbott. "Synaptic Depression and Cortical Gain Control". In: *Science* 275.5297 (1997), pp. 221–224. ISSN: 00368075. DOI: 10.1126/science.275.5297.221.
 - [24] K. J. Friston. "Functional and effective connectivity: A review". In: *Brain connectivity* 1.1 (2011), pp. 13–36. ISSN: 2158-0022. DOI: 10.1089/brain.2011.0008.
 - [25] L. Berdondini et al. "Active pixel sensor array for high spatio-temporal resolution electrophysiological recordings from single cell to large scale neuronal networks". In: *Lab on a chip* 9.18 (2009), pp. 2644–2651. ISSN: 1473-0197. DOI: 10.1039/b907394a.
 - [26] J.-O. Muthmann et al. "Spike Detection for Large Neural Populations Using High Density Multielectrode Arrays". In: *Frontiers in neuroinformatics* 9 (2015), p. 28. ISSN: 1662-5196. DOI: 10.3389/fninf.2015.00028.
 - [27] I. Obeid and P. D. Wolf. "Evaluation of spike-detection algorithms for a brain-machine interface application". In: *IEEE transactions on bio-medical engineering* 51.6 (2004), pp. 905–911. ISSN: 0018-9294. DOI: 10.1109/TBME.2004.826683.
 - [28] A. Maccione et al. "A novel algorithm for precise identification of spikes in extracellularly recorded neuronal signals". In: *Journal of neuroscience methods* 177.1 (2009), pp. 241–249. ISSN: 0165-0270. DOI: 10.1016/j.jneumeth.2008.09.026.
 - [29] H.-L. Chan et al. "Detection of neuronal spikes using an adaptive threshold based on the max-min spread sorting method". In: *Journal of neuroscience methods* 172.1 (2008), pp. 112–121. ISSN: 0165-0270. DOI: 10.1016/j.jneumeth.2008.04.014.
 - [30] F. Lieb, H.-G. Stark, and C. Thielemann. "A stationary wavelet transform and a time-frequency based spike detection algorithm for extracellular recorded data". In: *Journal of neural engineering* 14.3 (2017). ISSN: 1741-2552. DOI: 10.1088/1741-2552/aa654b.
 - [31] C. Nick et al. "DrCell – A Software Tool for the Analysis of Cell Signals Recorded with Extracellular Microelectrodes". In: *Signal Processing: An International Journal* 7 (2013), pp. 96–109.
 - [32] R. Bestel, A. W. Daus, and C. Thielemann. "A novel automated spike sorting algorithm with adaptable feature extraction". In: *Journal of neuroscience methods* 211.1 (2012), pp. 168–178. DOI: <https://doi.org/10.1016/j.jneumeth.2012.08.015>.
-

-
- [33] M. S. Lewicki. "A review of methods for spike sorting: The detection and classification of neural action potentials". In: *Network: Computation in Neural Systems* 9.4 (1998), R53–R78. ISSN: 0954-898X. DOI: 10.1088/0954-898X_9_4_001.
 - [34] B. Kadirvelu, Y. Hayashi, and S. J. Nasuto. "Inferring structural connectivity using Ising couplings in models of neuronal networks". In: *Scientific reports* 7.1 (2017), p. 8156.
 - [35] S. De Blasi. "Simulation of Large Scale Neural Networks for Evaluation Applications". In: *arXiv preprint arXiv:1805.08626* (2018).
 - [36] A. L. Hodgkin and A. F. Huxley. "A quantitative description of membrane current and its application to conduction and excitation in nerve". In: *The Journal of Physiology* 117.4 (1952), pp. 500–544. ISSN: 00223751. DOI: 10.1113/jphysiol.1952.sp004764.
 - [37] T. P. Vogels and L. F. Abbott. "Signal propagation and logic gating in networks of integrate-and-fire neurons". In: *The Journal of neuroscience: the official journal of the Society for Neuroscience* 25.46 (2005), pp. 10786–10795. DOI: 10.1523/JNEUROSCI.3508-05.2005.
 - [38] E. M. Izhikevich. "Which model to use for cortical spiking neurons?" In: *IEEE transactions on neural networks* 15.5 (2004), pp. 1063–1070. ISSN: 1045-9227. DOI: 10.1109/TNN.2004.832719.
 - [39] E. M. Izhikevich. "Simple model of spiking neurons". In: *IEEE transactions on neural networks* 14.6 (2003), pp. 1569–1572. ISSN: 1045-9227. DOI: 10.1109/TNN.2003.820440.
 - [40] A. Mason, A. Nicoll, and K. Stratford. "Synaptic transmission between individual pyramidal neurons of the rat visual cortex in vitro". In: *The Journal of neuroscience : the official journal of the Society for Neuroscience* 11.1 (1991), pp. 72–84. ISSN: 1529-2401.
 - [41] H. A. Swadlow. "Efferent neurons and suspected interneurons in motor cortex of the awake rabbit: axonal properties, sensory receptive fields, and subthreshold synaptic inputs". In: *Journal of neurophysiology* 71.2 (1994), pp. 437–453. ISSN: 0022-3077.
 - [42] A.-L. Barabási and M. Pósfai. *Network science*. 2016. ISBN: 1-107-07626-9.
 - [43] A.-L. Barabási and E. Bonabeau. "Scale-free networks". In: *Scientific American* 288.5 (2003), pp. 60–69. ISSN: 0036-8733.
 - [44] D. J. Watts and S. H. Strogatz. "Collective dynamics of 'small-world' networks". In: *Nature*. 393.6684 (1998), pp. 440–442. DOI: 10.1038/30918.
 - [45] R. Cohen and S. Havlin. "Scale-free networks are ultrasmall". In: *Physical review letters* 90.5 (2003). ISSN: 1079-7114. DOI: 10.1103/PhysRevLett.90.058701.
 - [46] O. Sporns, C. J. Honey, and R. Kötter. "Identification and classification of hubs in brain networks". In: *PloS one* 2.10 (2007), e1049. ISSN: 1932-6203. DOI: 10.1371/journal.pone.0001049.
 - [47] P. Bonifazi et al. "GABAergic hub neurons orchestrate synchrony in developing hippocampal networks". In: *Science (New York, N.Y.)* 326.5958 (2009), pp. 1419–1424. ISSN: 1095-9203. DOI: 10.1126/science.1175509.
 - [48] M. Catanzaro, M. Boguñá, and R. Pastor-Satorras. "Generation of uncorrelated random scale-free networks". In: *Physical review. E, Statistical, nonlinear, and soft matter physics* 71.2 Pt 2 (2005), p. 027103. ISSN: 1539-3755. DOI: 10.1103/PhysRevE.71.027103.
 - [49] E. M. Izhikevich. "Polychronization: computation with spikes". In: *Neural computation* 18.2 (2006), pp. 245–282. ISSN: 0899-7667. DOI: 10.1162/089976606775093882.
 - [50] P. Erdos. "Graph theory and probability". In: *canad. J. Math* 11.11 (1959), pp. 34–38.
 - [51] A. Hagberg, P. Swart, and D. S. Chult. *Exploring network structure, dynamics, and function using NetworkX*. Tech. rep. Los Alamos National Lab.(LANL), Los Alamos, NM (United States), 2008.
-

-
- [52] P. Song and X.-J. Wang. "Angular path integration by moving "hill of activity": a spiking neuron model without recurrent excitation of the head-direction system". In: *The Journal of neuroscience : the official journal of the Society for Neuroscience* 25.4 (2005), pp. 1002–1014. ISSN: 1529-2401. DOI: 10.1523/JNEUROSCI.4172-04.2005.
 - [53] M. Garofalo et al. "Evaluation of the performance of information theory-based methods and cross-correlation to estimate the functional connectivity in cortical networks". In: *PloS one* 4.8 (2009), e6482. ISSN: 1932-6203. DOI: 10.1371/journal.pone.0006482.
 - [54] V. P. Pastore et al. "SpiCoDyn: A Toolbox for the Analysis of Neuronal Network Dynamics and Connectivity from Multi-Site Spike Signal Recordings". In: *Neuroinformatics* 16.1 (2018), pp. 15–30.
 - [55] S. Ito et al. "Extending transfer entropy improves identification of effective connectivity in a spiking cortical network model". In: *PloS one* 6.11 (2011), e27431. ISSN: 1932-6203. DOI: 10.1371/journal.pone.0027431.
 - [56] B. Gourévitch and J. J. Eggermont. "Evaluating information transfer between auditory cortical neurons". In: *Journal of neurophysiology* 97.3 (2007), pp. 2533–2543. ISSN: 0022-3077. DOI: 10.1152/jn.01106.2006.
 - [57] D. H. Perkel, G. L. Gerstein, and G. P. Moore. "Neuronal Spike Trains and Stochastic Point Processes". In: *Biophysical Journal* 7.4 (1967), pp. 391–418. ISSN: 00063495. DOI: 10.1016/S0006-3495(67)86596-2.
 - [58] M. S. Masud, R. Borisyuk, and L. Stuart. "Advanced correlation grid: Analysis and visualisation of functional connectivity among multiple spike trains". In: *Journal of neuroscience methods* 286 (2017), pp. 78–101. ISSN: 0165-0270. DOI: 10.1016/j.jneumeth.2017.05.016.
 - [59] T. Isomura et al. "Connection-Strength Estimation of Neuronal Networks by Fitting for Izhikevich Model". In: *Electrical Engineering in Japan* 187.4 (2014), pp. 42–50. ISSN: 04247760. DOI: 10.1002/eej.22517.
 - [60] T. Isomura et al. "Accurate connection strength estimation based on variational bayes for detecting synaptic plasticity". In: *Neural computation* 27.4 (2015), pp. 819–844. ISSN: 0899-7667. DOI: 10.1162/NECO_a_00721.
 - [61] K. J. Friston et al. "Network discovery with DCM". In: *NeuroImage* 56.3 (2011), pp. 1202–1221. ISSN: 1095-9572. DOI: 10.1016/j.neuroimage.2010.12.039.
 - [62] C. Diekmann et al. "Discovering functional neuronal connectivity from serial patterns in spike train data". In: *Neural computation* 26.7 (2014), pp. 1263–1297. ISSN: 0899-7667. DOI: 10.1162/NECO_a_00598.
 - [63] D. Poli et al. "From functional to structural connectivity using partial correlation in neuronal assemblies". In: *Journal of neural engineering* 13.2 (2016), p. 026023. ISSN: 1741-2552. DOI: 10.1088/1741-2560/13/2/026023.
 - [64] M. Ding, Y. Chen, and S. L. Bressler. "Granger Causality: Basic Theory and Application to Neuroscience". In: *Handbook of time series analysis*. Ed. by B. Schelter, J. Timmer, and M. Winterhalder. Weinheim: Wiley-VCH, 2006, pp. 437–460. ISBN: 9783527609970. DOI: 10.1002/9783527609970.ch17.
 - [65] M. Chávez, J. Martinerie, and M. van Quyen. "Statistical assessment of nonlinear causality: Application to epileptic EEG signals". In: *Journal of neuroscience methods* 124.2 (2003), pp. 113–128. ISSN: 0165-0270. DOI: 10.1016/S0165-0270(02)00367-9.
 - [66] Y. B. Saalmann et al. "The pulvinar regulates information transmission between cortical areas based on attention demands". In: *Science (New York, N.Y.)* 337.6095 (2012), pp. 753–756. ISSN: 1095-9203. DOI: 10.1126/science.1223082.
 - [67] A. Nakhnikian et al. "Behavior modulates effective connectivity between cortex and striatum". In: *PloS one* 9.3 (2014), e89443. ISSN: 1932-6203. DOI: 10.1371/journal.pone.0089443.
-

-
- [68] A. K. Seth. "A MATLAB toolbox for Granger causal connectivity analysis". In: *Journal of neuroscience methods* 186.2 (2010), pp. 262–273. ISSN: 0165-0270. DOI: 10.1016/j.jneumeth.2009.11.020.
 - [69] N. Timme et al. "Multiplex networks of cortical and hippocampal neurons revealed at different timescales". In: *PloS one* 9.12 (2014), e115764. ISSN: 1932-6203. DOI: 10.1371/journal.pone.0115764.
 - [70] P. Barthó et al. "Characterization of neocortical principal cells and interneurons by network interactions and extracellular features". In: *Journal of neurophysiology* 92.1 (2004), pp. 600–608. ISSN: 0022-3077. DOI: 10.1152/jn.01170.2003.
 - [71] V. Pasquale et al. "Self-organization and neuronal avalanches in networks of dissociated cortical neurons". In: *Neuroscience* 153.4 (2008), pp. 1354–1369. ISSN: 0306-4522. DOI: 10.1016/j.neuroscience.2008.03.050.
 - [72] L. Berdondini et al. "Extracellular recordings from locally dense microelectrode arrays coupled to dissociated cortical cultures". In: *Journal of neuroscience methods* 177.2 (2009), pp. 386–396. ISSN: 0165-0270. DOI: 10.1016/j.jneumeth.2008.10.032.
 - [73] A. Maccione et al. "Multiscale functional connectivity estimation on low-density neuronal cultures recorded by high-density CMOS Micro Electrode Arrays". In: *Journal of neuroscience methods* 207.2 (2012), pp. 161–171. ISSN: 0165-0270. DOI: 10.1016/j.jneumeth.2012.04.002.
 - [74] V. P. Pastore et al. "ToolConnect: A Functional Connectivity Toolbox for In vitro Networks". In: *Frontiers in neuroinformatics* 10 (2016), p. 13. ISSN: 1662-5196. DOI: 10.3389/fninf.2016.00013.
 - [75] M. Brosch and C. E. Schreiner. "Correlations between neural discharges are related to receptive field properties in cat primary auditory cortex". In: *The European journal of neuroscience* 11.10 (1999), pp. 3517–3530. ISSN: 0953-816X.
 - [76] T. Kiemel and A. H. Cohen. "Estimation of coupling strength in regenerated lamprey spinal cords based on a stochastic phase model". In: *Journal of computational neuroscience* 5.3 (1998), pp. 267–284. ISSN: 1573-6873.
 - [77] D. Eytan et al. "Dopamine-induced dispersion of correlations between action potentials in networks of cortical neurons". In: *Journal of neurophysiology* 92.3 (2004), pp. 1817–1824. ISSN: 0022-3077. DOI: 10.1152/jn.00202.2004.
 - [78] P. Bedenbaugh and G. L. Gerstein. "Multiunit normalized cross correlation differs from the average single-unit normalized correlation". In: *Neural computation* 9.6 (1997), pp. 1265–1275. ISSN: 0899-7667.
 - [79] M. Chiappalone et al. "Dissociated cortical networks show spontaneously correlated activity patterns during in vitro development". In: *Brain research* 1093.1 (2006), pp. 41–53. ISSN: 0006-8993. DOI: 10.1016/j.brainres.2006.03.049.
 - [80] E. Juergens and R. Eckhorn. "Parallel processing by a homogeneous group of coupled model neurons can enhance, reduce and generate signal correlations". In: *Biological cybernetics* 76.3 (1997), pp. 217–227. ISSN: 0340-1200. DOI: 10.1007/s004220050334.
 - [81] Y. Jimbo, T. Tateno, and H. Robinson. "Simultaneous Induction of Pathway-Specific Potentiation and Depression in Networks of Cortical Neurons". In: *Biophysical Journal* 76.2 (1999), pp. 670–678. ISSN: 00063495. DOI: 10.1016/S0006-3495(99)77234-6.
 - [82] T. Schreiber. "Measuring information transfer". In: *Physical review letters* 85.2 (2000), pp. 461–464. ISSN: 1079-7114. DOI: 10.1103/PhysRevLett.85.461.
 - [83] M. Lungarella and O. Sporns. "Mapping information flow in sensorimotor networks". In: *PLoS computational biology* 2.10 (2006), e144. ISSN: 1553-7358. DOI: 10.1371/journal.pcbi.0020144.
-

-
- [84] O. Stetter et al. "Model-free reconstruction of excitatory neuronal connectivity from calcium imaging signals". In: *PLoS computational biology* 8.8 (2012), e1002653. ISSN: 1553-7358. DOI: 10.1371/journal.pcbi.1002653.
 - [85] L. A. Overbey and M. D. Todd. "Dynamic system change detection using a modification of the transfer entropy". In: *Journal of Sound and Vibration* 322.1-2 (2009), pp. 438–453. ISSN: 0022460X. DOI: 10.1016/j.jsv.2008.11.025.
 - [86] M. Shimono and J. M. Beggs. "Functional clusters, hubs, and communities in the cortical microconnectome". In: *Cerebral Cortex* 25.10 (2014), pp. 3743–3757.
 - [87] S. De Blasi et al. "Total spiking probability edges: A cross-correlation based method for effective connectivity estimation of cortical spiking neurons". In: *Journal of neuroscience methods* 312 (2019), pp. 169–181.
 - [88] A. Date, E. Bienenstock, and S. Geman. "On the temporal resolution of neural activity". In: *Society for Neuroscience Abstracts (Brown University, Division of Applied Mathematics)* (1998).
 - [89] M. Abeles and I. Gat. "Detecting precise firing sequences in experimental data". In: *Journal of neuroscience methods* 107.1-2 (2001), pp. 141–154.
 - [90] A. Pazienti, M. Diesmann, and S. Grün. "Bounds of the ability to destroy precise coincidences by spike dithering". In: *International Symposium on Brain, Vision, and Artificial Intelligence*. Springer. 2007, pp. 428–437.
 - [91] A. Pazienti et al. "Effectiveness of systematic spike dithering depends on the precision of cortical synchronization". In: *Brain research* 1225 (2008), pp. 39–46.
 - [92] D. A. Butts et al. "Temporal precision in the neural code and the timescales of natural vision". In: *Nature* 449.7158 (2007), p. 92.
 - [93] M. D. Humphries and K. Gurney. "Network 'small-world-ness': a quantitative method for determining canonical network equivalence". In: *PloS one* 3.4 (2008), e0002051.
 - [94] L. Pan et al. "An in vitro method to manipulate the direction and functional strength between neural populations". In: *Frontiers in Neural Circuits* 9 (2015), p. 32. ISSN: 1662-5110. DOI: 10.3389/fncir.2015.00032.
 - [95] T. B. DeMarse et al. "Feed-forward propagation of temporal and rate information between cortical populations during coherent activation in engineered in vitro networks". In: *Frontiers in neural circuits* 10 (2016), p. 32.
 - [96] D. Poli et al. "Synchronicity among hippocampal co-cultures in a four-chamber in vitro system". In: *GNB2018* (2018).
 - [97] V. Braitenberg. "Anatomical basis for divergence, convergence, and integration in the cerebral cortex". In: *Sensory Functions*. Elsevier, 1981, pp. 411–419.
 - [98] L. Pan et al. "Propagation of action potential activity in a predefined microtunnel neural network". In: *Journal of neural engineering* 8.4 (2011), p. 046031.
 - [99] G. J. Brewer et al. "Toward a self-wired active reconstruction of the hippocampal trisynaptic loop: DG-CA3". In: *Frontiers in neural circuits* 7 (2013), p. 165.
 - [100] J.-M. C. Bouteiller et al. "Paired-pulse stimulation at glutamatergic synapses-pre-and postsynaptic components". In: *Engineering in Medicine and Biology Society (EMBC), 2010 Annual International Conference of the IEEE*. IEEE. 2010, pp. 787–790.
 - [101] D. E. Carlson et al. "Multichannel electrophysiological spike sorting via joint dictionary learning and mixture modeling". In: *IEEE Transactions on Biomedical Engineering* 61.1 (2014), pp. 41–54.
 - [102] V. P. Pastore et al. "Identification of excitatory-inhibitory links and network topology in large-scale neuronal assemblies from multi-electrode recordings". In: *PLoS computational biology* 14.8 (2018), e1006381.

-
- [103] H. Liu et al. "Use of a Neural Circuit Probe to Validate in silico Predictions of Inhibitory Connections". In: *bioRxiv* (2017).
 - [104] S. Ullo et al. "Functional connectivity estimation over large networks at cellular resolution based on electrophysiological recordings and structural prior". In: *Frontiers in neuroanatomy* 8 (2014), p. 137. ISSN: 1662-5129. DOI: 10.3389/fnana.2014.00137.
 - [105] V. Mwaffo, S. Butail, and M. Porfiri. "Analysis of pairwise interactions in a maximum likelihood sense to identify leaders in a group". In: *Frontiers in Robotics and AI* 4 (2017), p. 35.
 - [106] E. M. Izhikevich and R. FitzHugh. "FitzHugh-Nagumo model". In: *Scholarpedia* 1.9 (2006), p. 1349. ISSN: 1941-6016. DOI: 10.4249/scholarpedia.1349.
 - [107] J. Vitay, H. Dinkelbach, and F. Hamker. "ANNarchy: a code generation approach to neural simulations on parallel hardware". In: *Frontiers in neuroinformatics* 9 (2015), p. 19. ISSN: 1662-5196. DOI: 10.3389/fninf.2015.00019.
 - [108] J. Xu et al. "Information transmission in human cerebral cortex". In: *Physica D: Nonlinear Phenomena* 106.3-4 (1997), pp. 363–374. ISSN: 01672789. DOI: 10.1016/S0167-2789(97)00042-0.